Human monoclonal antibodies to the spike subdomain 1 neutralize SARS-CoV-2 and its variants of concern

A doctoral dissertation presented by
Filippo Bianchini

Under the supervision of
Prof. Davide F. Robbiani

Submitted to the
Faculty of Biomedical Sciences
Università della Svizzera italiana

For the degree of
Ph.D. in Biomedical Sciences

July 24th, 2024

INDEX

1. **ABSTRACT** 1
2. **INTRODUCTION** 2
2.1. THE IMMUNE SYSTEM 2
2.2. B LYMPHOCYTES 4
2.2.1. B cell development 4
2.2.2. B cell receptor complex 5
2.2.4. B cell activation 7
2.2.5. Germinal center 9
2.2.6. Antibody-secreting cells 10
2.2.7. Memory B cells 12
2.3. ANTIBODIES 13
2.3.1. Antibody structure and isotype 13
2.3.2. V(D)J recombination 17
2.3.3. Somatic hypermutation 18
2.3.4. Class switch recombination 19
2.3.5. Fc receptors 19
2.3.6. Antibody functions 21
2.3.7. Bispecific antibodies 22
2.4. SARS-CoV-2 25
2.4.1. Coronavirus taxonomy and history 25
2.4.2. SARS-CoV-2 proteins 26
2.4.3. SARS-CoV-2 Spike glycoprotein and cell entry mechanism 27
2.4.4. SARS-CoV-2 genome replication 30
2.4.5. SARS-CoV-2 evolution and variants 31
2.4.6. SARS-CoV-2 neutralizing antibodies 33
3. **AIMS OF THE THESIS** 37
4. **PUBLISHED MANUSCRIPT** 38
5. **UNPUBLISHED DATA** 71
5.1. RESULTS 71
5.2. MATERIALS AND METHODS 77
6. **DISCUSSION** 78
7. **ADDENDUM** 83
8. **BIBLIOGRAPHY** 87

1. ABSTRACT

Progress in the fight against COVID-19 is jeopardized by the emergence of SARS-CoV-2 variants that diminish or abolish the efficacy of vaccines and antiviral monoclonal antibodies. Novel immune therapies are therefore needed, that are broadly effective against present and future coronavirus threats. In principle, this could be achieved by focusing on portions of the virus that are both functionally relevant and averse to change.

The subdomain 1 (SD1) of SARS-CoV-2 Spike protein is adjacent to the receptor binding domain (RBD) and its sequence is conserved across SARS-CoV-2 variants, with the exception of one mutation each in the Alpha (A570D) and Omicron BA.1 (T547K) variants and two mutations in the Omicron BA.2.86 (E554K and A570V) variant.

To specifically identify and study human antibodies targeting SD1, we designed a flow cytometry-based strategy that combines negative selection of B cells binding to the RBD with positive selection of those binding to an SD1-RBD fusion protein. Among the 25 characterized human monoclonal antibodies, 16 are SD1-specific and 6 of them recognize the SD1-RBDs corresponding to all 12 main variants of concern that were tested.

Antibody sd1.040 also neutralizes SARS-CoV-2 pseudovirus variants, including the latest variants Omicron BQ.1.1, EG.5.1, and BA.2.86. Structural studies suggest that this antibody likely locks the Spike trimer in a conformation where the protomers are loosely associated and the fusion peptide is not completely exposed. sd1.040 synergizes with an antibody to the RBD (rbd.042) for neutralization and protects mice when these two antibodies are formulated in a bispecific antibody. Thus, naturally occurring antibodies can neutralize SARS-CoV-2 variants by binding to SD1 and can act synergistically against SARS-CoV-2 in preclinical models.

To improve our bispecific antibody, we characterized 37 new RBD antibodies for binding to the 12 main variants of concern. We selected 10 cross-reactive RBD antibodies and tested them in neutralization of ancestral pseudovirus. Three antibodies, rbd.106, rbd.112, and rbd.141, showed broader cross-reactivity and higher neutralizing potency than rbd.042. These antibodies represent promising candidates for the design of a new bispecific antibody.

2. INTRODUCTION

2.1. THE IMMUNE SYSTEM

Our body is constantly threatened by infectious pathogens and toxic molecules from the surrounding environment, in addition to the intrinsic risk of cell dysregulation and neoplastic disease. For these reasons, evolution led to the development of a complex network of specialized cells and effector molecules to protect us, known as immune system.

The cells of the immune system are collectively called leukocytes and originate from the hematopoietic stem cells of the bone marrow. These pluripotent stem cells can differentiate into two lineages: myeloid and lymphoid. The myeloid lineage includes macrophages, dendritic cells, and granulocytes, but also non-immune cells like erythrocytes and megakaryocytes. The lymphoid progenitors differentiate into natural killer cells (NK cells), B lymphocytes (B cells) and T lymphocytes (T cells)[1].

An effective immune response begins with the immunological recognition of the antigen. Historically the term "antigen" derived from "antibody generation". But nowadays all the molecules or substances able to elicit an immune reaction are referred to as antigens. Cells of the myeloid lineage belong to the innate arm of the immune system and generally recognize antigens through germline encoded pattern recognition receptors (PRRs). PRRs are activated by molecular structures shared among microorganisms known as pathogen-associated molecular patterns (PAMPs). Among the most common PAMPs there are lipopolysaccharides, peptidoglycans, mannose-rich oligosaccharides, and unmethylated CpG DNA. Unlike the myeloid lineage cells, B and T cells belong to the adaptive arm of the immune system and express highly variable antigen receptors which are the result of random recombination at particular genome loci. This process takes place during lymphocyte maturation, resulting in a different B or T cell receptor for each lymphocyte. This diversity in receptor repertoire allows the immune system to recognize any possible pathogen with higher affinity and specificity, even those pathogens that have never been encountered before[2–4].

Having recognized the pathogen, each cell type has a particular immune effector function. Macrophages, dendritic cells, and granulocytes are phagocytes. They can engulf and kill pathogens and then expose part of them on their surface to activate other leukocytes, and in particular T cells. All the cells that can perform this function are named antigen presenting cells (APCs), and dendritic cells, followed by macrophages, are considered the strongest APCs of the immune system. Granulocytes, also known as polymorphonucleated leukocytes, are divided into neutrophils, eosinophils, basophils, and mast cells. All of them present granules containing toxic

molecules and enzymes which are released upon activation to kill pathogens. Neutrophils are involved mainly in the defense against extracellular microorganism that can be phagocytosed, while eosinophils and basophils act against bigger parasites. Mast cells play a role in the defense from parasitic worms, but they are known mainly for their involvement in allergic reactions. NK cells play an important role in cancer prevention by killing abnormal cells. They also kill cells that have been infected by viruses. B cells are mostly known for being antibody-producing cells. B cells development and function will be explained more in detail in the following chapters. T cells are very heterogeneous and orchestrate the immune response at multiple levels. Once activated by their antigen, naïve T cells differentiate into T effector cells. There are three main categories of effector T cells. Cytotoxic T cells ($CD8^+$) kill the cells infected by intracellular pathogens and have an important role in the anti-cancer immune response. Helper T cells ($CD4^+$) provide signals to stimulate other leukocytes activation and influence their behavior based on the type of pathogen (e.g., induction of different antibody isotypes). Regulatory T cells ($CD4^+$) limit the immune response to avoid autoimmune diseases or excessive immune activation against environmental antigens[1,4].

Myeloid leukocytes and NK cells are generally classified as actors of the so-called "innate immunity". These cells express germline encoded receptors with broad specificity and are able to induce an immune reaction within hours from the pathogen encounter. On the other side, B and T lymphocytes need to be activated from cells of the innate immunity in order to differentiate into effector cells and proliferate, and this process usually requires days or weeks. However, B and T cells are more efficient and specific in recognizing the pathogen than innate immune cells. Because the development of effector B and T cells requires previous encounter with the pathogen, it is considered as an individual adaptation, from which the term "adaptive immunity" to describe this branch of the immune response.

Another important feature of adaptive immunity is the ability of developing immunological memory. Activated B and T cells can differentiate into memory cells, which are quiescent. In case of reinfection by the same or similar pathogen, memory cells rapidly reactivate, providing long-lasting immunity[5]. Long-term epigenetic changes elicited by antigen recognition have been observed also in cells of the innate immunity. This phenomenon has different features from adaptive memory, and it has been called "trained immunity"[6,7].

2.2. B LYMPHOCYTES

2.2.1. B cell development

B cells are one of the two main types of lymphocytes in the adaptive immune response and are responsible for the production of antibodies and the maintenance of humoral immunity[4]. The "B" in B cells originates from the fact that these cells develop in the *bursa of Fabricius* of birds[8]. In mammals, they are generated from hematopoietic stem cells, which reside in bone marrow microenvironmental niches made by stromal cells. Different cell types, including osteoblasts, reticular cells, and fibroblast-like cells, are responsible for the production of pro-survival and differentiation factors for B cells[9]. Guided by the factors produced, hematopoietic stem cells differentiate into multipotent progenitors (MPP) and then into common myeloid or lymphoid progenitors (CMPs or CLPs, respectively). B lymphocytes derive from CLPs, passing through subsequent developmental stages defined as:

1. Pre-pro-B cells ➔ they are found in contact with CXCL12-secreting stromal cells. Pre-pro-B cells are characterized by the expression of the surface marker CD45R and the transcription factor EBF1. Upon binding to the *Igh* locus, EBF1 promotes D_HJ_H recombination (details in the *VDJ recombination* section), which marks the entrance into the pro-B cell stage.
2. Pro-B cells ➔ in the bone marrow, pro-B cells migrate towards IL-7-secreting stromal cells. At this stage they start to express the co-receptor CD19 and the B cell receptor (BCR) components Igα and Igβ (details in the *B cell receptor complex* section). The expression of PAX5, induced by EBF1, determines the upregulation of B cell specific genes and the downregulation of non-B lineage genes. PAX5 also promotes V_HD_H recombination and progression to the pre-B cell stage[10,11].
3. Pre-B cells ➔ if the V(D)J recombination of the *Igh* locus is successfully completed, the rearranged μ heavy chain is expressed on the surface of the pre-B cells in combination with a surrogate light chain (SLC). The SLC is made by two separate and germline encoded proteins: VpreB and λ5. The surface expression of heavy chain and SLC in the so-called pre-BCR complex induces proliferation of the pre-B cells. When the surface expression of the pre-BCR decreases and light chain recombination starts, cells enter the late-pre-B cell stage. At the end, if the pre-B cells succeed in rearranging both heavy and light chain alleles, they express them as transmembrane IgM in the BCR complex and become immature B cells[12,13].
4. Immature B cells ➔ they migrate from the bone marrow toward the spleen and other lymphoid organs. Once they have reached their new location, immature B cells start to express the surface markers CD21 and CD23, together with the IgD version of their BCR complex, while

maintaining the expression of the IgM. At this stage, immature B cells also acquire the ability to recirculate into the bloodstream, finally becoming mature naïve B cells. Naïve B cells have been divided into two subtypes: follicular B (FOB) and marginal zone B (MZB) cells[14,15].

5a. Follicular B cells ➔ the differentiation of immature B cells into FOB cells requires weak BCR signaling. They recirculate through blood and lymphatic vessels and can be found in lymph node primary follicles and in the bone marrow. After interaction with helper T cells, FOB cells form the germinal centers and produce high-affinity antibodies against pathogens (details in the *Germinal center* section)[16]. In general, FOB cells present a more diverse repertoire of antibody genes when compared with MZB[15].

5b. Marginal zone B cells ➔ they develop from immature B cells experiencing strong (tonic) BCR signaling. MZB cells localize in the outer white pulp of the spleen and express higher levels of MHC class II compared with FOB cells. For this reason, they are strong APCs and contribute to the activation of T follicular helper cells. MZB cells can rapidly differentiate into IgM secreting plasmablasts in response to blood-borne pathogens, in both a T cell-dependent or -independent manner[17].

It is important to specify that the developmental processes described until this point refer to a group of B cells classified as B-2 in mouse. Another group, defined as B-1, has also been identified in the pleura and peritoneal cavities[18]. B-1 cells seem to be important to maintain tissue homeostasis and for the production of natural antibodies (i.e., antibodies that arise without any stimulation from external antigens), but their developmental pathway is still unclear[15]. Our understanding of human B-1 cells origin and function is still poor[19,20]. In this thesis, I will focus on B-2 cells and I will not further discuss B-1 cells.

2.2.2. B cell receptor complex

Naïve B cells express a transmembrane version of their antibody on the surface, which allows them to directly recognize the antigen in its native form. Transmembrane immunoglobulins have a short cytoplasmic tail which does not allow signal transduction. Activation signals are mediated by two other transmembrane proteins, named Igα (or CD79A) and Igβ (or CD79B). Igα and Igβ form dimers which are held together by disulfide bridges and are non-covalently associated with the immunoglobulin. Together with the transmembrane immunoglobulin, the Igα-Igβ chains form the so-called BCR complex[21].

Igα and Igβ cytoplasmic domains contain immunoreceptor tyrosine-based activation motifs (ITAMs) and are associated with tyrosine kinases of the Src family. When BCR molecules are cross-linked by a multivalent antigen, they are brought in proximity of each other. The clustering allows Src kinases

associated with a BCR to phosphorylate ITAM motifs of the Igα-Igβ chains from another BCR. The tyrosine kinase Syk can then bind the phosphorylated ITAMs and it is itself phosphorylated by Src kinases, leading to Syk full activation. Syk then phosphorylates adaptor proteins starting a signal transduction cascade which at the end brings to the activation of distinct pathways like: Ras-MAP kinase, phosphatidylinositol-specific phospholipase C (PLC), protein kinase Cβ (PKC-β) and PI3-kinase[22] (***Figure 1***).

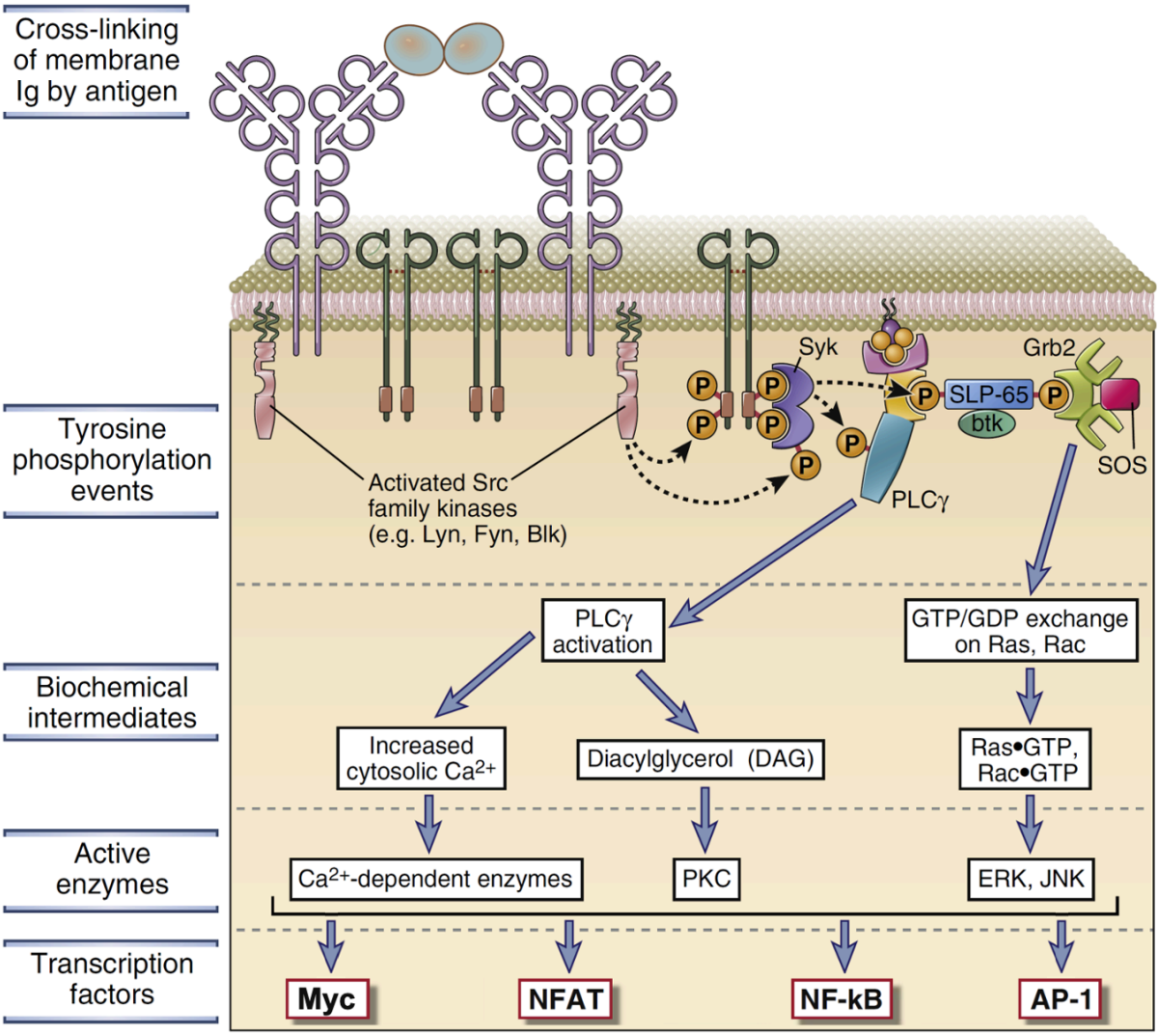

Figure 1. Schematic representation of BCR signaling pathway. *Upon BCR cross-linking by multimeric antigens, kinases from the Src family can phosphorylate Igα-Igβ ITAM motifs. Phosphorylated ITAMs recruit the kinase Syk, which phosphorylates other adaptor proteins and enzymes, leading to the activation of several pathways. The cascade results in a change of gene expression mediated by transcription factors like Myc, NFAT, NF-kB, and AP-1. Different stages of the signaling cascade are separated by dashed lines. Arrows indicate the sequence of events. (Figure adapted from Cellular and Molecular Immunology, Abbas et al., 2018[1])*

Another important contribution to B cell activation is provided by the type 2 complement receptor CR2 (or CD21). This receptor is expressed on the surface

of mature B cells in complex with the proteins CD19 and CD81. Together, CR2, CD19, and CD81 are called *B cell coreceptor complex*. CR2 can recognize the complement protein C3d, which can be covalently bound to the microbial surface. When this happens, the B cell coreceptor complex is brought in proximity of the BCR, which is also bound to the microbial surface in an antigen-specific way. The cytoplasmic tail of CD19 is then phosphorylated by the kinases of the BCR, allowing the recruitment and activation of PI3-kinase and enhancement of B cell stimulation. CD81 seems to be necessary for the correct localization of the B cell coreceptor complex at the membrane[23].

2.2.3. B cell tolerance

In order to avoid autoimmunity, B cells that express a BCR recognizing self-antigens have to be negatively selected. This selection can happen during B cells maturation in the bone marrow (central tolerance) or for mature B cells in the periphery (peripheral tolerance).

- Central tolerance ➔ when an immature B cell recognizes self-antigens present in the bone marrow at high concentration, BCRs cross-linking can directly induce the apoptosis of the cell (clonal deletion). If this is not the case, the B cell can also reactivate RAG1 and RAG2 expression and try to recombine another light chain allele, with the aim to produce a new non-autoreactive BCR (process known as receptor editing). B cells with low affinity for self-antigens can downregulate the BCR and become unresponsive (anergy)[24,25].
- Peripheral tolerance ➔ mature B cells can still die by apoptosis or become anergic if they recognize self-antigens without stimulation from helper T cells. Due to the somatic mutations that the BCR can acquire during the process of affinity maturation (details in the *Germinal center* section), B cells are more prone to develop peripheral self-reactivity compared to T cells. However, various inhibitory receptors can set a threshold preventing B cell activation against self-antigens[15].

2.2.4. B cell activation

BCR signaling is usually insufficient to induce B cell proliferation and antibody secretion. When a B cell recognizes a protein antigen, the latter is internalized, digested, and displayed on the B cell surface as peptides bound to MHC class II molecules. This process allows previously activated helper CD4 T cells to interact with the B cells specific for the same antigen. Helper T cells then secrete cytokines that induce B cell differentiation, proliferation and antibody isotype switching. Antigens that require the presence of T cells to elicit a B cell response are defined as thymus-dependent antigens.

Thymus-independent antigens are usually microbial-derived (e.g., bacterial polysaccharides) and can directly induce antibody production. This can be

achieved through extensive cross-linking of the BCR, in case of repetitive epitopes, or by recognition of other bacterial components by the B cell.
Antibodies induced by thymus-independent antigens are usually IgM and show lower affinity for the antigen than antibodies against thymus-dependent antigens. This is because interaction with T cells is usually required for both isotype switching and affinity maturation[4].
Due to the very small frequency of naïve B and T cells specific for the same antigen, the chance of an encounter is estimated to be around 1 in $10^8/10^{12}$. To improve the chances, B and T cells are retained in specialized structures of the peripheral lymphoid tissue, the lymph nodes. Naïve B cells express the chemokine receptor CXCR5, which directs them to the primary lymphoid follicles once they have arrived in the lymph node through the lymphatic vessels. CXCL13 is the natural ligand of CXCR5, and it is expressed by stromal cells and follicular dendritic cells located in the primary lymphoid follicle. The antigens are also transported into the lymph nodes through the lymph. Once there, they can directly interact with B cells or be caught and presented by follicular dendritic cells or macrophages. In the latter case, the antigen is always presented in its undigested and native form. Upon antigen recognition, B cells start expressing CCR7 and migrate to the boundary with the T-cell area, where stromal and dendritic cells express CCR7 ligands, like CCL21[26,27].
Vice versa, naïve T cells only express CCR7 and are localized in the T-cell area of the lymph node. When they recognize the antigen presented by a dendritic cell, T cells start to express CXCR5 and proliferate. Some of them differentiate into effector T cells and migrate outside of the lymphoid tissue, while others move to the boundary with the follicle and become follicular helper T cells[28].
The convergence of activated B and T cells to the boundary maximizes the chances of an encounter between cells specific for the same antigen. If this happens, T cells increase the expression of surface molecules and cytokines that promote B cell activation. Activated B cells migrate toward the medullary cords, in proximity of the efferent lymphatic vessels, and start proliferating to establish a primary focus (~5 days post infection). Some of these proliferating B cells differentiate into plasmablasts and start secreting antibodies. At the very beginning of the immune response, these antibodies are germline IgM. Later, plasmablasts may undergo isotype switching and low levels of somatic hypermutation. Plasmablasts usually die in few days, but some of them could differentiate into plasma cells. These terminally differentiated cells lose the expression of the MHC class II and have low level of surface immunoglobulin, and therefore are not able to contact T cells anymore. They also lose the ability to switch antibody isotype and to perform somatic hypermutation. Plasma cells can stay in the lymph node as short-lived cells, or migrate into the bone marrow and continue the antibody production[1,4].

2.2.5. Germinal center

Some of the B cells that have been activated by their T cell counterpart migrate toward the primary lymphoid follicle and continue to proliferate, forming a germinal center. When a germinal center is initiated inside a primary lymphoid follicle, this one becomes a secondary lymphoid follicle.

The expansion of the germinal center pushes the surrounding resting B cells to the periphery of the follicle, which takes the name of mantle zone[4]. The germinal center is divided in two regions called dark and light zones based on their histological appearance. Most of the B cells in the dark zone are actively proliferating and are called centroblasts. The B cells of the light zone are called centrocytes and proliferate at lower frequency than centroblasts. The light zone is also highly populated by follicular dendritic cells and follicular helper T cells, which contribute to the less dense appearance of this region[29] (***Figure 2***).

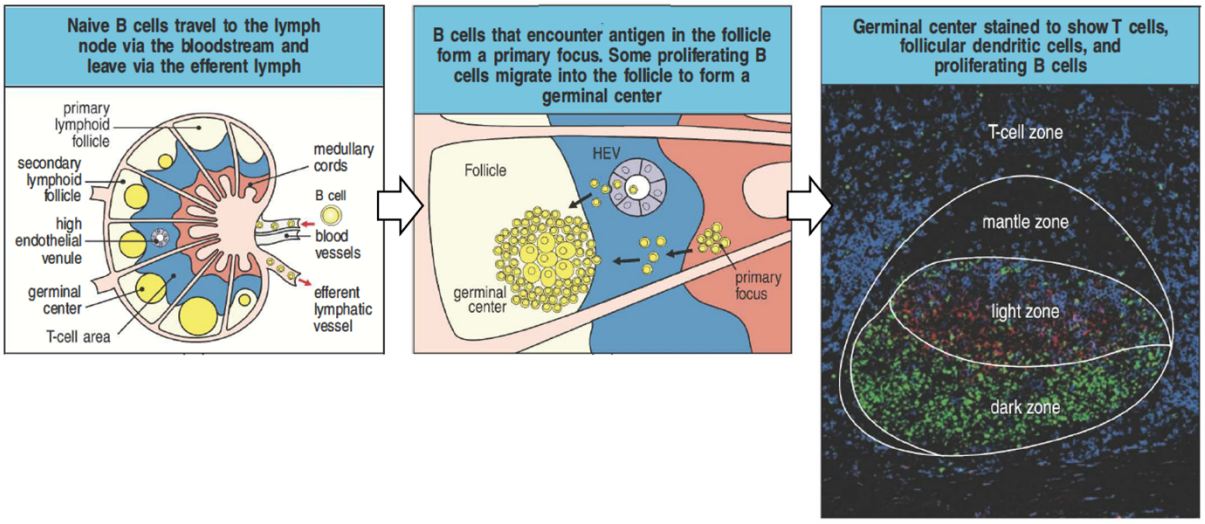

Figure 2. Lymph node and germinal center structures. *The first panel (left) shows the anatomy of an entire lymph node, with different colors for the medullary cords (red), the T cell area (blue) and the lymphoid follicle (yellow). It also shows the evolution from primary to secondary lymphoid follicle. The second panel (center) is the magnification of a secondary lymphoid follicle. Some of the activated B cells in the primary focus migrate back toward the follicle and form a germinal center. The third panel (right) shows immunofluorescent staining of a real germinal center. Proliferating cells (in this case centroblasts) are stained in green and are found mainly in the dark zone. Follicular dendritic cells are stained in red and localize in the light zone, while T cells are stained in blue and can be found in both the T-cell zone and in the light zone. (Figure adapted from Janeway's Immunobiology, Murphy and Weaver, 2016[4])*

Germinal centers are known to be the structures where B cells undergo affinity maturation. This process consists of the induction of new mutations in the variable regions of the antibody genes (details in the *Somatic hypermutation* section), followed by selection of the B cells with increased

affinity for the antigen. What we know about this process derives mainly from mouse models. It seems that, after the initial encounter with helper T cells, B cells migrate first to the light zone of the germinal center. Here they can be retained up to 12 h, before moving to the dark zone. In the dark zone the B cells undergo somatic hypermutation while proliferating, before entering quiescence and moving back to the light zone. Newly emerged B cells are tested in the light zone for their ability to bind and present the antigen to the T cells. B cells cycle between dark and light zones multiple times in order improve antibody affinity through the cumulative acquisition of mutations[30].
As mentioned above, B cells can directly interact with soluble antigens through the BCR, but they can also acquire antigens previously captured by follicular dendritic cells. Follicular dendritic cells can bind the antigen only when it is opsonized by complement proteins or by previously existing IgGs[26]. Furthermore, it has been hypothesized that follicular dendritic cells could play a suppressive role in this phase by capturing and presenting antibody-opsonized antigens that activate the suppressive receptor FcγRIIB expressed by germinal center B cells[31]. It also seems that BCR signaling alone does not contribute to positive selection, which is mainly dependent on T cell signaling. B cells with improved BCR affinity can outcompete the surrounding cells and internalize more antigen, which is processed and presented on MHC II[30,32,33]. If the affinity is too low and the B cell fails to receive positive signaling from T cells, in most of the cases it will undergo apoptosis[34]. However, some cells with low affinity have shown to survive and differentiate into memory B cells. These cells arise in the early stages of the germinal center and, consistent with this observation, they usually bear few mutations in the variable region of their antibody[35,36]. The factors determining the decision between apoptosis and differentiation remain poorly understood.
The first antibody-secreting cells arise before the formation of the germinal center as short-lived plasmablasts which migrate to the spleen and in the bone marrow. Germinal center-derived long-lived plasma cells originate later, and after memory B cells. They then migrate to the bone marrow[35,37]. Antibodies produced by antibody secreting cells show higher affinity for the antigen and higher number of mutations compared with memory B cells ones, but it is still not clear how affinity plays a direct role in B cell differentiation[31].

2.2.6. Antibody-secreting cells

The term antibody-secreting cells (ASCs) refers to both plasmablasts and plasma cells. The mechanism determining which B cells differentiate into ASCs and whether they will be plasmablasts or plasma cells is still not clear, even though high BCR affinity could be associated with preferential differentiation to ASCs[38].
Although ASCs are the final stage of differentiation of activated B cells, they can be considered a completely different cell due to the extensive changes in

gene expression and chromatin remodeling. Among the most important transcription factors involved in ASC differentiation are IRF4, BLIMP1 (highly expressed in plasmablasts but not in plasma cells), and XBP1, which are necessary for the unfolded protein response and immunoglobulin production. These transcription factors not only activate the ASC specific gene program, but also repress B cell specific genes like Pax5. Whether plasma cells derive from plasmablasts or are a direct product of the germinal center is still under debate. The main difference between these two cell types is their ability to proliferate, which is lost in plasma cells[39].

Both plasmablasts and plasma cells can express the receptors S1PR1 and CXCR4, which allow them to enter in the bloodstream and home to the bone marrow, respectively[40]. However, only plasma cells can survive in the bone marrow for long periods, becoming long-lived plasma cells. It is demonstrated that the longevity of plasma cells is due to extrinsic factors derived from the microenvironment, although the precise location and composition of bone marrow niches are still elusive[39,41]. Many cell types could actually be involved in the maintenance of long-lived plasma cells, including megakaryocytes, eosinophils, fat cells, and mesenchymal stromal cells[38]. They are thought to provide extrinsic survival signals like CXCL12, VCAM1, APRIL, TNF, and IL-6[39]. Among them, APRIL seems to be one of the most important factors, inducing the expression of the anti-apoptotic protein MCL1 in ASCs[42]. MCL1 has a very short half-life, suggesting that ASCs exiting from the niche could rapidly undergo apoptosis due to a lack of APRIL signaling. Interestingly, both APRIL and IL-6 signaling require the activity of nitric oxide synthase. Nitric oxide also has a short half-live, supporting the model that long living plasma cells can survive only in the particular microenvironment of the niche[43].

Another important factor controlling plasma cell homeostasis seems to be serum antibody levels. In fact, plasma cells express the inhibitory Fc receptor FcγRIIB, which induces plasma cell apoptosis when activated[44].

Only 0.1-1% of human bone marrow cells are long-lived plasma cells. Based on this observation, it has been estimated that a maximum of 10^9 plasma cells can home to the bone marrow [45,46]. These cells are always found in the proximity of stromal cells expressing CXCL12 (ligand of CXCR4), supporting the hypothesis that new ASCs could enter the bone marrow and displace already present plasma cells from the niche. Without the survival signals of the niche, displaced plasma cells would rapidly die, probably as a consequence of endoplasmic reticulum stress[47].

Based on these assumptions, it has been predicted that, in humans, the concentration of serum antibodies specific for an antigen would decrease of 50% in around 23 years. However, because the minimal protective concentration of serum antibodies can be different from one pathogen to another, in some cases the protection provided by the humoral immune memory could be life-long[47–49].

2.2.7. Memory B cells

Around 40% of human peripheral blood B cells are memory B cells[50], while in mice they account only for 5%[51]. Memory B cells are characterized by higher stability (decades)[52] and faster activation kinetics compared with naïve B cells[53]. They can arise at the early stage of the immune response from activated B cells in the primary focus (germinal center-independent memory B cells) or later from the germinal center (germinal center-derived memory B cells)[54]. It seems that activated B cells expressing BCRs with low affinity for the antigen tend to differentiate in memory B cells, while higher affinity BCRs promote differentiation into plasma cells[55,56]. However, other factors are believed to play a role in deciding the B cell fate, such as antigen availability[57] and pro-survival signals from the local microenvironment[53].

The molecular mechanisms driving memory B cell differentiation is still not clear, though. No master transcription factor has been identified for this cell subtype, but it seems that an important role is played by BACH2. The expression of the transcription factor BACH2 is suppressed by the interaction with T helper cells. However, memory B cells develop in conditions of low level or absence of T cell help, allowing maintenance of BACH2 expression. BACH2 suppresses MYC and mTORC1 pathways[58,59], that are known to be necessary respectively for proliferation and biomass increase in germinal center B cells[60,61]. Memory B precursor cells do not proliferate and, indeed, BACH2-deficient germinal center B cells are not able to generate memory B cells[58].

From mouse experiments it seems that the memory B cell population is quite heterogeneous. $CD80^{-}CD73^{-}$ IgM-expressing memory B cells likely originated in a germinal center-independent manner and tend to generate germinal center B cells upon activation. On the other hand, $CD80^{+}CD73^{+}$ IgG1-expressing memory B cells likely derive from the germinal center and rapidly develop into plasmablasts upon reactivation, forming just a small population of germinal center cells[62]. Another subset of memory B cells discovered in humans is characterized by the expression of inhibitory receptors and the lack of CD21 and CD27. These cells, are less sensitive to in vitro antigen stimulation and require T cell-derived cytokines to be reactivated[63]. Their function is still not clear, but some hypotheses are that they could be exhausted cells, cells specialized in antigen presentation, or cells that are less dependent on antigen for reactivation compared to conventional memory B cells[53].

Memory B cells are also known to recirculate in the bloodstream to then reach other lymphoid organs[64], but a subpopulation residing long-term in the draining lymph node of origin has also been observed[65]. Resting memory B cells are found mainly in the subcapsular region of the lymph nodes, in close proximity of memory T follicular helper cells and macrophages. It is believed that these macrophages are specialized in capturing antigens like viruses and

immune complexes and passing them to the nearby B cells. Memory B cells then internalize the antigen and present it to memory T cells via MHC II molecules, reactivating them. The proximity of macrophages, B and T cells would explain the speed and strength of recalled responses[66].
Most of the plasmablasts generated after reimmunization derive from memory B cells. On the other hand, once reactivated, only few memory B cells form secondary germinal centers, which are mainly composed of naïve B cells[67]. The reasons why memory B cells are rarely forming germinal centers are not clear. One of the factors involved could be the presence of antibodies competing for the same antigen recognized by memory B cells. These antibodies could either be present before boosting or being rapidly produced by reactivated memory B cells, but in both cases they are believed to cause epitope-masking[53,68].
Despite lower BCR affinity for the antigen, memory B cells have shown higher clonal diversity compared with plasma cells. It seems that the memory B cell pool is enriched in non-immunodominant clones, that however cross-react with antigens derived from distinct viral variants[69,70]. This is consistent with what observed in a mouse model of West Nile virus infection. While antibodies from long-lasting plasma cells were more efficient against reinfections with the same virus, memory B cells secreted antibodies were recognizing at similar extend original virus and viral variants[71].

2.3. ANTIBODIES

2.3.1. Antibody structure and isotype

Antibodies were the first immune component involved in pathogen recognition to be identified, and they are now the most characterized. They are first expressed on the surface of B cells as immunoglobulins, and then secreted as proper antibodies following B cell activation and differentiation into plasma cells. Secretion of antibodies is considered the main effector function of B cells in adaptive immunity[4].
Antibodies are proteins made of two immunoglobulin heavy chains (IgH) of approximately 50 kDa and two immunoglobulin light chains of 25 kDa. IgH chains are encoded by a locus on human chromosome 14, while immunoglobulin light chains can be either kappa (Igκ), encoded by human chromosome 2, or lambda (Igλ), on human chromosome 22. Heavy and light chains are held together by disulfide bridges forming a “Y” shaped structure. (***Figure 3A)***.
Each short arm is made by the N-terminal portions of one IgH chain and by a light chain. Antibody variability concentrates at the N-terminus of each chain where there are three loops named complementarity-determining regions (CDR1, CDR2, and CDR3) which form the antigen binding pocket. For this reason, the short arms of the antibody are also called Fragments antigen

binding (Fab). The C-terminal domain of the immunoglobulin is instead much more conserved in the same species and is called constant (C) region or Fragment crystallizable (Fc), for historical reasons (***Figure 3B)***.

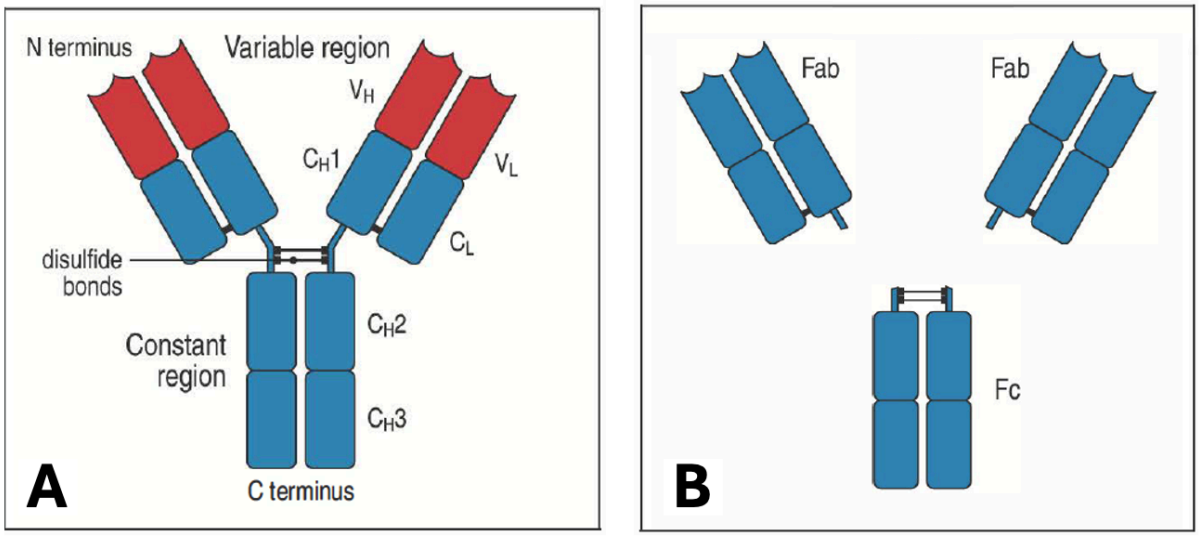

Figure 3. Schematic structure of an antibody molecule (IgG). (A) *Structure of an antibody molecule with annotations for each variable (V_H and V_L, in red) and constant (C_H1, C_H2, C_H3, and C_L, in blue) domain. Disulfide bridges between the two heavy chains and between heavy and light chains are also shown.* ***(B)*** *Division of the antibody molecule into Fab and Fc. (Figure adapted from Janeway's Immunobiology, Murphy and Weaver, 2016[4])*

In humans, there are five types of C regions encoded by different exon clusters (Cα, Cε, Cγ, Cμ, and Cδ)[4,72]. Based on the sequence of the C region, human antibodies can be classified in five main isotypes with different functional and structural features:

- Immunoglobulin A (IgA, exon cluster Cα) ➔ IgA antibodies are fundamental in the defense of mucosal surfaces, where they are the most abundant isotype[73]. They are particularly efficient in inducing antibody-dependent cellular cytotoxicity (ADCC) by macrophages and granulocytes, but not by NK cells. They can also activate the complement cascade[74,75]. IgA antibodies in serum are mostly monomeric. However, they can form dimers through a C-terminal 18 amino acid extension (tailpiece) which forms disulfide bridges with a 15 kDa polypeptide called joining (J) chain. Only dimeric IgA can bind the polymeric immunoglobulin receptor (pIgR), which is expressed on the basolateral surface of mucosal epithelial cells. This receptor mediates IgA transcytosis and release at the mucosal surface. The release requires cleavage of pIgR, thus secretory IgA is made of dimeric IgA connected by J-chain and associated with the extracellular part of pIgR, called the secretory component (SC)[73,76]. Humans have two IgA subclasses: IgA1 and IgA2. IgA1 is more glycosylated than IgA2 and has a hinge region

between Fab and Fc, which is 13 amino acids longer. It seems that the difference in glycosylation is responsible for the stronger pro-inflammatory activity of IgA2 compared with IgA1[77,78]. IgA1 and IgA2 have similar serum half-life (~6 days), but IgA1 is more abundant than IgA2 (3.0 VS 0.5 mg/mL of serum) representing 90% and 10% of the total serum monomeric IgA, respectively. However, both IgA1 and IgA2 can form dimers and their proportion at mucosal sites and in mucosal secretions is more variable[4,73].

- Immunoglobulin E (IgE, exon cluster Cε) ➔ IgE antibodies are involved in defense against parasites and in allergic reactions. They are the less abundant antibody isotype in human serum (~50 ng/mL) and they have short half-life (~1.5 days). However, the strong affinity of IgE for the FcεRI seems to prolong their half-life in tissues for up to 2 weeks, reducing their diffusion back to the bloodstream[4,79]. FcεRI is mainly expressed on mast cells, basophils, monocytes, and macrophages[80]. When IgE antibodies bound to FcεRI recognize a multivalent antigen, the consequent clustering of antibody-receptor complexes activates the signaling cascade that finally results in cell degranulation[81]. The consequent release of molecules like histamine, heparin, and serotonin is responsible for the typical symptoms of allergic reactions[79].

- Immunoglobulin G (IgG, exon cluster Cγ) ➔ immunoglobulins of the G isotype can in human be further distinguished into four subclasses (IgG1-4). IgG1, IgG2, and IgG4 have the longest serum half-life among all antibody isotypes (approximately 21 days). This is due to their ability to bind the neonatal Fc receptor (FcRn) at endosomal acidic pH. FcRn binding prevents lysosomal degradation of IgGs and recycles them to the cell surface. Antibodies of the IgG3 subclass can also bind FcRn, but they are easily displaced by IgG1 antibodies. This explains their shorter half-life in comparison with the other IgG subclasses (~7 days). Each IgG subclass has peculiar features:

    - IgG1 (adult serum level ~9 mg/mL): they are potent activators of the complement cascade and they can induce ADCC[82]. From the translational point of view, IgG1 antibodies show desirable features like high yield of production and purification from transfectoma cells and good stability in storage buffers. For these reasons and their long half-life *in vivo*, most of the antibodies currently approved in the clinic are cloned into IgG1 expression vectors[80], including the monoclonal antibodies discussed within this thesis.
    - IgG2 (adult serum level ~3 mg/mL): they have limited capacity of activating the complement cascade, and do so only at high

concentrations[83]. Fc-mediated effector functions are negligible and limited to the activating receptor FCγRIIa[80].

- IgG3 (adult serum level ~1 mg/mL): they activate the complement cascade and bind Fc receptors more efficiently than IgG1[83,84]. However, IgG1 have been preferentially chosen for clinical application because of IgG3's shorter serum half-life (~7 days), tendency to form aggregates, and manufacturing issues (IgG3 antibodies cannot be purified with protein A)[80].
- IgG4 (adult serum level ~0.5 mg/mL): this isoform has low complement activation and ADCC activities[82], although able to bind stimulatory Fc receptors like FcγRI, FcγRII ,and FcγRIIIa[85]. IgG4 antibodies have the peculiar feature that they undergo Fab arm exchange process. During this process, the antibody splits into two dimers made by one heavy and one light chain each, that can reassociate with dimers from other IgG4 antibodies. This recombination gives origin to natural bispecific antibodies[86].

- Immunoglobulin M (IgM, exon cluster Cμ) ➔ most of the IgM antibodies are found in the blood as pentameric molecules connected by J-chain, similarly to what was previously described for IgA. A minor part of pentameric IgM can bind pIgR and be transported to mucosal surfaces[87]. In human adults, IgM antibodies reach a serum concentration of ~1.5 mg/mL and have a half-life of ~10 days[4]. They are potent activators of the complement cascade[88] and they can bind the FcμR expressed by B, T, and NK cells. The intracellular portion of FcμR has several tyrosine residues but lack of canonical immunoreceptor tyrosine-based inhibition or activation motifs (ITIM and ITAM), suggesting that it could modulate the immune response in multiple ways[89,90].

- Immunoglobulin D (IgD, exon cluster Cδ) ➔ IgD antibodies have a half-life of ~3 days in human adult plasma and are the second less abundant isotype, reaching around 0.03 mg/mL[4]. Most naïve B cells express on the cell surface both IgD and IgM through alternative splicing[91]. Circulating $IgM^{-}IgD^{+}$ B cells are rare and usually anergic[92], but hypermutated $IgM^{-}IgD^{+}$ plasma cells can be found in human tonsils[93]. From there, IgD-secreting cells can enter the circulation and reach other mucosal districts, like the salivary and mammary glands or the middle ear, where they are thought to play a role in mucosal immunity binding both commensals and pathogens[94]. It seems that IgD antibodies can interact with cells of the innate immune system like basophils, mast cells, monocytes, and dendritic cells in a Fc-independent way. The receptor involved in this interaction is still unknown[95–97].

2.3.2. V(D)J recombination

The human antibody repertoire is estimated to possess greater than 10^{11} antibody specificities. A single individual's antibody repertoire is limited by genetics, B cell number, and previous antigen encounters. To reach such diversity, a limited number of gene segments (***Figure 4***) are rearranged in a process known as V(D)J recombination. The final V-region of the IgH chain is a product of the assembly of Variable (V), Diversity (D), and Join (J) segments, while light chains are made by V and J segments only[4].

Number of functional gene segments in human immunoglobulin loci

Segment	Light chains		Heavy chain
	κ	λ	H
Variable (V)	34–38	29–33	38–46
Diversity (D)	0	0	23
Joining (J)	5	4–5	6
Constant (C)	1	4–5	9

Figure 4. Total number of gene segments for each immunoglobulin locus in human genome. *The reported numbers have been obtained excluding the pseudogenes. Variability derives from genetic polymorphism, that results in possible different numbers of gene segments in different individuals. Most of the diversity in the antibody repertoire is due to the high number V segments, while D and J segments are much less abundant. (Figure from Janeway's Immunobiology, Murphy and Weaver, 2016[4])*

Each V, D, and J segment is flanked by recombination signal sequences (RSS), which are made of a heptamer motif (consensus 5'-CACAGTG-3') and a nonamer sequence (consensus 5'-ACAAAAACC-3') separated by a spacer sequence of 23 nucleotides, in the case of J and IgH V segments, or 12 nucleotides for D and light chain V segments[98,99] (***Figure 5***).

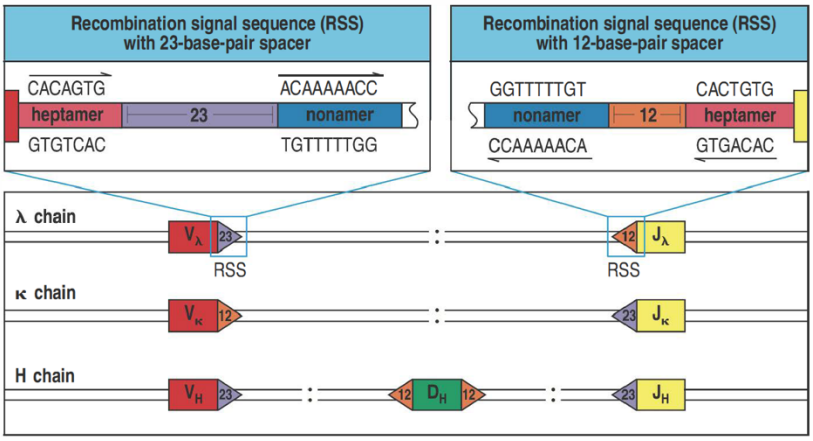

Figure 5. RSS organization. *Heptamers and nonamers are separated by spacers of 23 (violet) or 12 (orange) bp. Joining of gene segments happens only between RSS with 23 and 12 bp spacers, ensuring the correct V(D)J arrangement. (Figure from Janeway's Immunobiology, Murphy and Weaver, 2016[4])*

The RSS are recognized by the lymphoid-specific proteins Recombination-activated gene (RAG1-RAG2) recombinase. The RAG1-RAG2 complex introduces a nick between the RSS and the coding sequence, then it captures another RSS with a different spacer length and repeats the process. This step guarantees that only gene segments flanked by different spacers (23/12) can be fused[100]. The nicking generates a free 3'-OH that can attack the opposite DNA strand with formation of a hairpin structure. The two hairpins (one per RSS) activate the non-homologous end joining pathway (NHEJ) which joins the DNA segments in an imprecise way that contributes to the variability of this region[101,102]. During V(D)J recombination of the IgH locus, B lymphocytes also express the terminal deoxynucleotidyl transferase, which adds random nucleotides in the site of junction[103].
V(D)J recombination starts from the D-J segments of both IgH alleles at the same time. Instead, V-DJ rearrangement is first accomplished on one of the two alleles and, if successful, recombination of the second IgH allele is repressed epigenetically (allelic exclusion)[104,105]. If the B cell manages to express a functional pre-BCR, pre-BCR signaling induces the recombination of the Igκ locus. In a similar way to the IgH V(D)J recombination, if the first Igκ allele is successfully recombined, the second one is silenced. If both Igκ alleles fail to generate a productive light chain, then the Igλ alleles are recombined[1].
Of the three hypervariable loops that form the antigen binding site of the antibody (CDRs), the first two (CDR1, CDR2) are fully encoded by the V segment in both heavy and light chains. CDR3 is encoded by the V-J junction in light chains and also includes the full D segment in heavy chains. For this reason, diversity in CDR3 is much greater than that observed in CDR1 and CDR2[4].

2.3.3. Somatic hypermutation

The primary antibody repertoire is large and develops in the absence of antigens. Once a B cell is activated and forms a germinal center, the process of somatic hypermutation can further modify the V-region of the antibody with the aim to increase its affinity for a specific antigen: affinity maturation. In the germinal center, the interaction with follicular helper T cells induces the expression of the activation-induced cytidine deaminase (AID) in B cells. AID is a member of the APOBEC family of cytidine deaminases, and it acts only on single-stranded DNA. This would explain why AID acts only on genes that are actively transcribed[1,4,106]. AID converts cytosine bases (C) into uracils (U), which trigger the activation of the mismatch repair (MMR) or the base excision repair (BER) pathways when detected in DNA. Both MMR and BER can repair the DNA without inserting any mutation[107,108]. If this does not happen, during DNA replication the U can cause a C-T (thymine base) transition mutation. Furthermore, non-canonical MMR and BER pathways using error-prone

polymerases can also introduce mutations that are fixed after the first round of replication. In particular, non-canonical MMR tend to introduce mutations at A:T (A is adenine base) residues near the U, while non-canonical BER results in C-G (G is guanine base) transversion at the site of U[72,109].

2.3.4. Class switch recombination

Antibodies are first expressed in the form of IgM and IgD on the surface of naïve B cells. Upon B cell activation, the same antibody specificity can be expressed as a different isotype, including IgA, IgE, and IgG. This process, called isotype switching, allows the cells to modify the effector activity of the antibody without influencing its specificity[4,72]. Differently from the expression of IgM or IgD, which is based on alternative splicing[91], the isotype switch is due to irreversible DNA recombination, making it impossible for the cell to express more than one isotype[72]. The C-region of each isotype is encoded by a specific exon cluster (Cα, Cε, Cγ, Cμ, and Cδ) with its own promoter. With the exception of Cδ, there is a switch (S) region made of 1-10 kb of repetitive sequence between the promoter and each coding sequence. When the promoter of an exon cluster is actively transcribed, the S region unwinds and becomes accessible to AID[110,111]. As previously described, AID can convert C into U and activate MMR or BER pathways. However, when this happens on two Cs that are nearby on opposite DNA strands, MMR or BER pathways can lead to a double strand break and to the activation of the ATM-dependent DNA damage response. The likelihood of this event is maximized by the CG-rich composition of the S region[72,112]. A DNA double-strand break is necessary in the S region of both Cμ and the exon cluster encoding the new isotype. Then, the NHEJ repair pathway can join the two ends, deleting the intervening DNA which always includes Cμ and Cδ[4,113].

The choice of the new isotype is not random, but it is guided by cytokines. The promoters of exon clusters respond to different combinations of cytokines, inducing transcription and recombination of the downstream S region[114]. For instance, IL-4 seems to induce class switching toward IgE and IgG isotypes, and IL-10 toward IgG1 and IgG3. IgG2a and IgG3 are induced by interferon-γ, while IgA by the transforming growth factor-β (TGF-β). IL-9 and IL-13 are also involved in the transcription of the IgE locus[72].

2.3.5. Fc receptors

If the Fab regions of an antibody determine its specificity and affinity for the antigen, the Fc portion allows activation of the effector branches of the immune system. This includes triggering of the complement cascade and interaction with numerous Fc receptors (FcRs) expressed by a variety of cells[1,4].

Each antibody isotype can activate a specific class of FcRs through its Fc portion. Isotype specificity is indicated by Greek letters: FcαR for IgA, FcεR for IgE, FcγR for IgG, and FcμR for IgM[115]. However, this distinction is simplistic and most FcRs can bind different classes or subclasses of antibodies. The nomenclature is determined by the isotype with the highest affinity for that particular receptor[116]. Affinity also determines under which conditions the FcRs get activated. High-affinity FcRs can bind monomeric antibodies in the absence of antigen and cluster only when the antigen is encountered, while low-affinity FcRs only recognize immune complexes that cause their direct aggregation[117,118].

Few FcRs are single-chain proteins, but most of them are complexes of 2-3 non-covalently associated subunits. The FcRα subunit contains the extracellular domain responsible for antibody binding. The signal transduction is mediated by other subunits, like the widely expressed FcRγ[4,116]. The intracellular domain of monomeric FcRs or FcRγ contains ITAMs that are phosphorylated upon FcR clustering, similarly to what was previously described for BCR activation[119]. The signal transduction cascade leads to a variety of cell responses that depend on many factors, like the cell type expressing the FcR, the combination of activated FcRs, and the abundance of each antibody isotype. Among the responses induced by FcR activation there is degranulation and release of cytotoxic, vasoactive or pro-inflammatory molecules, production of cytokines, chemokines or growth factors, phagocytosis, endocytosis, and transcytosis[116]. However, it has been observed that some ITAM-containing FcRs, like FcεRI, can also generate inhibitory signals through the recruitment of SH2 domain-containing inositol phosphatase (SHIP1). This seems to limit or modulate the downstream effects of FcR activation[120,121]. The only FcR containing ITIMs instead of ITAMs is FcγRIIB, which is also the only FcR expressed by B lymphocytes. The clustering of FcγRIIB does not trigger any negative signal per se, but suppresses positive signals when co-aggregated with other stimulatory receptors by SHIP1 recruitment[122,123].

FcRs are expressed by almost all myeloid cells, some lymphoid cells, and few non-hematopoietic cells. Most of the cells express multiple types of FcRs at variable levels. This heterogeneity is further complicated by the fact that antibody isotypes can be found at different concentrations in different tissues and some of them have both monomeric and polymeric forms. For these reasons, FcRs are thought to be involved in numerous physiological and pathological conditions, but the study of their mechanisms of action is not trivial[116] (***Figure 6***).

Receptor	FcγRI (CD64)	FcγRII-A (CD32)	FcγRII-B2 (CD32)	FcγRII-B1 (CD32)	FcγRIII (CD16)	FcεRI	FcεRII (CD23)	FcαRI (CD89)	Fcα/μR
Structure	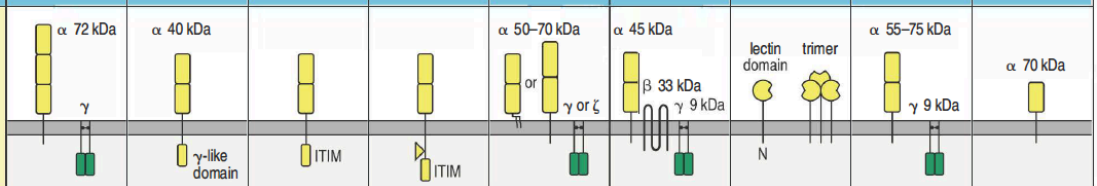								
Binding Order of affinity	IgG1 $10^8\ M^{-1}$ 1) IgG1=IgG3 2) IgG4 3) IgG2	IgG1 $2 \times 10^6\ M^{-1}$ 1) IgG1 2) IgG3=IgG2* 3) IgG4	IgG1 $2 \times 10^6\ M^{-1}$ 1) IgG1=IgG3 2) IgG4 3) IgG2	IgG1 $2 \times 10^6\ M^{-1}$ 1) IgG1=IgG3 2) IgG4 3) IgG2	IgG1 $5 \times 10^5\ M^{-1}$ IgG1=IgG3	IgE $10^{10}\ M^{-1}$	IgE $2–7 \times 10^7\ M^{-1}$ (trimer) $2–7 \times 10^6\ M^{-1}$ (monomer)	IgA1, IgA2 $10^7\ M^{-1}$ IgA1=IgA2	IgA, IgM $3 \times 10^9\ M^{-1}$ 1) IgM 2) IgA
Cell type	Macrophages Neutrophils Eosinophils Dendritic cells	Macrophages Neutrophils Eosinophils Platelets Langerhans cells	Macrophages Neutrophils Eosinophils	B cells Mast cells	NK cells Eosinophils Macrophages Neutrophils Mast cells	Mast cells Basophils	Eosinophils B cells	Macrophages Eosinophils† Neutrophils	Macrophages B cells
Effect of ligation	Uptake Stimulation Activation of respiratory burst Induction of killing	Uptake Granule release (eosinophils)	Uptake Inhibition of stimulation	No uptake Inhibition of stimulation	Induction of killing (NK cells)	Secretion of granules	Degranulation	Uptake Induction of killing	Uptake

Figure 6. Human FcRs - summary. *The table summarizes in a simplistic way the main features of each FcR, from the structure to the preference for isotype binding, including the cell types that express the receptor and its effects upon activation. (Figure from Janeway's Immunobiology, Murphy and Weaver, 2016[4])*

2.3.6. Antibody functions

The main function of an antibody is to neutralize pathogens or toxins. During infection, the neutralization power of an antibody reflects its ability to prevent or limit infection of susceptible cells and thus prevent or limit disease. Neutralization can be achieved by interfering with at least one of the multiple phases of the pathogen life cycle[124].

Some antibodies can crosslink pathogens and induce their aggregation. Polymeric antibodies like IgA and IgM are more likely to induce aggregation, but the phenomenon has been observed also with IgG antibodies. Aggregated bacteria are more efficiently trapped in the mucous and expelled[125,126], while aggregated viruses are less infective, possibly due to reduced numbers of virus-cell encounters[127].

Other antibodies can immobilize microorganisms, for example by binding to bacterial flagella[128], or induce conformational changes that destabilize the pathogen, making it non-infectious[129,130]. They can even directly inhibit the growth of the pathogen by binding the yeast cell wall[131,132], or affect gene expression and metabolism[133].

One of the most common and efficient neutralization mechanisms is the interference with pathogen attachment to the surface of target cells. This has been observed for many anti-viral antibodies that bind directly to the viral receptor recognition site or in its proximity, preventing the interaction by steric hindrance[134–138]. To achieve full neutralization, antibodies need to bind the virion with a ratio that depends mainly on antibody affinity and epitope

accessibility[139,140]. Bacteria and fungi also need to adhere to the cell surface of their specific target cell and resist hydrodynamic forces. For this reason, antibodies directed against adhesion molecules like adhesins and glucans have been shown to prevent infection[141–143].
In case of enveloped viruses, if the antibody does not prevent the attachment, it can still prevent the fusion between viral and cell membrane. This has been observed, for example, for HIV, West Nile, and influenza viruses[144–146].
If the antibody is internalized by the cell because it is bound to the pathogen or through FcRs, it can also interfere with the life cycle of intracellular pathogens. Some antibodies are thought to block viral genome release from the capsid[146] or its transport to the nucleus[147]. Some of them can even directly induce viral degradation via the proteasome[148].
Finally, antibodies can also inhibit budding of nascent viruses from the cell, inhibiting viral release. This was observed in particular with anti-neuraminidase antibodies in influenza A infection[149].
All the mechanisms of neutralization previously mentioned are directly mediated by the antibody molecule. In addition, antibodies can activate other branches of the effector immune system in order to eliminate the pathogen. One of the most important is the complement cascade, which can be initiated by the interaction of antigen-antibody complexes with the lectin C1q. Complement activation can lead to lysis of the pathogen or infected cell, enhanced phagocytosis mediated by complement receptors, and recruiting of leukocytes to the site of infection[150,151]. In one case, a non-neutralizing antibody against West Nile virus was shown to decrease viral load in mice through the C1q interaction[152].
Another important and indirect mechanism of antibody-mediated protection is the antibody-dependent cellular cytotoxicity (ADCC). ADCC occurs when an immunocomplex interacts with an effector cell expressing the right FcRs. As previously described, this kind of interaction can lead to multiple outcomes, among which the release of granules bearing cytotoxic molecules. This results in killing of the target cell or pathogen by lysis or induction of apoptosis[116,153].
An alternative to ADCC which is initiated in the same way and sometimes involves the same effector cells is phagocytosis. Pathogens that are covered (opsonized) by antibodies are more easily phagocytosed and cleared from the organism. This has been demonstrated for numerous pathogens[124,154,155].

2.3.7. Bispecific antibodies

As inferable from the name, a bispecific antibody is a man-made recombinant protein that can recognize two different epitopes. This useful feature can be exploited in multiple ways, making bispecific antibodies more versatile than their natural counterparts. There are two main categories of bispecific antibodies: IgG-like and non-IgG-like. IgG-like bispecific antibodies possess both Fab and Fc regions. The Fc makes them easier to purify and more stable,

in addition to increasing their half-life and allowing for the activation of FcRs. Non-IgG-like bispecific antibodies, on the other hand, do not include the Fc and are generally easier to produce and less immunogenic[156,157].

Because a bispecific antibody has two different Fabs, and each Fab is made of a heavy and a light chain, the main challenge in the production of bispecific antibodies is guaranteeing that the two heavy and the two light chains are correctly paired. In order to minimize the formation of side products, many strategies have been developed and reviewed elsewhere[158,159].

One possible strategy to make bispecific antibodies relies on the Knobs-into-Holes technology published by Schaefer et al. in 2011. This kind of bispecific antibody has the advantage of being among the most similar to naturally occurring antibodies, preserving the same properties of pharmacokinetics, tissue penetration, stability, and Fc-mediated effector functions. To guarantee the heterodimerization of the two heavy chains, the CH3 domain of one of them was modified with the introduction of a large amino acid side chain ("knob" mutation T366W), while three substitutions on the other heavy chain formed a cavity ("hole" mutations T366S, L368A, Y407V). The structure was further stabilized by the introduction of an additional disulfide bridge (S354C and Y349C on the "knob" and "hole" chains, respectively).

Another crucial step in the production of bispecific antibodies is ensuring the matching of heavy and light chains as it is in the correspondent parental antibodies. To achieve this goal, Schaefer et al. exchanged the CH1 and the CL domains of just one of the two couples of heavy-light chains. Thanks to the intrinsic highly specific heterodimerization properties of heavy and light chains, they were able to guarantee the right pairing of both the Fabs in the bispecific construct[160] (***Figure 7***).

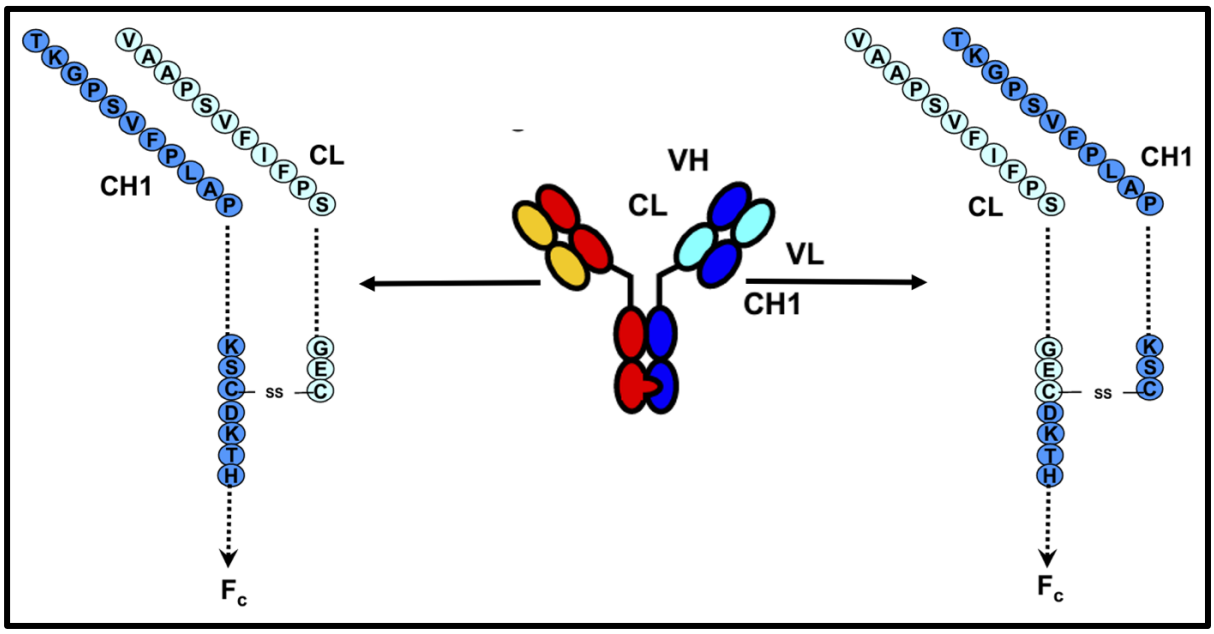

Figure 7. Schematic representation of the bispecific antibody developed by Schaefer et al. *At the center, the Knob-into-Holes modifications of the CH3 domains guarantee the heterodimerization of the heavy chains (red and blue). The CH1 domain of the blue heavy chain has been exchanged with the CL domain of the light-blue light chain to ensure correct Fab pairing. Indicated by arrows are the amino acid sequences of the CH1 and CL domains (wt sequence on the left, exchanged on the right). (Figure adapted from Immunoglobulin Domain Crossover as a Generic Approach for the Production of Bispecific IgG Antibodies, Schaefer et al., 2011*[160]*)*

The large majority of bispecific antibodies were to date developed to treat cancer[161]. A common strategy consists in using them as connectors between tumor cells and immune effector cells by targeting at the same time tumor antigens and immune cells surface molecules (e.g. CD3, CD16). As an alternative, bispecific antibodies targeting multiple immune checkpoints (e.g. PD-1, TIM-3) have been proposed to reactivate anti-cancer immune response[162,163]. Less frequently, bispecific antibodies have been used for high-specificity diagnostic and for treatment of diseases like diabetes and Alzheimer[159]. For the latter, a bispecific antibody targeting β-secretase 1 and transferrin receptor has been designed. The interaction with the transferrin receptor allows the construct to cross the blood-brain barrier, and then it prevents the formation of Amyloid-β plaques by inhibiting β-secretase 1[164].
When it comes to infectious diseases, cocktails of two or more antibodies are safer than single antibody treatment because the combination reduces the chances of the pathogen developing resistance. In this case, one advantage of bispecific antibodies over a cocktail consists in lower manufacturing costs and easier formulation[165]. Furthermore, in earlier work, our collaborators demonstrated that a bispecific antibody designed to bind two different epitopes of SARS-CoV-2 Spike glycoprotein (CoV-X2) had better binding and neutralization properties *in vitro* when compared with the combination of parental antibodies. This is probably due to the enhanced properties of the bispecific over natural antibodies, in particular the ability to bind with both arms simultaneously to the same Spike monomer[166].

2.4. SARS-CoV-2

2.4.1. Coronavirus taxonomy and history

Coronaviruses are enveloped viruses with icosahedral shape and approximately 80-220 nm in diameter. They have a single-strand, positive-sense RNA genome, between 26 and 32 kb[167]. They belong to the order Nidovirales, suborder Cornidovirinae, and family Coronaviridae. Coronaviridae family is further divided into Letovirinae and Orthocoronavirinae subfamilies. Orthocoronavirinae includes four genera: Alphacoronavirus (αCoV), Betacoronavirus (βCoV), Gammacoronavirus (γCoV), and Deltacoronavirus (δCoV). Coronaviruses have been found in many different animal species. αCoV and βCoV seem to infect mammals, while γCoV and δCoV infect mainly birds[168].

The first case of human infection from coronavirus was reported in 1960 by the virus B814[169]. Since then, seven different species of coronavirus have been found to infect and cause disease in humans. Two of them, 229E and NL63 are αCoVs, while HKU1, OC43, SARS-CoV, MERS-CoV, and SARS-CoV-2 are βCoVs. 229E, NL63, HKU1, and OC43 cause only mild symptoms and are therefore known as common-cold coronaviruses[167].

Severe Acute Respiratory Syndrome Coronavirus (SARS-CoV) started spreading in China in 2002. Unlike the previously known human coronaviruses, SARS-CoV was immediately recognized as dangerous pathogen with a fatality rate of around 9.6%. This allowed the fast implementation of strict quarantine protocols and eradication of the virus[170,171].

Ten years later, in 2012, another highly pathogenic coronavirus emerged and spread mainly in Saudi Arabia. This new virus was called Middle East Respiratory Syndrome Coronavirus (MERS-CoV) and possessed a fatality rate of around 36%[172,173].

The last coronavirus spillover happened in December 2019 in the city of Wuhan, in China. Several pneumonia cases were reported among people related to the Huanan Seafood Wholesale Market, and the causative agent was identified as the Severe Acute Respiratory Syndrome Coronavirus 2 (SARS-CoV-2). The disease caused by SARS-CoV-2 was named Coronavirus Disease-2019 (COVID-19) and was characterized by fever, dry cough, dyspnea, and diarrhea in mild patients, while the severe cases could present pneumonia, metabolic acidosis, septic shock, and bleeding[174,175]. SARS-CoV-2 worldwide spread was promoted by transmission through asymptomatic carriers, leading the World Health Organization (WHO) to declare the status of pandemic on March 11th, 2020[176,177]. Most of the world nations implemented control measures like travel restrictions, screenings, forced quarantine for infected people, social distancing, face mask wearing, and promotion of personal hygiene[178]. The WHO ended the status of emergency on

May 5th, 2023[177]. Up to December 2023, the number of deaths caused by SARS-CoV-2 infection was estimated at almost 7 million[179].
Bats have been identified as the main reservoir of human coronaviruses. It is commonly accepted that bat coronaviruses can be transmitted to humans through intermediate hosts. In particular, SARS-CoV was apparently transmitted to humans by palm civets, while MERS-CoV came from dromedary camels[180]. The precise origin of SARS-CoV-2 has not been elucidated yet, but its closest relative has been identified as the coronavirus RaTG13 of the horseshoe bat *Rhinolophus affinis*, in the province of Yunnan, China (96.2% genome sequence identity). *Malayan pangolin* has also been proposed as an intermediate host because of the detection of a closely related pangolin coronavirus in the Chinese provinces of Guangxi (PCoVGX, 85.5% identity) and Guangdong (PCoVGD, 92.4% identity)[181].

2.4.2. SARS-CoV-2 proteins

SARS-CoV-2 is a single stranded RNA virus with a genome of around 30'000 nucleotides. The genome contains two untranslated regions (UTRs), one at each end, and 14 open reading frames (ORFs) encoding for 4 structural proteins, 16 non-structural proteins (nsp), and 9 accessory proteins[182]. Most of the functional information on SARS-CoV-2 proteins have come from studies on previously known coronaviruses.
Structural proteins are responsible for the assembly of the viral particle. They are:

- Nucleocapsid protein (N) ➔ it directly binds the viral RNA and protects it by packaging it. N protein also keeps the RNA in an optimal conformation for transcription and replication. Furthermore, it can also regulate host cell pathways like apoptosis and cell cycle progression[183].
- Envelope protein (E) ➔ it is a short polypeptide that forms poorly selective homopentameric ion channels[184]. It localizes mainly at the ER-Golgi body intermediate compartment (ERGIC), while only small amount of E protein has been found in the final viral particles[185]. Interaction of the E and M proteins seems to be important for viral assembly into the ERGIC[186]. E protein is also involved in pathogenesis, probably due to its interaction with several host proteins[187–189].
- Membrane glycoprotein (M) ➔ by interacting with the other structural proteins, the M glycoprotein orchestrate viral particle assembly in the ERGIC and mediates nucleocapsid attachment to the membrane necessary for budding[190].
- Spike glycoprotein (S) ➔ it mediates recognition and attachment to the viral receptor on the surface of host cells and the subsequent viral entry[191] (details in the *SARS-CoV-2 Spike glycoprotein and cell entry mechanism* section).

Non-structural proteins are involved in viral RNA transcription and replication, but they can also interfere with cellular pathways to promote virus survival[182]. For example, nsp1 inhibits cellular mRNA translation[192], while nsp6 alters intracellular membrane trafficking and autophagosome formation[192]. nsp15 can degrade viral RNA to prevent the activation of the antiviral immune response[193].
nsp7, nsp8, nsp12, and nsp13 form the polymerase complex that allows viral genome replication. nsp7 stabilizes nsp8, which synthetizes the RNA primers necessary for the viral polymerase nsp12 to start the synthesis of the new RNA filament[194]. nsp13 is a helicase able to unwind nucleic acid secondary structures, and it also possesses mRNA capping activity[195,196].
Another important complex is made by nsp10, nsp14, and nsp16. nsp10 interacts with the other two components of the complex and enhances their enzymatic activities[197]. nsp16 is a 2'-O-methyltransferase which methylates viral RNA cap, mimicking cellular mRNA cap structure[198]. nsp14 has 3'-5' exoribonuclease activity and is responsible for the decreased incidence of mutations during coronavirus RNA replication compared with other RNA viruses. The limited proofreading activity of nsp14 is believed to allow the large genome size of coronaviruses[199,200].
The SARS-CoV-2 genome also encodes for 9 accessory proteins named ORF3a, 3b, 6, 7a, 7b, 8, 9b, 9c, and 10. Accessory proteins are usually smaller than nsp and they have no homologs in other viral groups[201]. Except for ORF9c and ORF10, whose production during SARS-CoV-2 infection is still uncertain, all the other accessory proteins contribute to changing the cellular environment to make it favorable for viral replication or promote viral escape[182]. ORF6 and ORF7a, for instance, seem to inhibit cellular translation[202,203], while ORF8 and ORF9b interfere with the immune response[204,205]. ORF3a forms ion channels that contribute to the release of viral particles from the infected cell. It can also interact with the viral structural proteins and be incorporated in the final virion, but its presence is not essential[206].

2.4.3. SARS-CoV-2 Spike glycoprotein and cell entry mechanism

The name "coronavirus" derives from the first electron microscopy image of a common cold coronavirus, obtained in 1967. In this image, the viral particles were surrounded by projections of around 200 Å, that together formed a crown-like structure ("*corona*", in Latin). We now know that the projections observed in electron microscopy were the coronavirus S glycoproteins[207].
As previously mentioned, the S glycoprotein is a structural protein fundamental for coronavirus infection because it mediates receptor binding and fusion of the viral envelope with the cellular membrane[191]. It is a transmembrane homotrimer present on the surface of the coronavirus

envelope. In SARS-CoV-2, each S protomer has a total length of around 1'273 amino acids, with small differences among SARS-CoV-2 variants[208].
During viral assembly, each S protomer undergoes proteolytic cleavage between amino acids R685 and S686[209]. This cleavage is operated mainly by the ubiquitously expressed protein convertase furin, but other convertases can compensate its action[210]. The cleavage divides the S protein in two subunits: the N-terminal S1 subunit, which is responsible for binding to the receptor, and the C-terminal S2 subunit, responsible for the fusion.
The S1 subunit presents four domains called N-terminal domain (NTD), receptor-binding domain (RBD) and subdomains 1 and 2 (SD1, SD2), also known as C-terminal domains 1 and 2 (CTD1, CTD2) (***Figure 8***). The SD1 connects both the N- and C-terminus of the RBD to the SD2[181,211], and its interaction with the adjacent NTD is fundamental for stabilization of the S1 subunit[212,213].

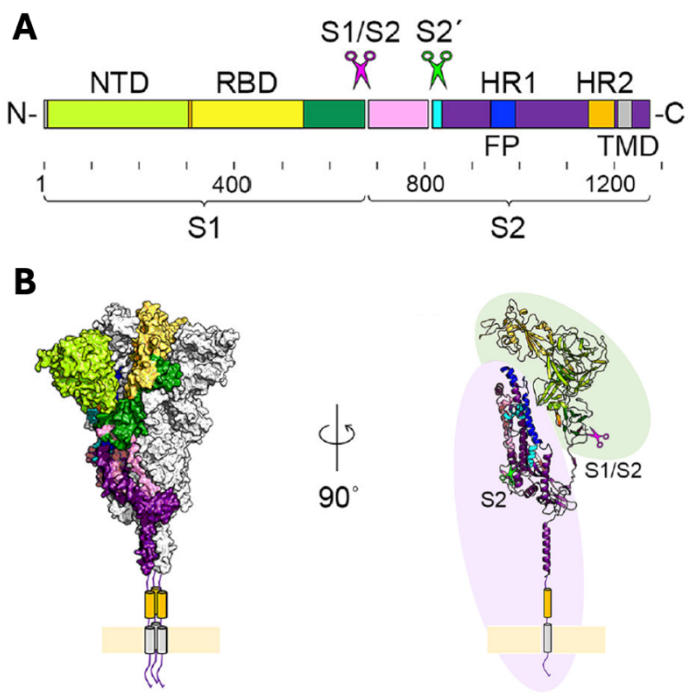

Figure 8. Structure of SARS-CoV-2 S glycoprotein. ***(A)*** *Representation of the S primary structure with annotations corresponding to the main functional domains and to the furin cleavage site (S1/S2) and TMPRSS2 cleavage site (S2').* ***(B)*** *Full atomic structure of the S trimer (left) and single protomer (right). The domains have the same colors as in (A). On the right, the cleavage sites are annotated and the S1 and S2 subunits are colored with green or violet background, respectively. (Figure adapted from Proteolytic Activation of SARS-CoV-2 Spike Protein, Takeda, M., 2022[208])*

The three RBD domains of the S protein form the apical part of the trimer and can change position from a closed (down) conformation to an open (up) conformation, which exposes the receptor binding motif (RBM). Only when the RBD is in the "up" conformation it can bind the receptor, which is the angiotensin converting enzyme 2 (ACE2) in the case of SARS-CoV-2[214,214]. It is believed that the S1/S2 cleavage can destabilize the S trimer and promote ACE2 binding facilitating the transition to the "up" conformation[215]. The mutation D614G, which emerged early in the pandemic and is conserved among SARS-CoV-2 variants, can also increase infectivity and proliferation of the virus by disrupting an inter-protomer interaction and promoting the "up"

conformation[216]. Because of its location in proximity to the S1/S2 cleavage site, D614G mutation can also increase furin cleavage efficiency[217].
After ACE2 binding, the S protein undergoes irreversible conformational changes that lead to the fusion of the viral envelope with the cellular membrane. However, this extensive remodeling requires a second proteolytic cleavage on top of the one already present at the S1/S2 site. The second cleavage takes place in the S2 subunit at the S2' site, between amino acids R815 and S816, but it first requires ACE2 binding[208]. Only after interaction with its receptor the S trimer exposes the S2' site, which becomes accessible to the transmembrane protease serine 2 (TMPRSS2)[215]. TMPRSS2 is expressed mainly in the prostate and by epithelial cells, including the ones of the airway epithelium. Thus, for cells expressing TMPRSS2, SARS-CoV-2 infection can happen already at the plasma membrane, through the so-called "early pathway". However, cells that express ACE2 but not TMPRSS2 can also be infected. In this case, SARS-CoV-2 does not fuse directly at the plasma membrane but enters the cell by endocytosis. Once in the endosome, the S2' site is cleaved by the lysosomal cathepsin L, triggering envelope fusion with the endosomal membrane. This second route, known as "late pathway", is less efficient than the early pathway, though[208].
When the S protein is in the prefusion conformation, the S2 subunit is packed around the three coiled-coil central helices and partially wrapped on top by the S1 subunit[209]. The proteolytic cleavage of the S2' site further destabilizes the S1-S2 interaction, causing the release of the S1 subunit from the S trimer. This dissociation triggers further conformational changes in the S2 subunit that involve two helices named heptad repeat 1 (HR1) and 2 (HR2). HR1 undergoes dramatic refolding, driving the insertion of the hydrophobic fusion peptide (FP) into the cell membrane. HR2 then interacts with HR1 and forces the transmembrane domain of the S protein to get close to the FP. These movements bring the envelope and the cell membranes near to each other, overcoming the repulsive forces and causing their fusion with release of the viral genome into the cell[211,218] (***Figure 9***).

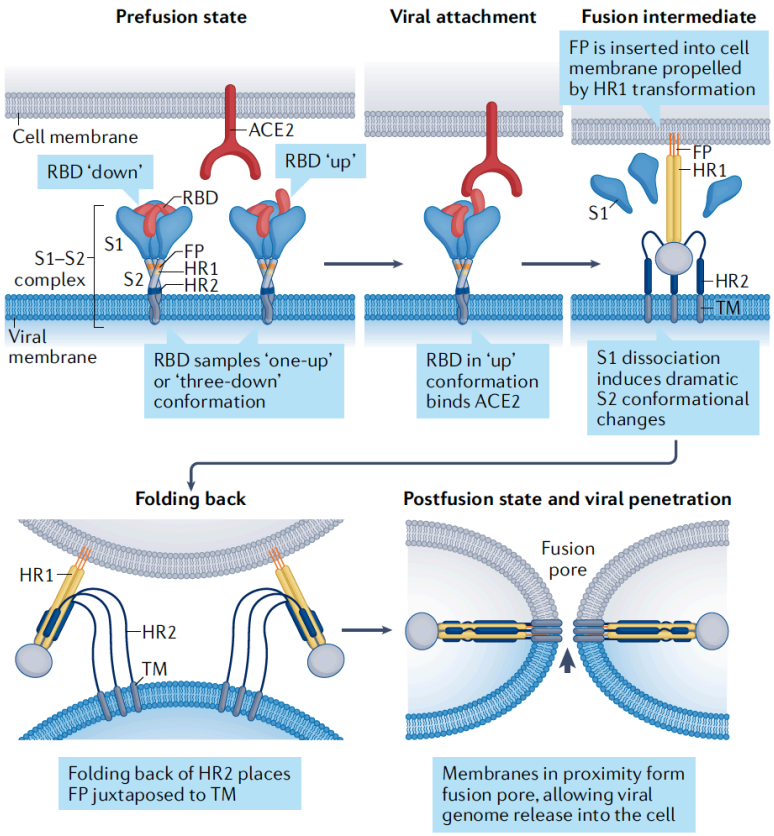

Figure 9. Model of S-mediated membrane fusion. *The mechanism of SARS-CoV-2 entry into the cell is described step by step. Once bound to the ACE2 receptor, the S trimer is cleaved in the S2' site. This causes destabilization and shedding of the S1 subunit, followed by major conformational changes of the S2 subunit. The fusion peptide inserts into the cell membrane and the HR1-HR2 interaction brings it near the viral envelope, inducing fusion. (Figure from Mechanisms of SARS-CoV-2 Entry into Cells, Jackson et al.,2022[211])*

2.4.4. SARS-CoV-2 genome replication

Once the virion fuses with the host cell, the viral genomic RNA (gRNA) is released into the cytoplasm, where the viral replication takes place. The gRNA is 5'-capped and 3'-polyadenilated and can be directly translated by cellular ribosomes into two polyproteins[219]. The production of one or the other polyprotein is determined by a programmed ribosomal frameshift. This mechanism is promoted by gRNA secondary structures and by the interaction of the nascent protein with the ribosome itself[220]. The two polyproteins are then cleaved into the previously mentioned 16 nsp by nsp3 and nsp5.

The newly produced nsp7, nsp8, and nsp12 form the complex of RNA-dependent RNA polymerase which is responsible for the synthesis of a full-length anti-genome (–gRNA) and a set of anti-sense subgenomic RNAs (sgRNAs). While the –gRNA is used as a template for the synthesis of new gRNA, the sgRNAs are transcribed into sg-mRNAs encoding the 4 structural proteins (N, E, M, S) and the 9 accessory proteins of SARS-CoV-2[221].

sgRNAs are synthesized through template switching from the gRNA region downstream the two ORFs encoding nsp. Each ORF encoding structural or accessory proteins presents a 5' transcription regulatory sequence (TRS), which causes the stall of the polymerase complex. This event can result in the dissociation of the complex and its translocation to the TRS adjacent to the 5' leader sequence of the gRNA, where the synthesis resumes. The translocation

is guided by TRS complementarity and likely facilitated by gRNA cyclization. As result of this process, all the sg-mRNAs and the gRNA share the same 3' terminal sequence and 5' leader sequence. Although most of the sg-mRNAs are polycistronic, it is believed that only the ORF immediately downstream the leader sequence is actively translated[219,222–224].

2.4.5. SARS-CoV-2 evolution and variants

As observed for other RNA viruses, SARS-CoV-2 also evolved rapidly, resulting in the emergence of numerous variants of interest and variants of concern (VOCs) since the beginning of the COVID-19 pandemic[225].

The main determinant of viral evolution is the fidelity of the viral polymerase. RNA viruses are known for their high mutation rate, ranging between ~10^{-4} and 10^{-6} mutations per nucleotide per replication cycle[226,227]. Despite the peculiar coronavirus proofreading system based on the exonuclease activity of nsp14[199], the SARS-CoV-2 mutation rate is estimated between 1×10^{-6} and 2×10^{-6} mutations per nucleotide per replication cycle, likely enough to guarantee fast SARS-CoV-2 evolution[228]. Mutations in the SARS-CoV-2 genome can also be a consequence of the activity of cellular antiviral proteins, like APOBEC family members[229] or adenosine deaminases ADAR1[230].

Another mechanism that plays an important role in βCoV evolution is recombination. Recombination happens when two virions with different genetic backgrounds infect the same cell, exchanging genome portions and generating viable progeny. This event is promoted by the discontinuous nature of coronavirus transcription based on template switching[231].

The aim of evolution is to increase the fitness of the virus. However, when we consider obligate parasites causing acute infection with a short window of infectivity, transmissibility becomes the leading fitness determinant[232,233]. SARS-CoV-2 binding and entry into the host cell are both mediated by the S glycoprotein. Therefore, it is not surprising that many of the mutations increasing SARS-CoV-2 transmissibility were found in S. These mutations usually improve S binding to ACE2 (e.g., D614G[234], N501Y[235]) or promote full S cleavage by furin, facilitating the membrane fusion process (e.g., P681H, P681R)[236].

Evolution can also enhance transmissibility through change of virus tissue tropism. This was observed for SARS-CoV-2 with the emerging of Omicron BA.1 variant. While ancestral SARS-CoV-2 mainly infected bronchial and lung cells, Omicron BA.1 had a preference for nasopharyngeal tissue, promoting transmission through aerosol[237].

During the first phase of the COVID-19 pandemic, when SARS-CoV-2 started spreading in the naïve population, improvement of transmissibility was likely the main goal of viral evolution. However, with the increase of population immunity due to natural infection and vaccination, overcoming host resistance became another important factor influencing SARS-CoV-2

evolution. Many mutations have been reported for SARS-CoV-2 causing antigenic evolution and immune escape, that means the loss or reduction of pathogen recognition by the humoral and cellular immunity[233]. Some of these mutations were discovered already in the S glycoprotein of early variants like Beta and Gamma (e.g., E484K)[238], but their numbers increased a lot during the late stages of the pandemic with the Omicron variant[239]. Most of the S mutations were observed in the RBD and NTD domains, which are the main targets of neutralizing antibodies[238]. In agreement with the predictions, Omicron variants showed much higher reinfection ability than previous VOCs[240].

Let's now look more in detail to the history and classification of SARS-CoV-2 VOCs. The very first VOC was identified by the WHO in United Kingdom in December 2020 and was named Alpha (lineage B.1.1.7)[241,242]. A few weeks later, another two variants were reported in South Africa, the Beta variant (lineage B.1.351)[243], and Brazil, the Gamma variant (lineage P.1)[244]. These three VOCs, although presenting enhanced transmissibility and immune escape compared with the ancestral strain, were next all replaced by the Delta variant (lineage B.1.617.2), that originated from India and recognized as VOC in May 2021[245,246]. Finally, in October 2021, the new Omicron variant emerged, bearing a much higher number of mutations compared with the previous VOCs. The first three sublineages of Omicron (BA.1, BA.2, and BA.3) emerged independently in different parts of the world, likely through convergent evolution and recombination[239,247]. Further inter-lineage recombination events likely led to the emergence of lineages BA.4, in December 2021, and BA.5, in January 2022[248]. The rise of Omicron variants led the pandemic in a new phase, which was characterized by the periodic emergence of closely related Omicron sublineages (e.g., BA.2, BA.2.75, BA.2.75.2) sharing multiple mutations in the S glycoprotein. This phase was different from the previous one, characterized by highly divergent variants[233,249].

Despite the unparalleled amount of data generated during SARS-CoV-2 pandemic[250], we still lack a clear model to explain the evolutionary origin of the VOCs. Three main hypotheses have been formulated to justify the sudden appearance of variants with high divergence from the previous ones:

- New variants could develop in countries with insufficient SARS-CoV-2 genomic surveillance, being detected only at later stage of their evolution and spreading[251,252].
- SARS-CoV-2 could infect and circulate in wild animal populations, acquiring new mutations before coming back to humans through a new spillover. Only Syrian hamsters, minks, and white-tailed deer have shown to transmit SARS-CoV-2[253–255]. However, the mutations acquired by SARS-

CoV-2 in these animals seem to support host-specific adaptation, more than an actual origin of VOCs in animal reservoirs[233].

- Immunocompromised individuals could fail in clearing SARS-CoV-2 infection and become long-term reservoirs for the virus[256]. In these people, evolutionary pressure could be determined by treatments or by the weak immune response. Virions sampled in chronically infected individuals indeed shared some mutations with known VOCs[257,258].

It is not easy to predict which will be the next steps in SARS-CoV-2 evolution. The most probable scenario is that the virus will reach endemic persistence with seasonal fluctuation in the number of cases. New Omicron variants could rise periodically, but severe disease would be limited by pre-existing immunity and updated vaccines.
However, we cannot exclude the emergence of a completely new variant that would evade immunity and show unpredictable features of transmissibility and virulence[233]. It is worth highlighting that the virulence, i.e. pathogenicity, of SARS-CoV-2 did not follow a linear trend during its evolution. Alpha, Beta, Gamma, and Delta variants were all more virulent than the ancestral lineage[259]. On the other hand, Omicron variants were characterized by lower virulence[260]. Despite the common belief that pathogens evolve to become less virulent and avoid host death, this is an oversimplification. In the case of SARS-CoV-2, severe disease usually manifests around the third week post-infection, while the infectious period spans between 2 and 15 days post-infection[261]. Disease severity thus has no or little influence over SARS-CoV-2 transmissibility. Furthermore, for some pathogens, virulence is just a by-product of other evolutionary acquired traits that improve viral fitness. An example is SARS-CoV-2 viral load, the increase of which can lead to enhanced transmission but also to more severe disease[233].

2.4.6. SARS-CoV-2 neutralizing antibodies

Despite the central role of vaccines in resolving the COVID-19 pandemic, some individuals may fail in developing an immune response upon SARS-CoV-2 vaccination (e.g., immunocompromised people or the elderly). Furthermore, vaccines are effective only if administered before infection, and an increasing fraction of the population is vaccine hesitant. For these reasons, since the beginning of the pandemic, several monoclonal antibodies (mAbs) have been and are currently being developed and approved for clinical use for both prevention and treatment of SARS-CoV-2 infection[262].
The main target used for antibody discovery is the S glycoprotein of SARS-CoV-2. This choice was driven by the important role that the S glycoprotein has in viral infection, mediating attachment to the target cell and viral entry[263].

RBD

Most of the mAbs approved for the clinic target the RBD[262]. This is partially due to early studies on SARS-CoV-2 convalescent sera showing that around 90% of serum neutralizing activity was due to RBD-specific antibodies[264].

Based on structural data and V(D)J sequence similarity, RBD antibodies have been divided into 4 main classes:

- Class I mAbs can bind only to the RBD in the "up" conformation and they block ACE2 binding by direct recognition of the RBM. Many of them are encoded by the VH3-53 or VH3-66 germ lines. Most of the class I mAbs lost their binding to SARS-CoV-2 VOCs due to RBD mutations like K417N, E484K and N501Y.
- Class II mAbs can bind the RBD in both "up" and "down" conformation. They can bind the RBM too and block ACE2, but they can also lock the RBDs in the "down" conformation, preventing RBM exposure. Most of them can bind adjacent RBDs using both arms at the same time. Class II mAbs can lose binding on the E484K and Q493R mutants, present in many VOCs.
- Class III mAbs can bind the RBD in both "up" and "down" conformation. They bind outside the RBM, but some of them can still prevent ACE2 recognition by steric hindrance. Most of these antibodies have shown to preserve at least partial activity on many VOCs.
- Class IV mAbs can bind only to the RBD in the "up" conformation and they do not prevent ACE2 binding. They recognize a highly conserved and probably cryptic epitope, preserving their neutralizing activity on multiple VOCs[263,265,266].

Unfortunately, the RBD is highly mutated in Omicron sublineages, which are characterized by both increased transmissibility and immune escape[267]. Even the most promising therapeutic RBD-antibodies showed a partial or complete loss of activity on the most recent Omicron sublineages. One of the best crossreactive RBD antibodies is Sotrovimab, derived from antibody S309 discovered in a SARS-CoV survivor[268]. Sotrovimab is a class III antibody which retains neutralizing activity on some of the most recent Omicron BA.2- and BA.5-derived variants (i.e. BA.2.75.2, BQ.1, BQ.1.1, XBB). However, its potency decreases when compared with the one on Delta variant (IC_{50} 98.6 ng/mL), reaching IC_{50} values between 422.3 and 1'238.0 ng/mL. Even worse are the antibodies developed by AstraZeneca and combined into the Evusheld cocktail: Cilgavimab (class III) and Tixagevimab (class I). Despite better neutralization on the Delta variant (IC_{50} 21.7 and 12.4 ng/mL, respectively), both of them completely lose their activity on the latest BA.2.75.2, BQ.1, BQ.1.1, and XBB variants. Very similar results to the Evusheld cocktail are observed for the Roche Regeneron cocktail made by Casirivimab (class I) and Imdevimab (class III), which is effective on Omicron BA.2 and BA.5 but not on the derived variants. Even the most recently discovered antibody

Bebtelovimab (class III), from Eli Lilly, completely loses its neutralizing activity on the BQ.1, BQ.1.1, and XBB variants, despite remaining a potent neutralizer of Omicron BA.2.75.2 (IC_{50} 0.6 ng/mL)[269].

NTD

Outside the RBD, the NTD of the S glycoprotein is another target of potent neutralizing antibodies. These mAbs seem to block the S conformational changes, preventing the pre- to post-fusion transition[270]. Unfortunately, most of the discovered NTD-specific mAbs bind a positively charged epitope named "NTD supersite", which is highly mutated in SARS-CoV-2 VOCs. mAbs that target the NTD outside the NTD supersite can have broad neutralizing potential[265,271].

SD1

The SD1 is also target of neutralizing antibodies, although generally less potent than the ones targeting the RBD and the NTD. Our group was the first to focus antibody discovery on this domain, guided by its high level of amino acid conservation among SARS-CoV-2 variants (see section: *Published data*, **Fig 1A**)[272]. Before the publication of my thesis project, only one human mAb targeting SD1 was reported, named P008_60, but it was a weak neutralizer of both pseudovirus and authentic virus VOCs (IC_{50} > 1'000 and 10'000 ng/mL, respectively)[273]. The potent SD1 neutralizing mAb S3H3 (IC_{50} around 10-100 ng/mL) was derived from a S-immunized mouse, but it completely lost its ability to neutralize the Omicron variant BA.2.86[274,275]. A single-chain variable fragment (scFv) binding SD1, N-612-004, was discovered using the mRNA display approach, but it showed to plateau at 40% of viral neutralization[276]. After our publication, few other SD1 mAbs have been published and characterized for neutralization on pseudovirus or authentic virus VOCs: C68.59 (IC_{50} between 6 and 577 ng/mL)[277], ADARC1, ADARC2 (IC_{50} between 53 and 162 ng/mL)[275], 12-16, 12-19 (IC_{50} between 19 and 99 ng/mL)[278], SD1-1, SD1-2, SD1-3 (IC_{50} < 100 ng/mL)[279] and MO11 (IC_{50} between 103 and 883 ng/mL)[280]. Most of these antibodies show high variability in their neutralization potency across different VOCs and also between pseudovirus and real virus. Furthermore, none of them can neutralize the Omicron variant BA.2.86 (with the exception of MO11, 12-16, and 12-19, which were not tested)[275,278,279]. The mechanism of neutralization by SD1-targeting antibodies is still not entirely clear. Both stabilization and destabilization of the S trimer have been proposed. mAbs SD1-1, SD1-2, and SD1-3 seem to neutralize by blocking ACE2 binding, but it has been hypothesized that they could also prevent oligomerization of S proteins by steric hindrance, inhibiting viral entry into the cell[279]. mAbs 12-16 and 12-19 also prevent ACE2 binding by locking the RBD in the "down" conformation. However, 12-16 and 12-19 bind a quaternary epitope made by both SD1 and

NTD and are likely different from the other SD1 antibodies in their mechanism of action[278]. One of the most interesting features of the SD1 mAbs is their broad cross-reactivity to SARS-CoV-2 variants. The high conservation of SD1, with only one mutation in the Alpha (A570D) and Omicron BA.1 (T547K) variants and two mutations in the Omicron BA.2.86 (E554K and A570V) variant, makes it a promising target for discovery of antibodies resistant to viral escape[272,275].

S2 subunit

Despite most of the mAbs developed against SARS-CoV-2 target the S1 subunit of the S, the S2 subunit is much more conserved among coronavirus variants and even across different coronaviruses[281]. Antibodies targeting the S2 region are more resistant to viral escape, but they are generally less potent than antibodies targeting the S1 region[263,265]. Some of these antibodies can bind the helices of the S fusion machinery, blocking the fusion process. This is the case for S2P6 and WS6, both able to neutralize multiple coronaviruses, but with a minimum IC50 against SARS-CoV-2 of 1'400 and 2'460 ng/mL, respectively[282,283].

Fusion peptide

A different class of S2-antibodies targets the fusion peptide (FP). Antibodies belonging to this class are also able to neutralize multiple coronaviruses, and they usually act by preventing S2' cleavage and the following conformational changes of the S[284]. In some cases, e.g. mAbs C77G12 and 76E1, FP-antibodies can increase their binding and neutralization when combined with class I antibodies mimicking ACE2 binding. This is due to conformational changes that lead to better exposure of the FP upon ACE2 binding to the S trimer[285,286].

3. AIMS OF THE THESIS

The overall aim of the thesis was to discover and characterize human antibodies to a conserved region of the SARS-CoV-2 Spike glycoprotein called subdomain 1 (SD1). The sub-aims included (1) devise a strategy to purify SD1-specific human memory B cells, (2) characterize the biochemical and functional features (e.g., binding, affinity, neutralization) of the antibodies that they express, (3) evaluate the efficacy of select SD1 antibodies against variants of concern and in preclinical models, (4) define the mechanism of neutralization by SD1 antibodies, (5) evaluate the effect of combining SD1 antibodies in bispecific formats. Sub-aims 3 and 4 were achieved thanks to collaboration with Dr. Daniel Ruzek for animal studies (Czech Academy of Sciences) and Dr. Christopher Barnes (Stanford University) for structural studies.

4. PUBLISHED MANUSCRIPT

Part of the experimental work included in this thesis was already published. The publication is reported below.

HUMAN NEUTRALIZING ANTIBODIES TO COLD LINEAR EPITOPES AND SUBDOMAIN 1 OF THE SARS-COV-2 SPIKE GLYCOPROTEIN

Filippo Bianchini[1]†, Virginia Crivelli[1]†, Morgan E. Abernathy[2]†, Concetta Guerra[1]†, Martin Palus[3,4]†, Jonathan Muri[1], Harold Marcotte[5], Antonio Piralla[6], Mattia Pedotti[1], Raoul De Gasparo[1], Luca Simonelli[1], Milos Matkovic[1], Chiara Toscano[1], Maira Biggiogero[7], Veronica Calvaruso[7], Pavel Svoboda[3,4,8,9], Tomás Cervantes Rincón[1], Tommaso Fava[1], Lucie Podešvová[1], Akanksha A. Shanbhag[1], Andrea Celoria[1], Jacopo Sgrignani[1], Michal Stefanik[4,10], Vaclav Hönig[3,4], Veronika Pranclova[3,11], Tereza Michalcikova[12], Jan Prochazka[12], Giuditta Guerrini[13], Dora Mehn[13], Annalisa Ciabattini[14], Hassan Abolhassani[5,15], David Jarrossay[1], Mariagrazia Uguccioni[1], Donata Medaglini[14], Qiang Pan-Hammarström[5], Luigi Calzolai[13], Daniel Fernandez[16], Fausto Baldanti[17,6], Alessandra Franzetti-Pellanda[7], Christian Garzoni[18], Radislav Sedlacek[12], Daniel Ruzek[3,4,8]*, Luca Varani[1]*, Andrea Cavalli[1,19]*, Christopher O. Barnes[2,20]*, Davide F. Robbiani[1]*

[1]Institute for Research in Biomedicine, Università della Svizzera italiana, Bellinzona, Switzerland. [2]Department of Biology, Stanford University, Stanford, CA, USA. [3]Institute of Parasitology, Biology Centre of the Czech Academy of Sciences, Ceske Budejovice, Czech Republic. [4]Veterinary Research Institute, Brno, Czech Republic. [5]Department of Biosciences and Nutrition, Karolinska Institutet, Huddinge, Sweden. [6]Microbiology and Virology Department, Fondazione IRCCS Policlinico San Matteo, Pavia, Italy. [7]Clinical Research Unit, Clinica Luganese Moncucco, Lugano, Switzerland. [8]Department of Experimental Biology, Faculty of Science, Masaryk University, Brno, Czech Republic. [9]Department of Pharmacology and Pharmacy, Faculty of Veterinary Medicine, University of Veterinary Sciences, Brno, Czech Republic. [10]Department of Chemistry and Biochemistry, Mendel University in Brno, Brno, Czech Republic. [11]Faculty of Science, University of South Bohemia, Ceske Budejovice, Czech Republic. [12]Czech Centre of Phenogenomics, Institute of Molecular Genetics of the Czech Academy of Sciences, Vestec, Czech Republic. [13]European Commission, Joint Research Centre (JRC), Ispra Italy. [14]Laboratory of Molecular Microbiology and Biotechnology, Department of Medical Biotechnologies, University of Siena, Siena, Italy. [15]Research Center for Immunodeficiencies, Pediatrics Center of Excellence, Children's Medical Center, Tehran University of Medical Sciences, Tehran, Iran. [16]Sarafan ChEM-H Macromolecular Structure Knowledge Center, Stanford University, Stanford, CA, USA. [17]Department of Clinical, Surgical, Diagnostic and Pediatric Sciences, University of Pavia, Pavia, Italy. [18]Internal Medicine and Infectious Diseases, Clinica Luganese Moncucco, Lugano, Switzerland. [19]Swiss Institute of Bioinformatics, Lausanne, Switzerland. [20]Chan Zuckerberg Biohub, San Francisco, CA, USA.
†These authors contributed equally to this work.
*Corresponding author.

Personal contribution:

- Study conception, experimental design and analysis,
- Design, generation, purification and characterization of reagents (i.e., monoclonal antibodies, RBD and SD1-RBD expression plasmids and proteins, Fab proteins),
- Execution of the experiments (i.e., buffy coat processing; B cell sorting, antibody PCRs, cloning, expression and purification; ELISA on plasma and mAbs; ACE2-competition ELISA; flow cytometry for antibody binding to cell surface expressed S), in particular Fig. 1D, 3B, 3C, 3D, 3E, 3F, 4A, 4F, S1D, S6A, S6B, S6C, S6D, S6E, S6F, S6G,
- Manuscript writing with input from all coauthors.

Status: published in Science Immunology (10.1126/sciimmunol.ade0958), March 2023.

CORONAVIRUS

Human neutralizing antibodies to cold linear epitopes and subdomain 1 of the SARS-CoV-2 spike glycoprotein

Filippo Bianchini[1]†, Virginia Crivelli[1]†, Morgan E. Abernathy[2]†, Concetta Guerra[1]†, Martin Palus[3,4]†, Jonathan Muri[1], Harold Marcotte[5], Antonio Piralla[6], Mattia Pedotti[1], Raoul De Gasparo[1], Luca Simonelli[1], Milos Matkovic[1], Chiara Toscano[1], Maira Biggiogero[7], Veronica Calvaruso[7], Pavel Svoboda[3,4,8,9], Tomás Cervantes Rincón[1], Tommaso Fava[1], Lucie Podešvová[1], Akanksha A. Shanbhag[1], Andrea Celoria[1], Jacopo Sgrignani[1], Michal Stefanik[4,10], Vaclav Hönig[3,4], Veronika Pranclova[3,11], Tereza Michalcikova[12], Jan Prochazka[12], Giuditta Guerrini[13], Dora Mehn[13], Annalisa Ciabattini[14], Hassan Abolhassani[5,15], David Jarrossay[1], Mariagrazia Uguccioni[1], Donata Medaglini[14], Qiang Pan-Hammarström[5], Luigi Calzolai[13], Daniel Fernandez[16], Fausto Baldanti[17,6], Alessandra Franzetti-Pellanda[7], Christian Garzoni[18], Radislav Sedlacek[12], Daniel Ruzek[3,4,8]*, Luca Varani[1]*, Andrea Cavalli[1,19]*, Christopher O. Barnes[2,20]*, Davide F. Robbiani[1]*

Copyright © 2023 The Authors, some rights reserved; exclusive licensee American Association for the Advancement of Science. No claim to original U.S. Government Works. Distributed under a Creative Commons Attribution License 4.0 (CC BY).

Emergence of severe acute respiratory syndrome coronavirus 2 (SARS-CoV-2) variants diminishes the efficacy of vaccines and antiviral monoclonal antibodies. Continued development of immunotherapies and vaccine immunogens resilient to viral evolution is therefore necessary. Using coldspot-guided antibody discovery, a screening approach that focuses on portions of the virus spike glycoprotein that are both functionally relevant and averse to change, we identified human neutralizing antibodies to highly conserved viral epitopes. Antibody fp.006 binds the fusion peptide and cross-reacts against coronaviruses of the four genera, including the nine human coronaviruses, through recognition of a conserved motif that includes the S2′ site of proteolytic cleavage. Antibody hr2.016 targets the stem helix and neutralizes SARS-CoV-2 variants. Antibody sd1.040 binds to subdomain 1, synergizes with antibody rbd.042 for neutralization, and, similar to fp.006 and hr2.016, protects mice expressing human angiotensin-converting enzyme 2 against infection when present as a bispecific antibody. Thus, coldspot-guided antibody discovery reveals donor-derived neutralizing antibodies that are cross-reactive with Orthocoronavirinae, including SARS-CoV-2 variants.

Downloaded from https://www.science.org on May 03, 2024

INTRODUCTION

The coronavirus (CoV) spike protein (S) is a trimeric glycoprotein of S1-S2 heterodimers that mediates binding to target cells and membrane fusion (*1*–*3*). Most severe acute respiratory syndrome CoV 2 (SARS-CoV-2) neutralizing antibodies that have been described to date target the receptor binding and N-terminal domains of S (RBD and NTD) (*4*–*6*). However, mutations in the viral genome, such as those found in SARS-CoV-2 variants of concern (VOCs), cause amino acid changes in the RBD and NTD that can diminish or abrogate the effectiveness of vaccines and antiviral monoclonal antibodies currently in the clinic (*7*–*10*). Thus, innovative approaches are needed to identify countermeasures that remain effective despite SARS-CoV-2 viral evolution and have the potential to combat the growing number of CoVs that cause infection in humans (*11*–*13*).

To this end, we used a bioinformatic approach to uncovering regions of S devoid of amino acid changes in SARS-CoV-2, which include highly conserved linear epitopes in the S2 domain. Donor-derived monoclonal antibodies from convalescent individuals specific for these regions were evaluated for neutralization of SARS-CoV-2 VOCs and for cross-reactivity to human and zoonotic CoVs across the four Orthocoronavirinae subfamilies. Through this strategy, we identified neutralizing antibodies to the fusion peptide (FP), to the stem helix near the heptad repeat 2 (HR2)

[1]Institute for Research in Biomedicine, Università della Svizzera italiana, Bellinzona, Switzerland. [2]Department of Biology, Stanford University, Stanford, CA, USA. [3]Institute of Parasitology, Biology Centre of the Czech Academy of Sciences, Ceske Budejovice, Czech Republic. [4]Veterinary Research Institute, Brno, Czech Republic. [5]Department of Biosciences and Nutrition, Karolinska Institutet, Huddinge, Sweden. [6]Microbiology and Virology Department, Fondazione IRCCS Policlinico San Matteo, Pavia, Italy. [7]Clinical Research Unit, Clinica Luganese Moncucco, Lugano, Switzerland. [8]Department of Experimental Biology, Faculty of Science, Masaryk University, Brno, Czech Republic. [9]Department of Pharmacology and Pharmacy, Faculty of Veterinary Medicine, University of Veterinary Sciences, Brno, Czech Republic. [10]Department of Chemistry and Biochemistry, Mendel University in Brno, Brno, Czech Republic. [11]Faculty of Science, University of South Bohemia, Ceske Budejovice, Czech Republic. [12]Czech Centre of Phenogenomics, Institute of Molecular Genetics of the Czech Academy of Sciences, Vestec, Czech Republic. [13]European Commission, Joint Research Centre (JRC), Ispra Italy. [14]Laboratory of Molecular Microbiology and Biotechnology, Department of Medical Biotechnologies, University of Siena, Siena, Italy. [15]Research Center for Immunodeficiencies, Pediatrics Center of Excellence, Children's Medical Center, Tehran University of Medical Sciences, Tehran, Iran. [16]Sarafan ChEM-H Macromolecular Structure Knowledge Center, Stanford University, Stanford, CA, USA. [17]Department of Clinical, Surgical, Diagnostic and Pediatric Sciences, University of Pavia, Pavia, Italy. [18]Internal Medicine and Infectious Diseases, Clinica Luganese Moncucco, Lugano, Switzerland. [19]Swiss Institute of Bioinformatics, Lausanne, Switzerland. [20]Chan Zuckerberg Biohub, San Francisco, CA, USA.
†These authors contributed equally to this work.
*Corresponding author. Email: ruzekd@paru.cas.cz (D.R.); luca.varani@irb.usi.ch (L.V.); andrea.cavalli@irb.usi.ch (A.C.); cobarnes@stanford.edu (C.O.B.); drobbiani@irb.usi.ch (D.F.R.)

region, and to the subdomain 1 (SD1) that are broadly cross-reactive and protective in vivo. Collectively, our data add to the growing body of evidence suggesting the potential use of broadly neutralizing antibodies for prophylaxis or therapy against emerging SARS-CoV-2 VOCs and future zoonotic spillover events.

RESULTS

Protective and broadly cross-reactive human antibodies to FP and HR2 coldspots

We hypothesized that some regions of S may be under selective pressure to maintain their amino acid sequence unchanged because it is essential for their function or to maintain proper quaternary structure. To determine whether these regions exist, we analyzed 10,480,461 SARS-CoV-2 sequences from GISAID (*14*). We identified 15 regions with infrequent amino acid changes, which we called "coldspots" that were defined as >17 consecutive amino acids with a frequency of substitutions of <0.1%. One coldspot includes the S2′ cleavage site and a portion of the FP (amino acids 814 to 838), which is a substrate of the TMPRSS2 and cathepsin proteases; a second one is at the stem helix that precedes the HR2 region (amino acids 1142 to 1161); and three coldspots span sequences at the discontinuously encoded SD1 (see data file S1). Both FP and HR2 coldspots are devoid of amino acid changes in SARS-CoV-2 VOCs, whereas changes are rare in SD1 (Fig. 1, A and B, and fig. S1A).

To determine whether antibodies to the FP and HR2 coldspots occur naturally in response to SARS-CoV-2 infection, we evaluated plasma samples from a coronavirus disease 2019 (COVID-19) convalescent cohort by enzyme-linked immunosorbent assay (ELISA; n = 67). High levels of immunoglobulin G (IgG) antibodies binding to peptides at the FP and HR2 coldspots were found in convalescent individuals (Fig. 1C). In comparison, IgG levels were low to undetectable in samples from uninfected controls, in prepandemic samples obtained after documented common cold CoV infection, and in most COVID-19–vaccinated individuals, except for some who received inactivated virus–based vaccines (fig. S1B). To examine the molecular features of coldspot antibodies, we used flow cytometry to isolate B cells specific for FP and HR2 peptides from those individuals with high antibody levels in plasma (Fig. 1D and fig. S1, C and D). We obtained 55 (FP) and 100 (HR2) paired IgG heavy and light chain antibody sequences, some of which clustered in expanded clones of related antibodies (fig. S1E). The average number of V gene somatic nucleotide mutations was high: 42 for FP (range: 6 to 76) and 28 for HR2 antibodies (range: 8 to 92; Fig. 1E).

Twenty-nine monoclonal antibodies, including at least one representative for each of the expanded clones, were recombinantly expressed and tested in ELISA (data file S1). Ten of 11 FP antibodies bound to the peptide with half-maximal effective concentrations (EC_{50}) between 25 and 119 ng/ml. The EC_{50} values of the same antibodies to S were on average 4.8-fold higher, except for antibody fp.007, where the observed EC_{50} value declined from 177 to 58 ng/ml (Fig. 1F and fig. S2). Similarly, all 18 HR2 antibodies bound to the peptide with EC_{50} values between 7 and 117 ng/ml, and with an average of 1.3-fold higher EC_{50} value to S. Several of the antibodies were broadly cross-reactive because they bound to representative S trimers of SARS-CoV-2 VOCs, Middle East respiratory syndrome (MERS), and human coronavirus 229E (HCoV-229E) as well as to FP and HR2 peptides corresponding to other CoVs. Most FP antibodies recognized CoVs of the four genera (alpha to delta, including all nine CoVs associated with human disease), and some HR2 antibodies cross-reacted not only with beta- but also with alpha- and gammacoronaviruses (Fig. 1F, figs. S2 and S3, and data file S2) (*11*, *15*, *16*).

To evaluate the antibodies' ability to neutralize SARS-CoV-2, we used a previously established SARS-CoV-2 pseudovirus assay (*4*). The most potent FP antibody (fp.006) displayed a half-maximal inhibitory concentration (IC_{50}) of 737 ng/ml, whereas the best HR2 neutralizer (hr2.016) had an IC_{50} value of 10 ng/ml, which was lower than that of previously reported antibodies to this region that were tested alongside (CV3-25 and S2P6; Fig. 1G, fig. S4A, and data file S2) (*16*, *17*). Select anti-FP and anti-HR2 antibodies blocked infection regardless of TMPRSS2 expression by target cells, and, consistent with the view that they antagonize postattachment events, they did not interfere with angiotensin-converting enzyme 2 (ACE2) binding to S in ELISA but inhibited cell fusion (Fig. 1, H and I, and fig. S4, A and B). As expected, on the basis of the absence of amino acid changes at coldspot regions, some FP and HR2 antibodies were effective against pseudoviruses corresponding to SARS-CoV-2 VOCs and against ancestral and Omicron SARS-CoV-2 in vitro. In mice ACE2-humanized by inhalation of a modified adeno-associated virus (AAV-hACE2), we observed protection after challenge with the ancestral virus when administered either as pre- or postexposure prophylaxis (Fig. 1, G, J, and K; fig. S4, C and D; and data file S2). Thus, natural antibodies exist that can protect against SARS-CoV-2 by binding to highly conserved linear epitopes at functional regions of S.

Antibody fp.006 recognizes a partially cryptic epitope that is exposed by ACE2 binding

To gain insight into the mechanism of broad recognition by fp.006, we obtained a 2.0 Å–resolution crystal structure of its Fab in complex with the $_{812}$PSKRSFIEDLLFNKVTLADA$_{831}$ FP peptide (Fig. 2 and table S1). In the bound structure, FP residues 813 to 825 adopt an α-helical conformation, extending an amphipathic helix observed in prefusion S trimer structures. The helical peptide sits within a groove that is formed by fp.006 complementarity-determining region 3 (CDR3) loops, which mediate most epitope contacts (Fig. 2A). Additional contacts with heavy chain CDR1 and CDR2 loops result in a total buried surface area (BSA) of 1466 Å^2 (686-Å^2 paratope BSA + 780-Å^2 epitope BSA) and are consistent with binding orientations of similarly described anti-FP antibodies (fig. S5, A to G) (*18*–*20*). Of the 13 antigenically distinct CoV FPs tested here, the majority of epitope residues contacted by fp.006 are highly conserved, explaining fp.006's breadth of binding (Fig. 1F and figs. S2B and S5B). In particular, three FP residues (R815, E819, and F823) are completely buried in the Fab groove and make extensive hydrogen bonds and hydrophobic interactions (Fig. 2, B to G). As a result, one face of the FP amphipathic helix comprises two polar residues that contact a polar patch on the edge of the Fab trough formed by CDRH2, and the opposite hydrophobic face engages hydrophobic residues in the CDRH3 loop (fig. S5, D and E). Residue R815, which is critical for TMPRSS2 and cathepsin cleavage (*3*, *21*, *22*), forms hydrogen bonds with the Fab CDRH1 loop and a cation-π interaction with Y52A in CDRH2 (Fig. 2D). Given the importance of R815 in protease cleavage, fp.006-mediated neutralization likely includes steric hindrance of

Downloaded from https://www.science.org on May 03, 2024

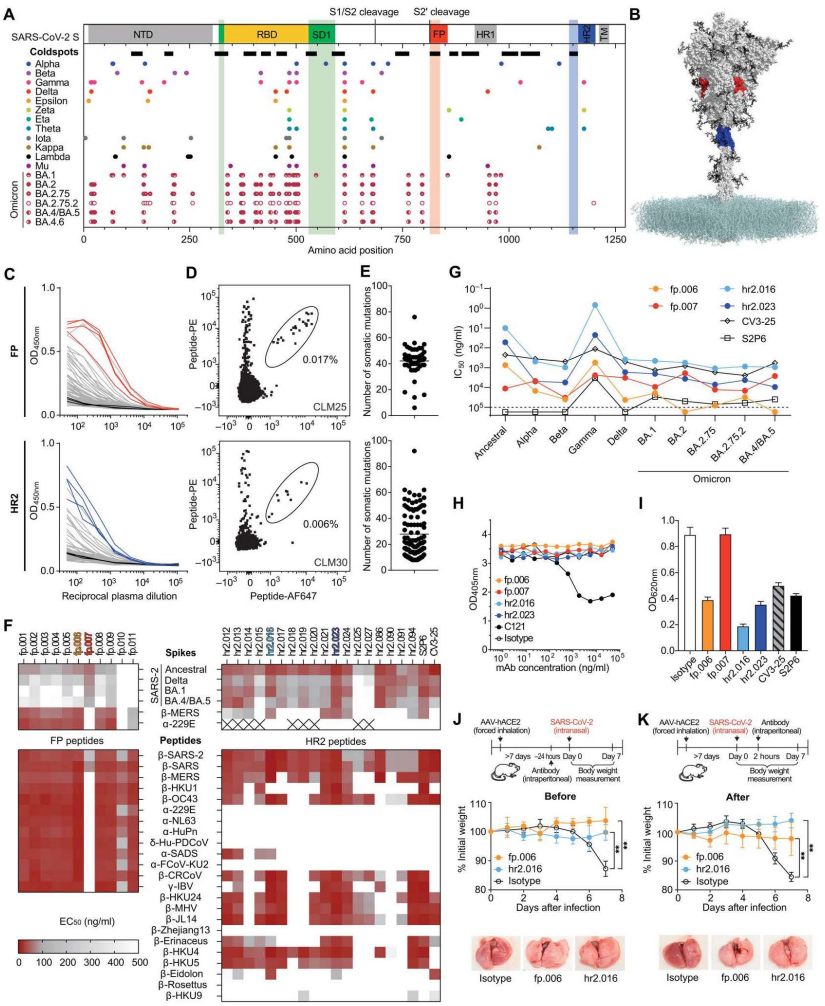

Fig. 1. Identification of virus-neutralizing coldspot antibodies. (**A**) Top: Cartoon diagram of the SARS-CoV-2 spike with highlighted coldspot areas at the FP (red), HR2 region (blue), and SD1 (green). Thick horizontal lines indicate the location of all coldspots (see also fig. S1A). Bottom: Amino acid (aa) changes in SARS-CoV-2 variants. Each circle represents a single amino acid substitution over ancestral virus. (**B**) Structure of the SARS-CoV-2 spike; FP (amino acids 814 to 838) and HR2 (amino acid 1142 to 1161) coldspots are in red and blue, respectively (PDB: 6XM4). (**C**) ELISA measurements of convalescent plasma IgG reactivity to FP (top) or HR2 (bottom) peptides. Optical density units at 450 nm (OD; *y* axis) and reciprocal plasma dilutions (*x* axis). Noninfected controls are in black; samples selected for cell sorting by flow cytometry are in red or blue. Two independent experiments. (**D**) Representative flow cytometry plots of B cells binding to fluorescently labeled FP (top) or HR2 (bottom) peptides. Numbers indicate the percentage of double-positive cells in the gate. (**E**) The number of heavy and light chain V gene somatic mutations of antibodies to the FP (top) or HR2 (bottom) peptides. (**F**) Heatmaps with ELISA EC_{50} values of monoclonal antibodies (mAbs) binding to the S of CoVs (top) and to the FP and HR2 peptides (bottom) corresponding to the CoV species, whose genus is indicated by Greek letters. The monoclonal antibodies to the HR2 region S2P6 (*16*) and CV3-25 (*17*) were assayed alongside for comparison. Cross indicates not tested. Two experiments. (**G**) Graph with IC_{50} values of monoclonal antibodies neutralizing pseudoviruses corresponding to the indicated VOC. Two experiments. (**H**) ACE2 binding to ancestral S in ELISA in the presence of select FP and HR2 antibodies. Dotted line represents the limit of detection. Two experiments. (**I**) Inhibition of cell fusion by FP and HR2 antibodies. (**J** and **K**) fp.006 and hr2.016 antibodies protect in vivo. Top: Diagram of the experiment's timeline. Middle: Mouse weight over time after challenge with ancestral SARS-CoV-2 of AAV-hACE2 mice treated with antibodies either 24 hours before [(J); $n = 6$ per group, $P = 0.0022$ for both fp.006 and hr2.016 versus isotype at day 7] or 2 hours after [(K); $n = 5$ per group, $P = 0.0079$ for both fp.006 and hr2.016 versus isotype at day 7] the infection. Mann-Whitney *U* test; SD is shown. Bottom: Representative lung images at day 7.

TMPRSS2 and cathepsin binding and further processing of the S trimer for productive fusion. Superposition of the Fab-FP complex crystal structure with a prefusion S trimer structure revealed an approach angle incompatible with Fab binding, which explains the weak binding observed for FP antibodies to prefusion S trimers (Figs. 1F and 2C). Thus, cleavage by cellular proteases at the S2′ site and antibody recognition of this partially cryptic epitope likely involve transient conformational changes that are necessary to expose the FP epitope.

In agreement with this view, ACE2 engagement of cell surface–expressed S, which is known to alter S conformation, increased fp.006 binding 5.8-fold in a flow cytometry assay, and the addition

Downloaded from https://www.science.org on May 03, 2024

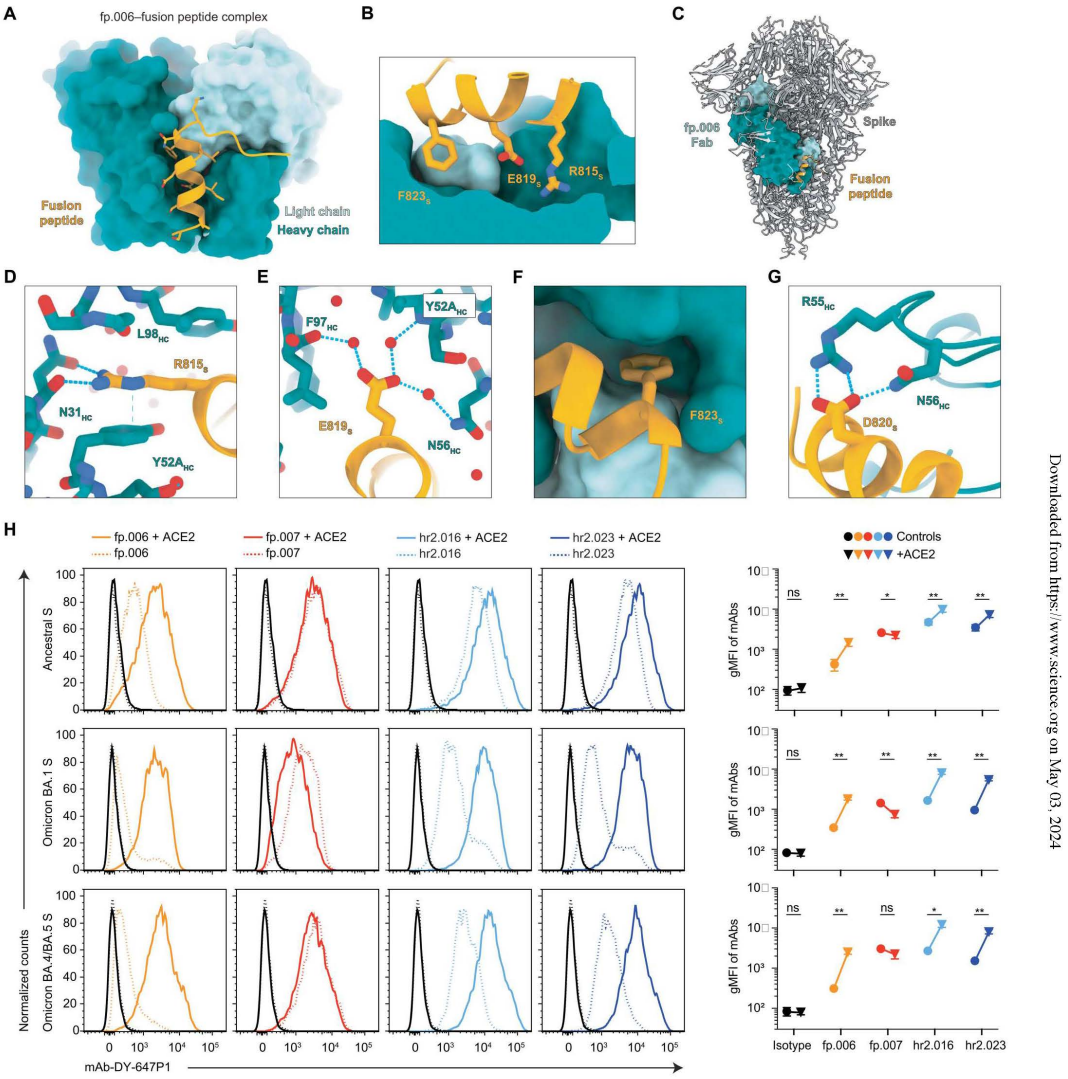

Fig. 2. SARS-CoV-2 FP recognition by fp.006. (**A**) Overview of the complex structure of fp.006 Fab (surface representation; heavy chain in teal and light chain in light teal) bound to the SARS-CoV-2 FP (orange cartoon) with interacting side chains represented as sticks. (**B**) Visualization of FP residues F823, E819, and R815 resting in a deep groove formed at the antibody paratope, with coloring as in (A). (**C**) Overlay of the fp.006-FP crystal structure with a cryo-EM structure of the SARS-CoV-2 prefusion S trimer (PDB: 6VXX). Models were aligned on Cα atoms of FP residues 818 to 822 (helical in both structures) with a root mean square deviation of 0.97 Å. (**D**) Residue-level interactions between FP residue R815 and the antibody heavy chain include hydrogen bond formation with N31 and a cation-π interaction with Y52A. (**E**) Water-mediated interactions between FP residue E819 and heavy chain residues Y52A, N56, and F97. Water molecules are shown as red spheres. (**F**) Van der Waals contacts between FP residue F823 (orange stick) and residues that comprise a groove at the heavy and light chain interface (teal surfaces). (**G**) Interactions between FP residue D820 and fp.006 CDRH2 residues include a salt bridge with R55 and additional hydrogen bond formation with N56. Hydrogen bonds, salt bridges, and cation-π interactions are shown as dashed blue lines. (**H**) Flow cytometry detection of anti-FP and anti-HR2 antibody binding to SARS-CoV-2 S expressed on 293T cells. Left: Representative FACS plots (pregated on live singlet-GFP$^+$ cells). Black lines indicate isotype control in the presence (continuous line) or absence (dotted line) of soluble ACE2. Right: Quantification of the geometric mean fluorescent intensity (gMFI; $n = 3$). Two-tailed paired t test: $^*P < 0.05$, $^{**}P < 0.01$, $^{***}P < 0.001$, and $^{****}P < 0.0001$; SD is shown.

Downloaded from https://www.science.org on May 03, 2024

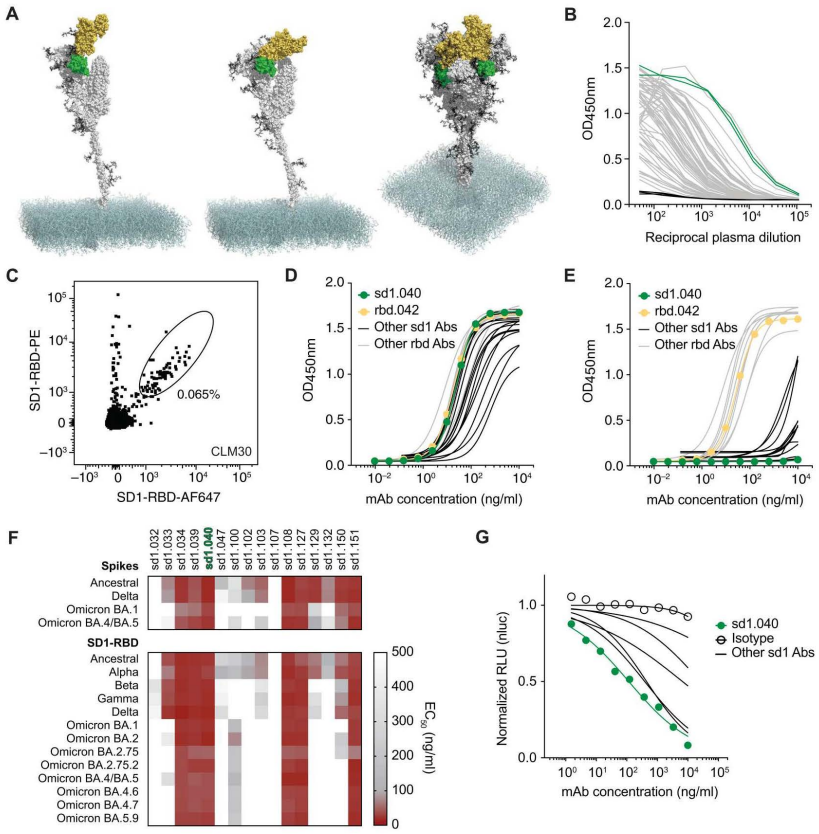

Fig. 3. Identification of broadly cross-reactive antibodies to SD1 and RBD. (**A**) Structure of the SARS-CoV-2 S. S protomer with RBD up (left) or down (middle) and S trimer with two down and one up (right; PDB: 6XM4). SD1 and RBD are in green and yellow, respectively. (**B**) Graph shows ELISAs measuring plasma IgG reactivity to SD1-RBD. Negative controls are in black; samples selected for sorting are in green. Mean of two independent experiments. A total of 82.1% of the plasma samples were positive (4 SD higher than the average AUC of the controls). (**C**) Representative flow cytometry plot of B cells binding to fluorescently labeled SD1-RBD. Percentage refers to gated cells. (**D** and **E**) ELISAs measuring the reactivity of monoclonal antibodies to SD1-RBD (D) and to RBD (E). Mean of two independent experiments. (**F**) Heatmaps with the binding (EC_{50}) of SD1 monoclonal antibodies to S (top) or SD1-RBD (bottom) proteins corresponding to SARS-CoV-2 VOC. Two experiments. (**G**) Graph shows normalized relative luminescence values in cell lysates of $293T_{ACE2}$ cells after infection with ancestral SARS-CoV-2 pseudovirus in the presence of increasing concentrations of broadly cross-reactive SD1 monoclonal antibodies. At least two independent experiments. RLU, relative luminescence units.

of soluble ACE2 synergized with fp.006 for neutralization (Fig. 2H and fig. S5, H and I). Consistent with the ELISA and neutralization data (Fig. 1, F and G), binding of fp.006 to S was weaker with Omicron by this assay, but ACE2 attachment improved it to levels similar to those of ancestral (5.3-fold for BA.1 and 8.2-fold for BA.4/BA.5; Fig. 2H). Therefore, ACE2 can induce conformational changes of S that expose the highly conserved FP epitope and favor neutralization. ACE2 attachment also increased the binding of hr2.016 and hr2.023 to both ancestral (2.3- and 2.4-fold) and Omicron S (4.9- and 5.8-fold for BA.1 and 4.6- and 5.3-fold for BA.4/BA.5, respectively; Fig. 2H) but did not improve the binding of fp.007, a neutralizing FP antibody that displays a different pattern of cross-reactivity from fp.006 (Figs. 1F and 2H). Therefore, optimal FP recognition by neutralizing fp.007-like antibodies does not require ACE2-induced conformational changes.

Antibodies to SD1 broadly neutralize VOCs

The SD1 of SARS-CoV-2 S is adjacent to the RBD, and its sequence is conserved across SARS-CoV-2 variants, except for substitutions A570D in Alpha (B.1.1.7) and T547K in Omicron BA.1 (B.1.1.529; Figs. 1, A and B, and 3A). To identify antibodies targeting SD1, we designed a flow cytometry–based strategy that combines negative selection of B cells binding to the RBD (amino acids 331 to 529) with positive selection of those binding to SD1-RBD (amino acids

Downloaded from https://www.science.org on May 03, 2024

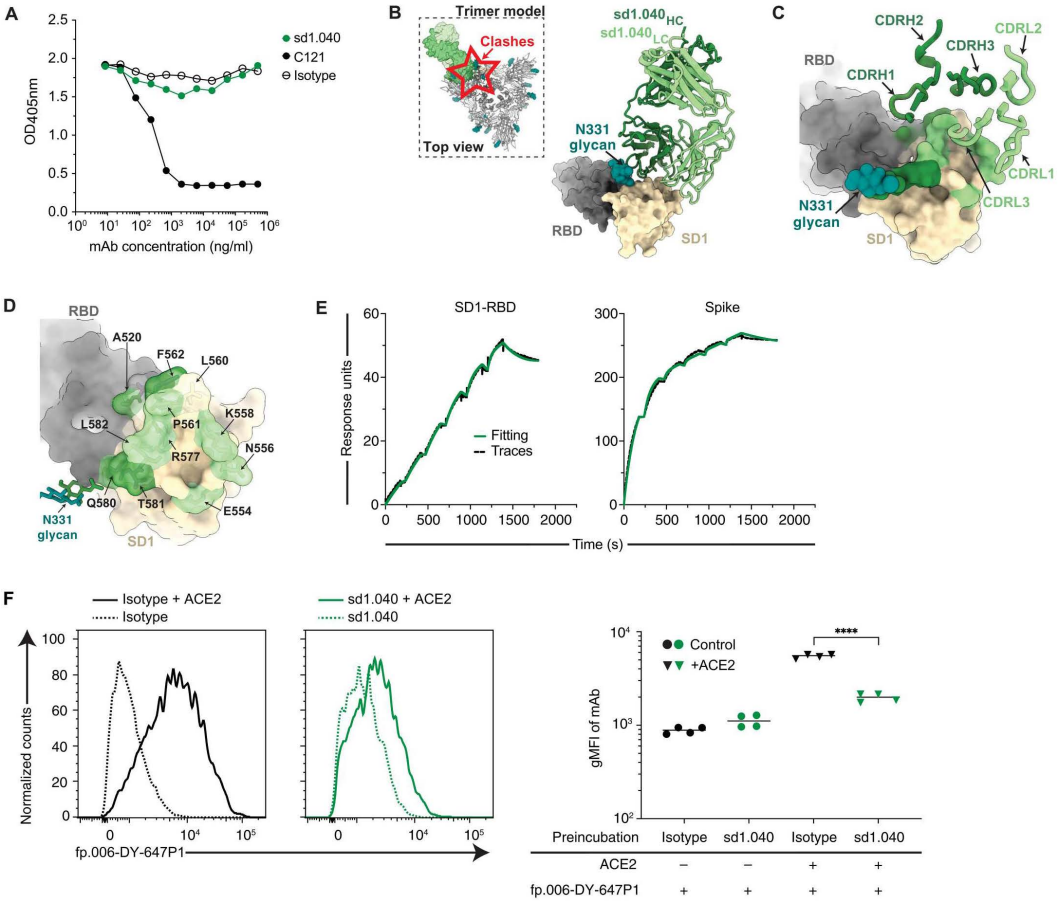

Fig. 4. Cryo-EM structure of sd1.040 in complex with SARS-CoV-2 S. (**A**) ACE2 binding to ancestral S in ELISA in the presence of sd1.040 or C121 control antibody. Representative of two experiments. (**B**) Structure of the sd1.040-S complex. Spike SD1 and RBD regions are shown as surface representations and colored wheat and gray, respectively. The sd1.040 Fab heavy chain (dark green) and light chain (light green) are shown as cartoons. The S N331-glycan that interacts with the sd1.040 Fab is shown as teal spheres. Inset: sd1.040 binding orientation on trimeric S shows clashes. (**C** and **D**) Surface rendering of sd1.040 epitope is highlighted on the SD1 and RBD surfaces, with sd1.040 CDR loops shown (ribbon). Most sd1.040 contacts are mediated by CDRH2, CDRL1, and CDRL3 loops. (**E**) SPR experiment showing the binding of sd1.040 Fab to ancestral SD1-RBD or S. (**F**) Antibody sd1.040 prevents ACE2-induced rearrangements. Flow cytometry detection of fp.006 binding to ancestral SARS-CoV-2 S expressed on 293T cells. Left: Representative FACS plots. Black lines indicate isotype control in the presence (continuous line) or absence (dotted line) of soluble ACE2. Right: Quantification of the geometric mean fluorescent intensity ($n = 4$). Two-tailed unpaired t test: $^{*}P < 0.05$, $^{**}P < 0.01$, $^{***}P < 0.001$, and $^{****}P < 0.0001$.

319 to 591; fig. S1C). Peripheral blood mononuclear cells (PBMCs) were obtained from individuals with high plasma IgG reactivity to SD1-RBD (Fig. 3B and fig. S6, A and B), and B cells enriched for binding to SD1 were sorted as single cells for antibody gene sequencing (Fig. 3C and fig. S6C).

Twenty-five monoclonal antibodies were cloned and produced. All 25 bound to SD1-RBD in ELISA, and 16 were SD1-specific (Fig. 3, D and E, and data file S1). Six of the SD1 antibodies cross-reacted with SD1-RBD proteins corresponding to all 12 CoV VOCs with EC_{50} values of 66.25 ng/ml or lower, whereas only two RBD antibodies cross-reacted with all variants' RBDs at low EC_{50} values (Fig. 3F; fig. S6, D to F; and data file S2). Select antibodies also bound effectively to the common SD1 variants T572I and E583D (fig. S6G). In pseudovirus-based neutralization assays, the best broadly cross-reactive SD1 antibody was sd1.040 (IC_{50} = 245 ng/ml; Fig. 3G and data file S2). These results demonstrate that naturally occurring antibodies can neutralize SARS-CoV-2 by binding to SD1.

Downloaded from https://www.science.org on May 03, 2024

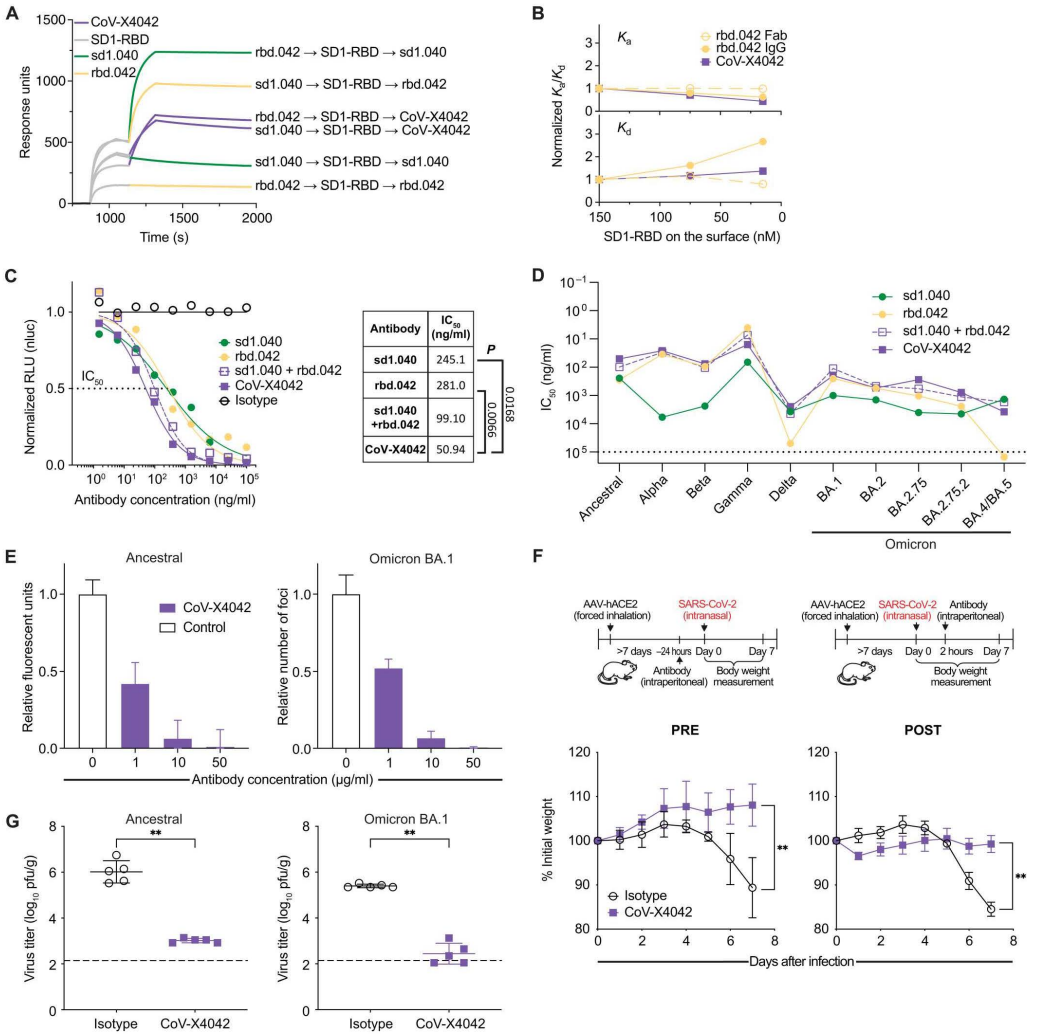

Fig. 5. In vitro neutralization and mouse protection by the bispecific antibody CoV-X4042. (**A**) SPR assay of the sequential binding of immobilized antibodies to SD1-RBD protein followed by either sd1.040, rbd.042, or CoV-X4042. (**B**) SPR analysis showing that both arms of CoV-X4042 bind simultaneously to the same SD1-RBD molecule because avidity is retained at decreasing SD1-RBD concentrations. Increasing normalized K_d values indicate loss of avidity. Solid lines, IgG; dashed lines, Fab (see also fig. S8A). (**C**) Normalized relative luminescence values in cell lysates of 293T_{ACE2} cells after infection with ancestral SARS-CoV-2 pseudovirus in the presence of increasing concentrations of CoV-X4042 or its parental monoclonal antibodies individually or as a cocktail. Isotype control is in black. Right: Mean IC_{50} values and significance (*P*) when parental antibodies are compared with CoV-X4042 ($n = 4$; Welch's *t* test, two-tailed). (**D**) Graph with IC_{50} values of bispecific and parental monoclonal antibodies neutralizing pseudoviruses corresponding to the indicated VOC. Mean of two independent experiments. (**E**) In vitro neutralization of SARS-CoV-2 by CoV-X4042. (**F**) CoV-X4042 protects in vivo. Top: Diagram of the experiment's timeline. Bottom: Mouse weight over time after challenge, with ancestral SARS-CoV-2, of AAV-hACE2 mice treated with antibodies either 24 hours before (PRE; $n = 5$ per group, $P = 0.0079$) or 2 hours after (POST; $n = 5$ per group, $P = 0.0079$; day 7) the infection. Mann-Whitney *U* test; SD is shown. (**G**) CoV-X4042 reduces viral titers in the lungs. Mice were treated with antibodies 24 hours before infection, and virus titers were evaluated on day 3 ($n = 5$ per group $P = 0.0079$ with both ancestral and Omicron BA.1; Mann-Whitney *U* test, SD is shown).

Downloaded from https://www.science.org on May 03, 2024

Antibody sd1.040 stabilizes the spike trimer

The mechanism of neutralization by sd1.040 does not involve inhibition of receptor binding because sd1.040, unlike C121 (*4*), failed to prevent ACE2 binding to S in ELISA (Fig. 4A). To gain insight into the neutralization mechanism, we formed a complex between sd1.040 Fabs bound to a prefusion S-2P trimer and used cryo–electron microscopy (cryo-EM) for structure determination. No intact Fab–S trimer structures were observed within the dataset (fig. S7, A to D). Instead, our 3.7 Å cryo-EM structure revealed sd1.040 Fabs in complex with S1 protomers, recognizing an epitope comprising SD1 residues 554 to 562 and 577 to 581 and RBD residues 520 to 524 (Fig. 4, B to D; fig. S7, A to D; and table S2). Superposition of the cryo-EM sd1.040–S protomer complex on published prefusion S structures, indiscriminate of RBD conformation, revealed minor clashes with the NTD of the adjacent protomer, similar to antibody P008_60 (*23*), which contrasts the recently described SD1-specific murine antibody S3H3 (Fig. 4B, inset, and fig. S7, E and F) (*24*). It is likely that sd1.040 binding to S requires minor local rearrangement of the NTD. Docking and molecular dynamics computational simulations suggested the presence of quaternary interactions between the antibody, SD1, and RBD on one protomer and NTD on another, which require minor rearrangement of the NTD hinging around residues 295 to 300 toward the end of the NTD (fig. S7, G and H). This rearrangement does not result in clashes with other S regions. The CDRH1 and CDRH3, which do not interact with RBD/SD1 in the cryo-EM protomer structure, are shown to directly contact the NTD in the simulations. These quaternary interactions are likely to stabilize the complex, which, by surface plasmon resonance (SPR), displays a ~20 times stronger binding affinity for S [dissociation constant (K_d) 0.2 nM] than for the SD1-RBD (K_d, 4.2 nM; Fig. 4E). To test the hypothesis that the mechanism of neutralization by sd1.040 is through the inhibition of S molecular rearrangements, we measured fp.006 binding to S by flow cytometry. ACE2 attachment in this assay improved fp.006 binding to S, which was, however, blocked by treatment with sd1.040 (Fig. 4F). Thus, sd1.040 interferes with conformational changes downstream of ACE2 attachment.

Bispecific antibody CoV-X4042 neutralizes VOCs and protects mice

On the basis of the breadth of binding exhibited by antibodies sd1.040 and rbd.042 against SARS-CoV-2 VOCs, their potency of neutralization, and preliminary experiments that indicated synergistic effects from combining them (Fig. 3, F and G, and fig. S6, F and H), we produced a bispecific antibody that includes the moieties of both antibodies, named CoV-X4042. CoV-X4042 has a natural IgG format including the entire Fc region and complementary modifications in the Fc and C_H1 (domain 1 of the constant portion of the Ig heavy chain)/C_L (light chain) regions that minimize the formation of undesired by-products (*25*). Consistent with the parental antibodies binding to distinct epitopes, both arms of CoV-X4042 can simultaneously engage the same SD1-RBD molecule (Fig. 5, A and B, and fig. S8). In pseudovirus-based neutralization assays, CoV-X4042, similar to the sd1.040/rbd.042 cocktail, exhibited substantial synergistic activity over either of the parental antibodies alone (Fig. 5C). CoV-X4042 neutralized pseudoviruses corresponding to VOCs and remained effective even when one of the parental antibodies lost efficacy (e.g., rbd.042 against Omicron BA.4/BA.5; Fig. 5D). Efficacy of the bispecific antibody was confirmed against ancestral and Omicron SARS-CoV-2 in vitro and by in vivo protection experiments showing that AAV-hACE2 mice treated with CoV-X4042, either as pre- or postexposure prophylaxis, maintained body weight and displayed diminished pathology and infectious virus titers in the lungs (Fig. 5, E to G). Therefore, bispecific antibodies composed of moieties that simultaneously target conserved neutralizing epitopes on SD1 and RBDs are effective against SARS-CoV-2 in preclinical mouse models of infection.

DISCUSSION

The evolving antigenic landscape of SARS-CoV-2 poses unanticipated challenges to the development of vaccines and immunotherapies. Monoclonal antibodies against the RBD that are potent against the ancestral virus were prioritized for clinical development (*26*–*30*). However, most of these antibodies lost efficacy because of amino acid changes in SARS-CoV-2 variants that possibly resulted from immune pressure (*8*, *10*, *27*, *31*–*33*). Although antibodies have been reported to broadly neutralize SARS-CoV-2 variants (e.g., anti-NTD antibodies, bebtelovimab, and sotrovimab), the majority of potent neutralizers recognize epitopes outside coldspot regions (*6*, *34*). The three RBD coldspots (residues 377 to 404, 418 to 438, and 454 to 476) partially comprise the conserved class 4 epitope, which has been identified as a potential target for eliciting cross-reactive antibodies against the sarbecovirus lineage (*35*–*39*). However, class 4 antibodies are weakly neutralizing and lack effectiveness against Omicron sublineages (*40*). Neutralizing antibodies that target the S2 region and act in the postattachment phase were recently described. Although generally weak neutralizers, some display broad reactivity against SARS-CoV-2 variants and even against more distant CoV species (*16*–*20*, *41*, *42*), which is analogous to what is observed with antibodies that target the FP of influenza and HIV-1 (*43*–*45*).

In contrast, we identified an antibody to the stem helix that precedes the HR2 region (hr2.016), which is, at the same time, potent (IC_{50} value of 10 ng/ml) and broadly cross-reactive with beta- and some alpha- and gammacoronaviruses. Similarly, we identified a panel of anti-FP neutralizing antibodies that broadly recognize more distant CoVs, including all nine of the known human CoVs. These results are consistent with the high degree of amino acid conservation at these regions of CoVs. IgG to FP and near the HR2 region was detected in convalescents and in individuals immunized with inactivated virus–based, but not with mRNA- or adenovirus-based, vaccines, suggesting that not all the current vaccines are equally proficient at inducing antibodies to these broadly conserved neutralizing epitopes. This is possibly because of amino acid changes made in vaccines to stabilize the S trimer that may reduce the accessibility of these epitopes (*18*). Future vaccine development may consider including these new targets to afford improved and broader effectiveness. However, it will be important to understand how neutralizing antibodies recognize native epitopes on the prefusion spike trimer to guide these efforts.

For FP-specific antibodies, we observed specific contacts with residue R815 in the S2′ cleavage site. Cleavage at this site during entry allows for the rearrangement of the S2 subunit and subsequent fusion with the host cell membrane. A recent publication comparing CoV FP binding antibodies hypothesizes that binding to this residue may be a feature that distinguishes neutralizing and non-

Downloaded from https://www.science.org on May 03, 2024

neutralizing FP antibodies (*19*). Another publication also posited that the mechanism of neutralization for cross-reactive FP antibodies was the steric occlusion of TMPRSS2 binding, rather than the prevention of fusogenic rearrangements, which supports the idea that binding to this highly conserved Arg is a key determinant for neutralizing FP antibodies (*18*). In addition to TMPRSS2 cleavage, viral fusion can proceed through cathepsin cleavage in the endosome downstream of the putative S2′ cleavage site (*2*, *3*). Consistent with the observation that FP antibodies are effective regardless of TMPRSS2 expression on target cells, superposition of fp.006 on the S structure indicates that access to the cathepsin site is also hindered by the antibody presence, suggesting that fp.006 neutralization may involve a second mechanism preventing the fusion of the viral and endosomal membranes in the cytoplasm.

We also report on human neutralizing antibodies that target SD1, a generally understudied but highly conserved region of S next to the RBD. Previous studies have demonstrated that quaternary interactions between the RBD and SD1 of one protomer with the NTD of the neighboring S1 protomer likely play a stabilizing role for prefusion S trimers (*46*). Our data suggest that antibody sd1.040 does not neutralize by interfering with ACE2 receptor binding. Instead, its function is likely linked to the inhibition of conformational changes that expose the fusion loop upon engagement of ACE2. This mechanism is distinct from that of murine antibody S3H3 that potentially functions by "locking" the release of S1 subunits from S2 (*24*).

Although the target sequences are conserved, FP, HR2, and SD1 antibodies are variably efficacious against VOC. This may reflect differences in the overall conformation of S variants that alter epitope accessibility as well as changes in residues contacted by the antibodies that are outside the coldspot region. For FP and HR2 antibodies, the observation that ACE2 attachment renders the epitopes more accessible and improves neutralization suggests that, for therapeutic purposes, it may be valuable to combine them with antibodies against the RBD that mimic ACE2 binding (*47*).

In recent work, broadly cross-reactive antibodies were identified through large-scale screening of more than 670,000 memory B cell antibodies or more than 4000 B cell cultures (*18*, *19*). By focusing on portions of the virus that are both functionally relevant and averse to change, the strategy described here represents a complementary, resource-savvy approach for the rapid identification of antibodies with the potential of being broadly cross-reactive against variants of a single virus or against multiple related virus species. This approach relies on the analysis of large collections of virus sequences, which at present are publicly available only for a handful of pathogens (e.g., more than 10 mio for SARS-CoV-2; 0.366 mio for influenza; 0.016 mio for HIV-1) (*14*, *48*, *49*) but are expected to become more broadly available for other pathogens in the future because of increased surveillance and ease of sequencing.

MATERIALS AND METHODS

Study design

This study was designed with the goal to identify broadly cross-reactive and cross-neutralizing monoclonal antibodies that could recognize all SARS-CoV-2 VOCs and likely remain effective against future VOCs. Through bioinformatic analysis, we identified highly conserved regions (coldspots) on the SARS-CoV-2 spike. We designed peptides and produced protein domains corresponding to these coldspots to specifically derive antibodies from the memory B cells of SARS-CoV-2 convalescent individuals. Monoclonal antibodies to coldspot regions were recombinantly produced and evaluated for cross-reactivity to coldspot peptides, SD1-RBD, and spike proteins in ELISA. The most interesting antibodies were further characterized in vitro for neutralization of SARS-CoV-2 VOC pseudoviruses and authentic viruses and in vivo with mice protection experiments. To define antibody recognition of viral epitopes, we used x-ray crystallography and cryo-EM to obtain the structures of fp.006 in complex with FP peptide and sd1.040 in complex with full spike trimer, respectively. The mechanism of action of the most interesting FP, HR2, and SD1 antibodies was further investigated by flow cytometry and other complementary methods.

Computational analyses of viral sequences

Sequences of reference for ancestral SARS-CoV-2 and its variants of interest and concern (Fig. 1A) were derived from ViralZone (https://viralzone.expasy.org/9556), matched the World Health Organization classification (www.who.int/en/activities/tracking-SARS-CoV-2-variants/), and were as follows: ancestral SARS-CoV-2 Wuhan-Hu-1 (19A; GenBank: QHO60594.1), Alpha (B1.1.7; GenBank: QWE88920.1), Beta (B.1.351; GenBank: QRN78347.1), Gamma (B.1.1.28.1; GenBank: QVE55289.1), Delta (B.1.617.2; GenBank: QWK65230.1), Epsilon (B.1.427; B.1.429; GenBank QQM19141.1), Zeta (B.1.1.28.2; GenBank; QQX30509.1), Eta (B.1.525; GenBank: QRF70806.1), Theta (B.1.1.28.3), Iota (B.1.526; GenBank: QRX49325.1), Kappa (B.1.617.1; GenBank: QTY83052.1), Lambda (B.1.1.1.C37; GenBank: QTJ90974.1), Mu (B.1.621), Omicron BA.1 (previously B.1.1.529; GenBank: UFO69279.1), Omicron BA.2 (GenBank: ULB15050.1), Omicron BA.3 (GISAID: EPI ISL 9092427), Omicron BA.4 (GenBank: UPP14409.1), and Omicron BA.5 (GenBank: UOZ45804.1). For the analysis of SARS-CoV-2 amino acid substitutions, viral sequences of S that were present in GISAID as of either 31 December 2020, 31 December 2021, or 29 April 2022 were downloaded. Sequences with a length of S corresponding between 1223 and 1323 amino acids and no undetermined amino acids were aligned to determine the frequency of amino acid changes over ancestral reference sequences using BLASTP version 2.5.0 with default settings. Frequencies were computed using an in-house–developed bash and C++ pipeline available at GitHub (https://github.com/cavallilab/coldspot). The models of the full S, glycosylated, and with a membrane, both closed and open conformation, were taken from a previous publication (*50*) and rendered with PyMOL 2.3.5 (Figs. 1B and 3A). For the phylogenetic analysis and peptide sequence alignment, sequences of the representative S protein of CoV species classified according to the International Committee on Taxonomy of Viruses taxonomical classification (https://talk.ictvonline.org/taxonomy/) (*51*) were derived from the National Center for Biotechnology Information taxonomy database (www.ncbi.nlm.nih.gov/data-hub/taxonomy/11118/) (*52*), aligned using ClustalW (SnapGene), and the phylogenetic tree was built using phylogeny.fr with default settings (*53*).

Downloaded from https://www.science.org on May 03, 2024

Study participants

COVID-19 convalescent cohort

Sixty-seven individuals, who were diagnosed with COVID-19 at the Clinica Luganese Moncucco (Switzerland) between March and November of 2020, were enrolled in the study, and written informed consent was obtained. Inclusion criteria were a SARS-CoV-2–positive nasopharyngeal swab test by real-time reverse transcription polymerase chain reaction (RT-PCR) or being a symptomatic close contact (same household) of a hospitalized participant and age of ≥18 years. Samples were 83 to 269 days after the onset of symptoms. The study was performed in compliance with all relevant ethical regulations under study protocols approved by the Ethical Committee of the Canton Ticino (ECCT): CE-3428 and CE-3960.

Control cohort

Seventeen individuals (≥18 years), with the absence of prior SARS-CoV-2 infection or vaccination, as confirmed by a negative serologic test, were enrolled between November 2020 and June 2021, and written informed consent was obtained (ECCT: CE-3428).

Vaccination cohort

Individuals (≥18 years), with the absence of prior SARS-CoV-2 infection and who received either mRNA-based (n = 11 for BNT162b2, samples obtained 75 to 136 days after the second dose; n = 5 for mRNA-1273, 85 to 120 days after the second dose), adenovirus-based (n = 19 for ChAdOx1-S, 90 days after the second dose; n = 4 for Ad26.COV2.S, 21 days after a single dose), or inactivated virus–based (n = 2 for Sinovac, 26 to 60 days after the second dose; n = 24 for Sinopharm, 6 to 60 days after the second dose) COVID-19 vaccines, were enrolled under approved protocols (ECCT: CE-3428 and CE-3960; Ethic Committee Karolinska Institutet: Dnr 2020-02646; Ethic Committee Tehran University of Medical Sciences: IR.TUMS.CHMC.REC.1399.098-B2; Ethical Committee for Clinical Experimentation of Regione Toscana Area Vasta Sud Est: ID 18869). Controls to the adenovirus-vaccinated group are prevaccination samples from the same participants.

Prepandemic common cold coronavirus convalescents

Six samples from individuals with confirmed common cold CoV infection were obtained 6 to 375 days after symptom onset at Policlinico San Matteo, Pavia (Institutional Review Board protocol no. P_20200029440).

Blood sample processing and storage

PBMCs from COVID-19 convalescents were obtained by Histopaque density centrifugation and stored in liquid nitrogen in the presence of fetal bovine serum (FBS) and dimethyl sulfoxide (DMSO). Anticoagulated plasma was aliquoted and stored at −20°C or less. Before experiments, aliquots of plasma were heat-inactivated (56°C for 1 hour) and then stored at 4°C. Similarly, frozen plasma aliquots from noninfected, common cold–infected, and vaccinated individuals were stored at 4°C after heat inactivation.

Peptides and recombinant proteins for biochemical studies

Peptides

Synthetic peptides containing the FP and HR2 coldspot sequences were designed and obtained (>75% purity) from GenScript (Hong Kong). Peptides were biotinylated (Biotin-Ahx) at the N terminus and amidated at the C terminus. The amino acid sequence of all peptides in this study is shown in fig. S2B.

Proteins

The CoV proteins were produced and purified as described (*54*).

S proteins

A codon-optimized gene encoding residues 1 to 1208 of the SARS-CoV-2 S ectodomain (GenBank: MN908947) was synthesized and cloned into the mammalian expression vector pcDNA3.1(+) by GenScript; the sequence contains proline substitutions at residues 986 and 987 (S-2P), a "GSAS" substitution at the furin cleavage site (residues 682 to 685), a C-terminal T4 fibritin trimerization motif, and a C-terminal octa-histidine tag. SARS-CoV-2 S ectodomains corresponding to the SARS-CoV-2 VOCs were based on the following: Delta, GenBank: QWK65230.1; Omicron BA.1, GenBank: UFO69279.1; and Omicron BA.4/BA.5, GenBank: UPP14409.1 + G3V. MERS and HCoV-229E S ectodomains were based on Protein Data Bank (PDB) 6NB3_A for MERS and PDB 6U7H_A for HcoV-229E (residues 17 to 1142). RBD and SD1-RBD proteins: Plasmids for the production of RBD and SD1-RBD proteins were similarly designed and obtained. RBD and SD1-RBD corresponding to ancestral SARS-CoV-2 were based on an early SARS-CoV-2 sequence isolate (GenBank: QHO60594.1) and included amino acids 331 to 529 and 319 to 591, respectively. RBD and SD1-RBD corresponding to the VOC were based on the following: Alpha, GenBank: QWE88920.1; Beta, GenBank: QRN78347.1; Gamma, GenBank: QVE55289.1; Delta, GenBank: QWK65230.1; Omicron BA.1, GenBank: UFO69279.1; Omicron BA.2, GenBank: UJE45220.1; Omicron BA.2.75, GenBank: UTM82166.1; Omicron BA.2.75.2, GenBank: UTM82166.1 + R343T + F483S; Omicron BA.4/BA.5, GenBank: UPP14409.1; Omicron BA.4.6, GenBank: UPP14409.1 + R341T; Omicron BA.4.7, GenBank: UPP14409.1 + R341S; and Omicron BA.5.9, GenBank: UPP14409.1 + R341I. SD1-RBD T572I and E583D were based on the ancestral SARS-CoV-2 sequence (GenBank: QHO60594.1) with T572I or E583D, respectively. For flow cytometry–based sorting experiments, ancestral SARS-CoV-2 RBD and SD1-RBD constructs were produced that included at the C terminus an Avitag (GLNDIFEAQKIEWHE) for site-directed biotinylation in addition to an octa-histidine tag for purification. ACE2 protein (human ACE2 fused at the C terminus with the Fc of mouse IgG) was produced as previously described (*54*), with the synthetic, codon-optimized nucleotide sequence of hACE2 (residues 18 to 740) fused at the C terminus to the Fc region of human IgG1 and cloned into a pcDNA3.1(+) vector by GenScript. All proteins were produced by transient polyethylenimine (PEI) transfection in Expi293F cells (Thermo Fisher Scientific), purified from the cell supernatants with proper affinity columns, and analyzed to ensure functionality, stability, lack of aggregation, and batch-to-batch reproducibility as previously described (*54*).

Enzyme-linked immunosorbent assays

To evaluate the ability of antibodies to bind to peptides and proteins of CoVs, we performed ELISAs.

Peptide ELISA

Ninety-six–well plates (Thermo Fisher Scientific, 442404) were coated with 50 μl per well of NeutrAvidin (2 μg/ml) (Life Technologies, 31000) solution in phosphate-buffered saline (PBS) overnight at room temperature. Plates were washed four times with washing buffer [PBS + 0.05% Tween 20 (Sigma-Aldrich)] and incubated with 50 μl per well of 50 nM biotinylated peptide solution in PBS for 1 hour at room temperature. After washing four times with

Downloaded from https://www.science.org on May 03, 2024

washing buffer, we incubated plates with 200 µl per well of blocking buffer (PBS + 2% bovine serum albumin + 0.05% Tween 20) for 2 hours at room temperature. Plates were then washed four times with washing buffer, and serial dilutions of monoclonal antibodies or plasma were added in PBS + 0.05% Tween 20 and incubated for 1 hour at room temperature. To screen for the presence of anti-cold-spot peptide IgGs, we assayed plasma samples at a 1:50 starting dilution followed by seven (Figs. 1C and 3B) or three (fig. S1B) threefold serial dilutions. Monoclonal antibodies were tested starting at the indicated concentrations and followed by threefold serial dilutions. Plates were subsequently washed four times with washing buffer and incubated with anti-human IgG secondary antibody conjugated to horseradish peroxidase (HRP) (GE Healthcare, NA933) at a 1:5000 dilution in PBS + 0.05% Tween 20. Last, after washing four times with washing buffer, we developed plates by the addition of 50 µl per well of the HRP substrate 3,3',5,5'-tetramethylbenzidine (Thermo Fisher Scientific, 34021) for 10 min. The developing reaction was stopped with 50 µl per well of 1 M H_2SO_4 solution, and absorbance was measured at 450 nm with an ELISA microplate reader (BioTek) with Gen5 software. The area under the curve (AUC) was obtained from two independent experiments and plotted with GraphPad Prism.

Protein ELISA

Experiments were performed with 96-well plates coated with 50 µl per well of a protein solution (5 µg/ml) in PBS overnight at room temperature and subsequently blocked and treated as described above. Monoclonal antibodies were tested starting at the indicated concentrations and followed by three-, four-, or fivefold serial dilutions. Cross-reactivity ELISAs on SD1-RBD variants were performed in 96-well plates with half-area (Corning, 3690) and using half of the volumes mentioned above.

ACE2 binding ELISA

Experiments were performed as previously described (*54*). Briefly, 96-well plates with half-area (Corning, 3690) were coated with 25 µl per well of a spike solution (5 µg/ml) in PBS and incubated overnight at 4°C. After washing, blocking was performed with 10% FBS in PBS for 1 hour at room temperature. Monoclonal antibodies were added at the indicated concentrations and followed by threefold serial dilutions in blocking buffer. After washing, 25 µl per well of a solution (5 µg/ml) of human ACE2 fused to the Fc portion of mouse IgG were added to the plate. Detection of ACE2 was performed with an alkaline phosphatase (AP)–conjugated anti-mouse IgG secondary antibody (Southern Biotechnology Associates, 1030-04) diluted 1:500 in blocking buffer.

Protein biotinylation for use in flow cytometry

Purified, Avi-tagged SARS-CoV-2 RBD and SD1-RBD (both corresponding to SARS-CoV-2 ancestral virus) were biotinylated using the Biotin-Protein Ligase-BIRA kit according to the manufacturer's instructions (Avidity). Ovalbumin (Ova) (Sigma-Aldrich, A5503-1G) was biotinylated using the EZ-Link Sulfo-NHS-LC-Biotinylation kit according to the manufacturer's instructions (Thermo Fisher Scientific). Biotinylated Ova and RBD were conjugated to streptavidin-BV711 (BD Biosciences, 563262), and SD1-RBD was conjugated to streptavidin-phycoerythrin (PE) (BD Biosciences, 554061) and streptavidin–Alexa Fluor 647 (AF647, BioLegend, 405237), respectively.

Single-cell sorting by flow cytometry

B cells from PBMCs of uninfected controls or of COVID-19 convalescent individuals were enriched using the pan–B cell isolation kit according to the manufacturer's instructions (Miltenyi Biotec, 130-101-638). The enriched B cells were subsequently stained in fluorescence-activated cell sorting (FACS) buffer (PBS + 2% fetal calf serum + 1 mM EDTA) with the following antibodies/reagents (all at 1:200 dilution) for 30 min on ice: anti–CD20-PE-Cy7 (BD Biosciences, 335828), anti–CD14-APC-eFluor 780 (Thermo Fisher Scientific, 47-0149-42), anti–CD16-APC-eFluor 780 (Thermo Fisher Scientific, 47-0168-41), anti–CD3-APC-eFluor 780 (Thermo Fisher Scientific, 47-0037-41), anti–CD8-APC-eFluor 780 (Invitrogen, 47-0086-42), and Zombie NIR (BioLegend, 423105), as well as fluorophore-labeled Ova and peptides. Live single Zombie-NIR$^-$CD14$^-$CD16$^-$CD3$^-$CD8$^-$CD20$^+$Ova$^-$peptide-PE$^+$peptide-AF647$^+$ B cells were single-cell–sorted into 96-well plates containing 4 µl of lysis buffer [0.5× PBS, 10 mM dithiothreitol, and RNasin ribonuclease inhibitors (3000 U/ml; Promega, N2615)] per well using a FACSAria III, and the analysis was performed with FlowJo software. The isolation of SD1-enriched B cells was performed similarly, except that sorted cells were live single Zombie-NIR$^-$CD14$^-$CD16$^-$CD3$^-$CD8$^-$CD20$^+$Ova$^-$RBD$^-$SD1-RBD-PE$^+$SD1-RBD-AF647$^+$. The gating strategy is shown in fig. S1C.

Antibody gene sequencing, cloning, and expression

Antibody gene sequences were identified as described previously (*4*). Briefly, single-cell RNA was reverse-transcribed (SuperScript III Reverse Transcriptase, Invitrogen, 18080-044), and the complementary DNA was stored at −20°C or used for subsequent amplification of the variable IGH, IGL, and IGK genes by nested PCR and Sanger sequencing. Amplicons from the first PCR reaction were used as templates for sequence- and ligation-independent cloning into antibody expression vectors. Recombinant monoclonal antibodies and Fabs were produced and purified as previously described (*55*). C121, C135 anti–SARS-CoV-2 antibodies, and isotype control anti–Zika virus antibody Z021 were previously published (*4*, *55*); the sequences of antibodies CV3-25 and S2P6 were derived from the literature [GenBank: MW681575.1 and MW681603.1 (*17*); PDB: 7RNJ (*16*)] and produced in-house starting from synthetic DNA (GenScript). The human IgG-like bispecific CoV-X4042 was designed on the basis of the variable regions of antibodies sd1.040 and rbd.042 in the CrossMAb format (*25*). Four pcDNA3.1(+) mammalian expression plasmids for CrossMAb production were synthesized (GenScript), used to transfect Expi293F cells (Thermo Fisher Scientific) in a 1:1:1:1 ratio, and purified from the cell supernatants as previously described (*54*). All of the antibodies were tested to ensure functionality, stability, and batch-to-batch reproducibility.

Cell lines

The 293T$_{ACE2/TMPRSS2}$ cell line was generated by transfecting 293T$_{ACE2}$ (*55*) cells with pCMV3-FLAG-TMPRSS2 (SinoBiological) using Lipofectamine 3000 (Invitrogen) and selected with hygromycin B (200 µg/ml) (Invivogen) 2 days after transfection. 293T cells for pseudotyped virus production were cultured in Dulbecco's modified Eagle's medium (DMEM) supplemented with 10% FBS. 293T$_{ACE2}$ cells were cultured in DMEM supplemented with 10% FBS, 1% nonessential amino acids, 1 mM sodium pyruvate, 1× penicillin/streptomycin, and blasticidin (5 µg/ml). Vero cells

Downloaded from https://www.science.org on May 03, 2024

were from the American Type Culture Collection (CCL-81), and Expi293F and 293FT cells were from Thermo Fisher Scientific (#A14528 and R70007). hMyD88-expressing 293 cells (Invivogen) were cultured in DMEM supplemented with 10% FBS, 1× penicillin/streptomycin, and puromycin (10 μg/ml). Secreted embryonic AP (SEAP) reporter 293 cells expressing hACE2 (Invivogen) were grown in DMEM supplemented with 10% FBS, 1× penicillin/streptomycin, puromycin (1 μg/ml), and Zeocin (100 μg/ml).

SARS-CoV-2–pseudotyped reporter viruses

The generation of plasmids to express a C-terminally truncated SARS-CoV-2 S protein (pSARS-CoV2-S_{trunc}), the HIV-1 structural/regulatory proteins (pHIV$_{NL}$GagPol), and the NanoLuc reporter construct (pCCNanoLuc2AEGFP) was previously described (*56*), and similar to the pSARS-CoV2-S_{trunc} plasmid for the Delta variant, they were gifted by P. Bieniasz and T. Hatziioannou (Rockefeller University, New York). Plasmids expressing Alpha, Beta, Gamma, Delta, Omicron BA.1, BA.2, BA.2.75, BA.2.75.2, and BA.4/BA.5 SARS-CoV-2-S_{trunc} variants were generated in-house by site-directed mutagenesis (QuikChange Multi Site-Directed Mutagenesis Kit, Agilent) starting from synthetic DNA (GenScript). The sequences corresponding to SARS-CoV-2 VOC were based on the following: Alpha (B1.1.7; GenBank QWE88920.1), Beta (B.1.351; GenBank QRN78347.1), Gamma (B.1.1.28.1; GenBank QRX39425.1), Delta (B.1.617.2; GenBank QWK65230), Omicron BA.1 (B.1.1.529; GenBank UFO69279.1), Omicron BA.2 (GenBank ULB15050.1), Omicron BA.2.75 (GenBank UTM82166.1), Omicron BA.2.75.2 (GenBank UTM82166.1 + R343T + F483S + D1196N), and Omicron BA.4/BA.5 (GenBank UPP14409.1 + G3V). In all pseudoviruses, the intracellular domain was similarly truncated, and the S1/S2 furin cleavage site was unchanged. The generation of pseudotyped virus stocks was as previously described, with minor modifications (*51*). Briefly, 293T cells were transfected with pHIV$_{NL}$GagPol, pCCNanoLuc2AEGFP, and pSARS-CoV2-S_{trunc} plasmids using PEI-MAX (Polysciences). At 24 hours after transfection, supernatants containing nonreplicating virions were harvested, filtered, and stored at −80°C. Infectivity was determined by titration on 293T$_{ACE2}$ and 293T$_{ACE2/TMPRSS2}$ cells.

Pseudotyped virus neutralization assay

The assay was performed as previously described (*56*). Briefly, three- or fourfold serially diluted monoclonal antibodies were incubated with the SARS-CoV-2–pseudotyped virus for 1 hour at 37°C. The mixture was subsequently incubated with 293T$_{ACE2}$ or 293T$_{ACE2/TMPRSS2}$ cells for 48 hours, after which the cells were washed once with PBS and lysed with Luciferase Cell Culture Lysis 5× reagent (Promega). NanoLuc Luciferase activity of lysates was then measured using the Nano-Glo Luciferase Assay System (Promega) with the GloMax Discover System reader (Promega). Relative luminescence units were then normalized to those derived from cells infected with SARS-CoV-2–pseudotyped virus in the absence of monoclonal antibodies. The IC_{50} value of monoclonal antibodies was determined using a four-parameter nonlinear regression curve fit (GraphPad Prism).

Inhibition of cell-cell fusion

Inhibition of spike-mediated cell-cell fusion was tested using an assay developed by Invivogen. Briefly, hMyD88-expressing 293 cells (Invivogen, catalog code 293-hmyd) were transfected with Wuhan pSARS-CoV2-S_{trunc} plasmid using jetOptimus (Polyplus). At 24 hours after transfection, cells were resuspended in complete media and incubated with antibodies (200 μg/ml) for 1 hour at 37°C before the addition of SEAP reporter 293 cells expressing hACE2 (Invivogen, catalog code hkb-hace2). Cells were cocultured for 24 hours, and cell-cell fusion was assessed by measuring SEAP activity into cell supernatant using QUANTI-Blue Solution (Invivogen) according to the manufacturer's protocol.

Focus reduction neutralization tests

The assay was performed similarly to how it was previously described (*4*). Briefly, the day before infection, Vero cells were seeded at 1×10^4 cells per well in 96-well plates. The antibodies were diluted to final concentrations in DMEM supplemented with 10% newborn calf serum, penicillin (100 U/ml), streptomycin (100 μg/ml), and 1% glutamine (Sigma-Aldrich, Prague, Czech Republic). Subsequently, the diluted samples were mixed with 1000 plaque-forming units (PFU) per well of ancestral SARS-CoV-2 (strain SARS-CoV-2/human/Czech Republic/951/2020) or Omicron (B.1.1.529-like; hCoV-19/Czech Republic/KNL_2021-110119140/2021) and incubated at 37°C for 90 min. The antibody-virus mixture was then applied directly to Vero cells (multiplicity of infection of ~0.1 PFU per cell) and incubated for 22 hours at 37°C and 5% CO_2. Cells were then fixed by cold acetone-methanol fixation (1:1, v/v) and blocked with 10% FBS. Cells were incubated with a rabbit (2019-nCoV) S1 antibody (1:50; Sino Biological, Duesseldorf, Germany) and then incubated for 1 hour at 37°C with secondary goat anti-rabbit antibodies conjugated with fluorescein isothiocyanate (1:250; Sigma-Aldrich, Prague, Czech Republic). Fluorescence intensity was measured using the Synergy H1 microplate reader (BioTek) with the following parameters: plate type (96-well plate), fluorescence (area scan) excitation/emission (490 nm/525 nm), optics (top) and gain (125), light source (xenon flash), lamp energy (high), reading speed (normal), delay (100 ms), and reading height (6 mm). For Omicron, fluorescent foci were manually counted using an Olympus IX71 epifluorescence microscope, and the numbers obtained were normalized to no-antibody control.

In vivo protection experiments

This study was performed in strict accordance with Czech laws and guidelines on the use of experimental animals and the protection of animals against cruelty (Animal Welfare Act No. 246/1992 Coll.). The protocol was approved by the Ethics Committee for Animal Experiments of the Institute of Parasitology, Institute of Molecular Genetics of the Czech Academy of Sciences, and by the Departmental Expert Committee for Approval of Projects of Experiments on Animals of the Czech Academy of Sciences (approvals 82/2020 and 101/2020). Thirteen- to 15-week-old female C57BL/6NCrl mice were ACE2-humanized by inhalation of a modified AAV (AAV-hACE2) as described previously (*54*). At least 7 days after the application of AAV-hACE2 virus particles, mice were intranasally infected with SARS-CoV-2 [1×10^4 PFU; ancestral strain SARS-CoV-2/human/Czech Republic/951/2020 or Omicron B.1.1.529-like; hCoV-19/Czech Republic/KNL_2021-110119140/2021, both isolated from clinical specimens at the National Institute of Public Health, Prague; passaged five times (six times for Omicron) in Vero E6 cells before use in this study] in a total volume of 50 μl of DMEM. Twenty-four hours before (preexposure

Downloaded from https://www.science.org on May 03, 2024

prophylaxis) or 2 hours after (postexposure prophylaxis) infection, mice were injected intraperitoneally with either hr2.016, CoV-X4042 (both at 300 μg), fp.006 (500 μg in preexposure or 300 μg in postexposure), or isotype control (either at 300 or 500 μg). Mice were culled at the indicated time points after infection, and their tissues were collected for analysis. Lung tissue was homogenized using Mixer Mill MM400 (Retsch, Haan, Germany) and processed as a 20% (w/v) suspension in DMEM containing 10% newborn calf serum. Homogenates were clarified by centrifugation at 14,000*g* (10 min at 4°C), and supernatant medium was used for plaque assay as previously described (*54*).

No sample size calculation was performed. The sample sizes were chosen on the basis of experience and previously published papers [e.g., (*57*, *58*)]. Details about groups and sample sizes for mouse virus challenge studies are provided in the figure legends. Experiments were successfully repeated at least twice. No data were excluded. The mice were randomly assigned to cages, and the cages were then randomized into groups. Blinding was not relevant to this study. The readouts of all experiments could be assessed objectively. Mouse weight loss was determined using body weight measurement as a readout, and plaque assay was used to quantify viral burden.

X-ray crystallography

fp.006 Fab in 1× Tris-buffered saline (TBS) (20 mM Tris and 150 mM NaCl) was mixed with the FP (PBS with 10% DMSO; PSKRSFIEDLLFNKVTLADA with N-terminal Biotin-Ahx and C-terminal amidation) at a 1:2 molar ratio (Fab:peptide). The sample was incubated overnight at room temperature and then concentrated to ~8.8 mg/ml using an Amicon spin filter with a 30-kDa molecular weight cutoff (Millipore-Sigma) after diluting with an additional sample volume of 1× TBS to decrease the proportion of PBS and DMSO in the complex.

Crystallization trials were set up using the sitting drop vapor diffusion method by mixing equal volumes of fp.006-FP complex and reservoir using a Douglas Oryx8 robot and commercially available 96-well crystallization screens (Hampton Research). Crystals were grown at 16°C and observed under multiple conditions. The single crystal that was used for structure determination of fp.006-FP was obtained in 0.2 M potassium phosphate monobasic (pH 4.8) and 20% (w/v) polyethylene glycol 3350 and was cryoprotected in a solution matching the reservoir and 30% glycerol and then cryocooled in liquid nitrogen.

X-ray diffraction data were collected at the Stanford Synchrotron Radiation Lightsource (SSRL) beamline 12-1 with an Eiger X 16M pixel detector (Dectris) at a wavelength of 0.979 Å and temperature of 100 K. Data from a single crystal were indexed and integrated in X-ray Detector Software (XDS)/Dials (*59*) and then merged using AIMLESS in CCP4 (*60*). Structures were determined using molecular replacement in PHASER (*61*) using two copies of each of the following individual chains as search models: V_H (variable region of Ig heavy chain; PDB: 4GXU chain M with CRH3 trimmed), V_L (variable region of Ig light chain; PDB: 6FG1 chain B with CDRL3 trimmed), C_H (PDB: 4GXU), and C_L (PDB: 6FG1). Coordinates were refined using iterative rounds of automated and interactive refinement in Phenix (*62*) and Coot (*63*), respectively. The final model contains 97.9% Ramachandran-favored residues, with 2.0% allowed and the remaining 0.1% Ramachandran outliers.

Detection of monoclonal antibody binding to S by flow cytometry

A total of 1.9×10^6 293T cells were plated in 60 mm–by–15 mm dishes (Corning, reference no. 430166) and cotransfected with two plasmids encoding green fluorescent protein (GFP) (2.25 μg) and the SARS-CoV-2 S protein (pSARS-CoV2-S_{trunc}; 2.25 μg) using 18 μg of PEI-MAX as a transfection reagent 24 hours later. Forty hours upon transfection, cells were collected by gentle pipetting, and 50,000 transfected cells per well (in U-bottom 96-well plates; Corning, reference no. 3799) were subsequently stained with prelabeled monoclonal antibodies (10 μg/ml) in the presence or absence of human ACE2 (30 μg/ml) in a total volume of 100 μl of PBS supplemented with 5% FBS and 2 mM EDTA for 2 hours at room temperature, similar to a previous report (Fig. 2H) (*18*). In Fig. 4F, cells were preincubated with sd1.040 or Z021 (isotype) antibodies at a final concentration of 10 μg/ml for 30 min at room temperature before the addition of ACE2 and prelabeled fp.006. Fluorescent labeling of monoclonal antibodies was performed with the DY-647P1-NHS-ester reagent (Dyomics, reference no. 647P1-01) according to the manufacturer's instructions. After staining, cells were washed twice, acquired with BD FACSCanto, and analyzed with FlowJo software.

Cryo-EM sample preparation

Concentrated and purified sd1.040 Fab was mixed with SARS-CoV-2 S-2P trimer at a 1.1:1 molar ratio (Fab:trimer) to a final concentration of 3 mg/ml and incubated at room temperature for 30 min. Immediately before the application of 3.1 μl of sample to a freshly glow-discharged 300-mesh Quantifoil R1.2/1.3 grid, fluorinated octyl-maltoside was added to a final concentration of 0.02% (w/v). Complex was vitrified by plunging into 100% liquid ethane after blotting for 3.5 s with Whatman no. 1 filter paper at 22°C and 100% humidity using a Mark IV Vitrobot (Thermo Fisher Scientific).

Cryo-EM data collection and processing

Single-particle movies were collected on a Titan Krios TEM (300 kV) using SerialEM automated data collection software (*64*) and a K3 camera (Gatan) behind a BioQuantum energy filter (Gatan) with a 20-eV slit size (0.85 Å/pixel). Specific collection parameters are summarized in table S2. Data processing followed a similar workflow as that previously described (*65*). Briefly, 9894 movies were patch motion–corrected for beam-induced motion including dose weighting within cryoSPARC v3.1 (*66*). CTF estimates were performed on non–dose-weighted micrographs, which were subsequently curated to remove poor fits and images with thick ice. An initial set of particles was generated using automated blob picking, of which a subset (300,000 particles) was used to generate four ab initio volumes. The entire particle stack (4,343,219 particles) was extracted, binned four times, and heterogeneously refined into the four ab initio volumes. Particles corresponding to the volume that best demonstrated features of a Fab bound to a protomer were cleaned up using two-dimensional (2D) classification and reextracted with 2× binning. The resulting particle stack (1,552,774 particles) was further 3D-classified in cryoSPARC ($k = 6$). Particles corresponding to the 3D volumes with well-defined secondary structural features were pooled and homogeneously refined with C1 symmetry. After CTF refinement and application of a mask for focus refinement on the RBD-SD1-Fab regions, the final

Downloaded from https://www.science.org on May 03, 2024

reconstructed volume achieved a global resolution of 3.7 Å based on gold standard FSC calculations.

Cryo-EM structure modeling and refinement

Coordinates for the sd1.040–S1 protomer complex were generated by docking individual domains from reference structures (individual spike domains, PDB: 6VXX–chain A; Fab heavy chain, PDB: 5AZE–chain H; Fab light chain, PDB: 7D0D–chain L) into cryo-EM density using UCSF Chimera (*67*). Initial models were rigid body–refined into cryo-EM density, followed by real-space refinement with morphing in Phenix. Sequence matching was interactively performed in Coot, and models were further refined in Phenix. Validation of model coordinates was performed using MolProbity (*68*).

Structural analyses

CDR and somatic mutation assignments were produced by IMGT V-QUEST (*69*). Graphics describing structures were made in Chimera X (*70*). BSAs were calculated using the online PDBePISA server (). Contacting residues are defined as those with less than 4 Å of distance between atoms of different chains. Hydrogen bond assignments were made using a 3.5 Å cutoff and an A-D-H angle greater than 90°. Root mean square deviation calculations were performed in PyMOL (Schrödinger). Antibody residues are numbered according to the Kabat convention.

SPR assays

The IgG antibody or Fab binding properties were analyzed at 25°C using a Biacore 8K instrument (GE Healthcare) with 10 mM Hepes (pH 7.4), 150 mM NaCl, 3 mM EDTA, and 0.005% Tween 20 as running buffer. SARS-CoV-2 antigens (SD1-RBD or S-2P) were immobilized on the surface of CM5 chips (Cytiva) through standard amine coupling. Increasing concentrations of IgG/Fab were injected using a single-cycle kinetic setting, and dissociation was followed for 10 min. Analyte responses were corrected for unspecific binding and buffer responses. Curve fitting and data analysis were performed with Biacore Insight Evaluation Software v.2.0.15.12933. Competition experiments were performed to obtain information on the IgG/Fab binding regions. The first antibody was immobilized on the surface of CM5 chips (Cytiva) through standard amine coupling; SD1-RBD was then flowed to form the SD1-RBD/antibody complex, and shortly thereafter, the second antibody was injected. If a binding event is detected at the final step, then the second antibody has a different epitope compared with the first (immobilized) antibody. If no binding event is detected, the two antibodies share overlapping epitopes. Competition experiments were also used to confirm the functionality of both arms of the CoV-X4042 bispecific. First, sd1.040 or rbd.042 antibodies were immobilized on the surface of CM5 chips (Cytiva) through standard amine coupling; then, SD1-RBD was flowed to form the RBD-SD1/antibody complex, and shortly thereafter, CoV-X4042 was injected. The analysis and comparison of kinetic parameters at different SD1-RBD concentrations were also performed as previously described (*54*) to assess the ability of CoV-X4042 to bind bivalently to a single SD1-RBD molecule.

Statistical analyses

Statistical significance between two groups of mice was determined using nonparametric two-tailed Mann-Whitney *U* tests. For paired samples, we used the two-tailed *t* test. For *P* value calculation of Fig. 5C, we used the more stringent Welch's *t* test, two-tailed, which does not assume equal variance of the two samples. Correlation between plasma IgG reactivity to SARS-CoV-2 RBD and SD1-RBD was assessed using Pearson's correlation analysis. $P < 0.05$ was considered statistically significant. In the figures, significance is shown as follows: ns $P \geq 0.05$ (not significant), $^{*}P < 0.05$, $^{**}P < 0.01$, $^{***}P < 0.001$, and $^{****}P < 0.0001$. Data and statistical analyses were performed with GraphPad Prism (version 8.4.3).

Supplementary Materials

This PDF file includes:
Figs. S1 to S8
Tables S1 and S2

Other Supplementary Material for this manuscript includes the following:
Data files S1 to S3
MDAR Reproducibility Checklist

View/request a protocol for this paper from *Bio-protocol*.

REFERENCES AND NOTES

1. P. S. Masters, The molecular biology of coronaviruses. *Adv. Virus Res.* **66**, 193–292 (2006).
2. P. V'kovski, A. Kratzel, S. Steiner, H. Stalder, V. Thiel, Coronavirus biology and replication: Implications for SARS-CoV-2. *Nat. Rev. Microbiol.* **19**, 155–170 (2021).
3. C. B. Jackson, M. Farzan, B. Chen, H. Choe, Mechanisms of SARS-CoV-2 entry into cells. *Nat. Rev. Mol. Cell Biol.* **23**, 3–20 (2022).
4. D. F. Robbiani, C. Gaebler, F. Muecksch, J. C. C. Lorenzi, Z. Wang, A. Cho, M. Agudelo, C. O. Barnes, A. Gazumyan, S. Finkin, T. Hägglöf, T. Y. Oliveira, C. Viant, A. Hurley, H.-H. Hoffmann, K. G. Millard, R. G. Kost, M. Cipolla, K. Gordon, F. Bianchini, S. T. Chen, V. Ramos, R. Patel, J. Dizon, I. Shimeliovich, P. Mendoza, H. Hartweger, L. Nogueira, M. Pack, J. Horowitz, F. Schmidt, Y. Weisblum, E. Michailidis, A. W. Ashbrook, E. Waltari, J. E. Pak, K. E. Huey-Tubman, N. Koranda, P. R. Hoffman, A. P. West Jr., C. M. Rice, T. Hatziioannou, P. J. Bjorkman, P. D. Bieniasz, M. Caskey, M. C. Nussenzweig, Convergent antibody responses to SARS-CoV-2 in convalescent individuals. *Nature* **584**, 437–442 (2020).
5. M. McCallum, A. De Marco, F. A. Lempp, M. A. Tortorici, D. Pinto, A. C. Walls, M. Beltramello, A. Chen, Z. Liu, F. Zatta, S. Zepeda, J. di Iulio, J. E. Bowen, M. Montiel-Ruiz, J. Zhou, L. E. Rosen, S. Bianchi, B. Guarino, C. S. Fregni, R. Abdelnabi, S.-Y. C. Foo, P. W. Rothlauf, L.-M. Bloyet, F. Benigni, E. Cameroni, J. Neyts, A. Riva, G. Snell, A. Telenti, S. P. J. Whelan, H. W. Virgin, D. Corti, M. S. Pizzuto, D. Veesler, N-terminal domain antigenic mapping reveals a site of vulnerability for SARS-CoV-2. *Cell* **184**, 2332–2347.e16 (2021).
6. Z. Wang, F. Muecksch, A. Cho, C. Gaebler, H.-H. Hoffmann, V. Ramos, S. Zong, M. Cipolla, B. Johnson, F. Schmidt, J. DaSilva, E. Bednarski, T. Ben Tanfous, R. Raspe, K. Yao, Y. E. Lee, T. Chen, M. Turroja, K. G. Milard, J. Dizon, A. Kaczynska, A. Gazumyan, T. Y. Oliveira, C. M. Rice, M. Caskey, P. D. Bieniasz, T. Hatziioannou, C. O. Barnes, M. C. Nussenzweig, Analysis of memory B cells identifies conserved neutralizing epitopes on the N-terminal domain of variant SARS-Cov-2 spike proteins. *Immunity* **55**, 998–1012.e8 (2022).
7. S. Iketani, L. Liu, Y. Guo, L. Liu, J. F.-W. Chan, Y. Huang, M. Wang, Y. Luo, J. Yu, H. Chu, K. K.-H. Chik, T. T.-T. Yuen, M. T. Yin, M. E. Sobieszczyk, Y. Huang, K.-Y. Yuen, H. H. Wang, Z. Sheng, D. D. Ho, Antibody evasion properties of SARS-CoV-2 Omicron sublineages. *Nature* **604**, 553–556 (2022).
8. E. Takashita, N. Kinoshita, S. Yamayoshi, Y. Sakai-Tagawa, S. Fujisaki, M. Ito, K. Iwatsuki-Horimoto, P. Halfmann, S. Watanabe, K. Maeda, M. Imai, H. Mitsuya, N. Ohmagari, M. Takeda, H. Hasegawa, Y. Kawaoka, Efficacy of antiviral agents against the SARS-CoV-2 Omicron subvariant BA.2. *N. Engl. J. Med.* **386**, 1475–1477 (2022).
9. R. E. Chen, E. S. Winkler, J. B. Case, I. D. Aziati, T. L. Bricker, A. Joshi, T. L. Darling, B. Ying, J. M. Errico, S. Shrihari, L. A. VanBlargan, X. Xie, P. Gilchuk, S. J. Zost, L. Droit, Z. Liu, S. Stumpf, D. Wang, S. A. Handley, W. B. Stine Jr., P.-Y. Shi, M. E. Davis-Gardner, M. S. Suthar, M. G. Knight, R. Andino, C. Y. Chiu, A. H. Ellebedy, D. H. Fremont, S. P. J. Whelan, J. E. Crowe Jr., L. Purcell, D. Corti, A. C. M. Boon, M. S. Diamond, In vivo monoclonal antibody efficacy against SARS-CoV-2 variant strains. *Nature* **596**, 103–108 (2021).
10. M. McCallum, N. Czudnochowski, L. E. Rosen, S. K. Zepeda, J. E. Bowen, A. C. Walls, K. Hauser, A. Joshi, C. Stewart, J. R. Dillen, A. E. Powell, T. I. Croll, J. Nix, H. W. Virgin, D. Corti, G. Snell,

Downloaded from https://www.science.org on May 03, 2024

D. Veesler, Structural basis of SARS-CoV-2 Omicron immune evasion and receptor engagement. *Science* **375**, 864–868 (2022).
11. J. A. Lednicky, M. S. Tagliamonte, S. K. White, M. A. Elbadry, M. M. Alam, C. J. Stephenson, T. S. Bonny, J. C. Loeb, T. Telisma, S. Chavannes, D. A. Ostrov, C. Mavian, V. M. Beau De Rochars, M. Salemi, J. G. Morris Jr., Independent infections of porcine deltacoronavirus among Haitian children. *Nature* **600**, 133–137 (2021).
12. J. D. Zehr, S. L. K. Pond, D. P. Martin, K. Ceres, G. R. Whittaker, J. K. Millet, L. B. Goodman, M. J. Stanhope, Recent zoonotic spillover and tropism shift of a canine coronavirus is associated with relaxed selection and putative loss of function in NTD subdomain of spike protein. *Viruses* **14**, 853 (2022).
13. M. A. Tortorici, A. C. Walls, A. Joshi, Y.-J. Park, R. T. Eguia, M. C. Miranda, E. Kepl, A. Dosey, T. Stevens-Ayers, M. J. Boeckh, A. Telenti, A. Lanzavecchia, N. P. King, D. Corti, J. D. Bloom, D. Veesler, Structure, receptor recognition, and antigenicity of the human coronavirus CCoV-HuPn-2018 spike glycoprotein. *Cell* **185**, 2279–2291.e17 (2022).
14. S. Khare, C. Gurry, L. Freitas, M. B. Schultz, G. Bach, A. Diallo, N. Akite, J. Ho, R. T. Lee, W. Yeo; Gisaid Core Curation Team, S. Maurer-Stroh, GISAID's role in pandemic response. *China CDC Wkly.* **3**, 1049–1051 (2021).
15. A. N. Vlasova, A. Diaz, D. Damtie, L. Xiu, T.-H. Toh, J. S.-Y. Lee, L. J. Saif, G. C. Gray, Novel canine coronavirus isolated from a hospitalized patient with pneumonia in East Malaysia. *Clin. Infect. Dis.* **74**, 446–454 (2022).
16. D. Pinto, M. M. Sauer, N. Czudnochowski, J. S. Low, M. A. Tortorici, M. P. Housley, J. Noack, A. C. Walls, J. E. Bowen, B. Guarino, L. E. Rosen, J. di Iulio, J. Jerak, H. Kaiser, S. Islam, S. Jaconi, N. Sprugasci, K. Culap, R. Abdelnabi, C. Foo, L. Coelmont, I. Bartha, S. Bianchi, C. Silacci-Fregni, J. Bassi, R. Marzi, E. Vetti, A. Cassotta, A. Ceschi, P. Ferrari, P. E. Cippà, O. Giannini, S. Ceruti, C. Garzoni, A. Riva, F. Benigni, E. Cameroni, L. Piccoli, M. S. Pizzuto, M. Smithey, D. Hong, A. Telenti, F. A. Lempp, J. Neyts, C. Havenar-Daughton, A. Lanzavecchia, F. Sallusto, G. Snell, H. W. Virgin, M. Beltramello, D. Corti, D. Veesler, Broad betacoronavirus neutralization by a stem helix–specific human antibody. *Science* **373**, 1109–1116 (2021).
17. M. F. Jennewein, A. J. MacCamy, N. R. Akins, J. Feng, L. J. Homad, N. K. Hurlburt, E. Seydoux, Y.-H. Wan, A. B. Stuart, V. V. Edara, K. Floyd, A. Vanderheiden, J. R. Mascola, N. Doria-Rose, L. Wang, E. S. Yang, H. Y. Chu, J. L. Torres, G. Ozorowski, A. B. Ward, R. E. Whaley, K. W. Cohen, M. Pancera, M. J. McElrath, J. A. Englund, A. Finzi, M. S. Suthar, A. T. McGuire, L. Stamatatos, Isolation and characterization of cross-neutralizing coronavirus antibodies from COVID-19+ subjects. *Cell Rep.* **36**, 109353 (2021).
18. J. S. Low, J. Jerak, M. A. Tortorici, M. McCallum, D. Pinto, A. Cassotta, M. Foglierini, F. Mele, R. Abdelnabi, B. Weynand, J. Noack, M. Montiel-Ruiz, S. Bianchi, F. Benigni, N. Sprugasci, A. Joshi, J. E. Bowen, C. Stewart, M. Rexhepaj, A. C. Walls, D. Jarrossay, D. Morone, P. Paparoditis, C. Garzoni, P. Ferrari, A. Ceschi, J. Neyts, L. A. Purcell, G. Snell, D. Corti, A. Lanzavecchia, D. Veesler, F. Sallusto, ACE2-binding exposes the SARS-CoV-2 fusion peptide to broadly neutralizing coronavirus antibodies. *Science* **377**, 735–742 (2022).
19. C. Dacon, C. Tucker, L. Peng, C.-C. D. Lee, T.-H. Lin, M. Yuan, Y. Cong, L. Wang, L. Purser, J. K. Williams, C.-W. Pyo, I. Kosik, Z. Hu, M. Zhao, D. Mohan, A. J. R. Cooper, M. Peterson, J. Skinner, S. Dixit, E. Kollins, L. Huzella, D. Perry, R. Byrum, S. Lembirik, D. Drawbaugh, B. Eaton, Y. Zhang, E. S. Yang, M. Chen, K. Leung, R. S. Weinberg, A. Pegu, D. E. Geraghty, E. Davidson, I. Douagi, S. Moir, J. W. Yewdell, C. Schmaljohn, P. D. Crompton, M. R. Holbrook, D. Nemazee, J. R. Mascola, I. A. Wilson, J. Tan, Broadly neutralizing antibodies target the coronavirus fusion peptide. *Science* **377**, 728–735 (2022).
20. X. Sun, C. Yi, Y. Zhu, L. Ding, S. Xia, X. Chen, M. Liu, C. Gu, X. Lu, Y. Fu, S. Chen, T. Zhang, Y. Zhang, Z. Yang, L. Ma, W. Gu, G. Hu, S. Du, R. Yan, W. Fu, S. Yuan, C. Qiu, C. Zhao, X. Zhang, Y. He, A. Qu, X. Zhou, X. Li, G. Wong, Q. Deng, Q. Zhou, H. Lu, Z. Ling, J. Ding, L. Lu, J. Xu, Y. Xie, B. Sun, Neutralization mechanism of a human antibody with pan-coronavirus reactivity including SARS-CoV-2. *Nat. Microbiol.* **7**, 1063–1074 (2022).
21. J. Jaimes, J. Millet, G. Whittaker, Proteolytic cleavage of the SARS-CoV-2 spike protein and the role of the novel S1/S2 site. *iScience* **23**, 101212 (2020).
22. M.-M. Zhao, W.-L. Yang, F.-Y. Yang, L. Zhang, W.-J. Huang, W. Hou, C.-F. Fan, R.-H. Jin, Y.-M. Feng, Y.-C. Wang, J.-K. Yang, Cathepsin L plays a key role in SARS-CoV-2 infection in humans and humanized mice and is a promising target for new drug development. *Signal Transduct. Target. Ther.* **6**, 134 (2021).
23. J. Seow, H. Khan, A. Rosa, V. Calvaresi, C. Graham, S. Pickering, V. E. Pye, N. B. Cronin, I. Huettner, M. H. Malim, A. Politis, P. Cherepanov, K. J. Doores, A neutralizing epitope on the SD1 domain of SARS-CoV-2 spike targeted following infection and vaccination. *Cell Rep.* **40**, 111276 (2022).
24. Q. Hong, W. Han, J. Li, S. Xu, Y. Wang, C. Xu, Z. Li, Y. Wang, C. Zhang, Z. Huang, Y. Cong, Molecular basis of receptor binding and antibody neutralization of Omicron. *Nature* **604**, 546–552 (2022).
25. W. Schaefer, J. T. Regula, M. Bähner, J. Schanzer, R. Croasdale, H. Dürr, C. Gassner, G. Georges, H. Kettenberger, S. Imhof-Jung, M. Schwaiger, K. G. Stubenrauch, C. Sustmann, M. Thomas, W. Scheuer, C. Klein, Immunoglobulin domain crossover as a generic approach for the production of bispecific IgG antibodies. *Proc. Natl. Acad. Sci. U.S.A.* **108**, 11187–11192 (2011).
26. D. Corti, L. A. Purcell, G. Snell, D. Veesler, Tackling COVID-19 with neutralizing monoclonal antibodies. *Cell* **184**, 3086–3108 (2021).
27. P. Chen, A. Nirula, B. Heller, R. L. Gottlieb, J. Boscia, J. Morris, G. Huhn, J. Cardona, B. Mocherla, V. Stosor, I. Shawa, A. C. Adams, J. Van Naarden, K. L. Custer, L. Shen, M. Durante, G. Oakley, A. E. Schade, J. Sabo, D. R. Patel, P. Klekotka, D. M. Skovronsky; BLAZE-1 Investigators, SARS-CoV-2 neutralizing antibody LY-CoV555 in outpatients with Covid-19. *N. Engl. J. Med.* **384**, 229–237 (2021).
28. R. L. Gottlieb, A. Nirula, P. Chen, J. Boscia, B. Heller, J. Morris, G. Huhn, J. Cardona, B. Mocherla, V. Stosor, I. Shawa, P. Kumar, A. C. Adams, J. Van Naarden, K. L. Custer, M. Durante, G. Oakley, A. E. Schade, T. R. Holzer, P. J. Ebert, R. E. Higgs, N. L. Kallewaard, J. Sabo, D. R. Patel, P. Klekotka, L. Shen, D. M. Skovronsky, Effect of bamlanivimab as monotherapy or in combination with etesevimab on viral load in patients with mild to moderate COVID-19: A randomized clinical trial. *JAMA* **325**, 632–644 (2021).
29. D. M. Weinreich, S. Sivapalasingam, T. Norton, S. Ali, H. Gao, R. Bhore, B. J. Musser, Y. Soo, D. Rofail, J. Im, C. Perry, C. Pan, R. Hosain, A. Mahmood, J. D. Davis, K. C. Turner, A. T. Hooper, J. D. Hamilton, A. Baum, C. A. Kyratsous, Y. Kim, A. Cook, W. Kampman, A. Kohli, Y. Sachdeva, X. Graber, B. Kowal, T. DiCioccio, N. Stahl, L. Lipsich, N. Braunstein, G. Herman, G. D. Yancopoulos; Trial Investigators, REGN-COV2, a neutralizing antibody cocktail, in outpatients with Covid-19. *N. Engl. J. Med.* **384**, 238–251 (2021).
30. A. Gupta, Y. Gonzalez-Rojas, E. Juarez, M. Crespo Casal, J. Moya, D. R. Falci, E. Sarkis, J. Solis, H. Zheng, N. Scott, A. L. Cathcart, C. M. Hebner, J. Sager, E. Mogalian, C. Tipple, A. Peppercorn, E. Alexander, P. S. Pang, A. Free, C. Brinson, M. Aldinger, A. E. Shapiro; COMET-ICE Investigators, Early treatment for Covid-19 with SARS-CoV-2 neutralizing antibody sotrovimab. *N. Engl. J. Med.* **385**, 1941–1950 (2021).
31. M. Hoffmann, N. Krüger, S. Schulz, A. Cossmann, C. Rocha, A. Kempf, I. Nehlmeier, L. Graichen, A.-S. Moldenhauer, M. S. Winkler, M. Lier, A. Dopfer-Jablonka, H.-M. Jäck, G. M. N. Behrens, S. Pöhlmann, The Omicron variant is highly resistant against antibody-mediated neutralization: Implications for control of the COVID-19 pandemic. *Cell* **185**, 447–456.e11 (2022).
32. E. C. Thomson, L. E. Rosen, J. G. Shepherd, R. Spreafico, A. da Silva Filipe, J. A. Wojcechowskyj, C. Davis, L. Piccoli, D. J. Pascall, J. Dillen, S. Lytras, N. Czudnochowski, R. Shah, M. Meury, N. Jesudason, A. De Marco, K. Li, J. Bassi, A. O'Toole, D. Pinto, R. M. Colquhoun, K. Culap, B. Jackson, F. Zatta, A. Rambaut, S. Jaconi, V. B. Sreenu, J. Nix, I. Zhang, R. F. Jarrett, W. G. Glass, M. Beltramello, K. Nomikou, M. Pizzuto, L. Tong, E. Cameroni, T. I. Croll, N. Johnson, J. Di Iulio, A. Wickenhagen, A. Ceschi, A. M. Harbison, D. Mair, P. Ferrari, K. Smollett, F. Sallusto, S. Carmichael, C. Garzoni, J. Nichols, M. Galli, J. Hughes, A. Riva, A. Ho, M. Schiuma, M. G. Semple, P. J. M. Openshaw, E. Fadda, J. K. Baillie, J. D. Chodera; ISARIC4C Investigators; COVID-19 Genomics UK (COG-UK) Consortium, S. J. Rihn, S. J. Lycett, H. W. Virgin, A. Telenti, D. Corti, D. L. Robertson, G. Snell, Circulating SARS-CoV-2 spike N439K variants maintain fitness while evading antibody-mediated immunity. *Cell.* **184**, 1171–1187.e20 (2021).
33. K. R. McCarthy, L. J. Rennick, S. Nambulli, L. R. Robinson-McCarthy, W. G. Bain, G. Haidar, W. P. Duprex, Recurrent deletions in the SARS-CoV-2 spike glycoprotein drive antibody escape. *Science* **371**, 1139–1142 (2021).
34. K. Westendorf, S. Žentelis, L. Wang, D. Foster, P. Vaillancourt, M. Wiggin, E. Lovett, R. van der Lee, J. Hendle, A. Pustilnik, J. M. Sauder, L. Kraft, Y. Hwang, R. W. Siegel, J. Chen, B. A. Heinz, R. E. Higgs, N. L. Kallewaard, K. Jepson, R. Goya, M. A. Smith, D. W. Collins, D. Pellacani, P. Xiang, V. de Puyraimond, M. Ricicova, L. Devorkin, C. Pritchard, A. O'Neill, K. Dalal, P. Panwar, H. Dhupar, F. A. Garces, C. A. Cohen, J. M. Dye, K. E. Huie, C. V. Badger, D. Kobasa, J. Audet, J. J. Freitas, S. Hassanali, I. Hughes, L. Munoz, H. C. Palma, B. Ramamurthy, R. W. Cross, T. W. Geisbert, V. Menachery, K. Lokugamage, V. Borisevich, I. Lanz, L. Anderson, P. Sipahimalani, K. S. Corbett, E. S. Yang, Y. Zhang, W. Shi, T. Zhou, M. Choe, J. Misasi, P. D. Kwong, N. J. Sullivan, B. S. Graham, T. L. Fernandez, C. L. Hansen, E. Falconer, J. R. Mascola, B. E. Jones, B. C. Barnhart, LY-CoV1404 (bebtelovimab) potently neutralizes SARS-CoV-2 variants. *Cell Rep.* **39**, 110812 (2022).
35. A. A. Cohen, P. N. P. Gnanapragasam, Y. E. Lee, P. R. Hoffman, S. Ou, L. M. Kakutani, J. R. Keeffe, H.-J. Wu, M. Howarth, A. P. West, C. O. Barnes, M. C. Nussenzweig, P. J. Bjorkman, Mosaic nanoparticles elicit cross-reactive immune responses to zoonotic coronaviruses in mice. *Science* **371**, 735–741 (2021).
36. A. A. Cohen, N. van Doremalen, A. J. Greaney, H. Andersen, A. Sharma, T. N. Starr, J. R. Keeffe, C. Fan, J. E. Schulz, P. N. P. Gnanapragasam, L. M. Kakutani, A. P. West, G. Saturday, Y. E. Lee, H. Gao, C. A. Jette, M. G. Lewis, T. K. Tan, A. R. Townsend, J. D. Bloom, V. J. Munster, P. J. Bjorkman, Mosaic RBD nanoparticles protect against challenge by diverse sarbecoviruses in animal models. *Science* **377**, eabq0839 (2022).
37. C. A. Jette, A. A. Cohen, P. N. P. Gnanapragasam, F. Muecksch, Y. E. Lee, K. E. Huey-Tubman, F. Schmidt, T. Hatziioannou, P. D. Bieniasz, M. C. Nussenzweig, A. P. West Jr., J. R. Keeffe, P. J. Bjorkman, C. O. Barnes, Broad cross-reactivity across sarbecoviruses exhibited by a subset of COVID-19 donor-derived neutralizing antibodies. *Cell Rep.* **36**, 109760 (2021).
38. D. R. Martinez, A. Schäfer, S. Gobeil, D. Li, G. De la Cruz, R. Parks, X. Lu, M. Barr, V. Stalls, K. Janowska, E. Beaudoin, K. Manne, K. Mansouri, R. J. Edwards, K. Cronin, B. Yount, K. Anasti,

Downloaded from https://www.science.org on May 03, 2024

S. A. Montgomery, J. Tang, H. Golding, S. Shen, T. Zhou, P. D. Kwong, B. S. Graham, J. R. Mascola, D. C. Montefiori, S. M. Alam, G. D. Sempowski, S. Khurana, K. Wiehe, K. O. Saunders, P. Acharya, B. F. Haynes, R. S. Baric, A broadly cross-reactive antibody neutralizes and protects against sarbecovirus challenge in mice. *Sci. Transl. Med.* **14**, eabj7125 (2021).

39. A. C. Walls, M. C. Miranda, A. Schäfer, M. N. Pham, A. Greaney, P. S. Arunachalam, M.-J. Navarro, M. A. Tortorici, K. Rogers, M. A. O'Connor, L. Shirreff, D. E. Ferrell, J. Bowen, N. Brunette, E. Kepl, S. K. Zepeda, T. Starr, C.-L. Hsieh, B. Fiala, S. Wrenn, D. Pettie, C. Sydeman, K. R. Sprouse, M. Johnson, A. Blackstone, R. Ravichandran, C. Ogohara, L. Carter, S. W. Tilles, R. Rappuoli, S. R. Leist, D. R. Martinez, M. Clark, R. Tisch, D. T. O'Hagan, R. Van Der Most, W. C. V. Voorhis, D. Corti, J. S. McLellan, H. Kleanthous, T. P. Sheahan, K. D. Smith, D. H. Fuller, F. Villinger, J. Bloom, B. Pulendran, R. S. Baric, N. P. King, D. Veesler, Elicitation of broadly protective sarbecovirus immunity by receptor-binding domain nanoparticle vaccines. *Cell* **184**, 5432–5447.e16 (2021).
40. C. Fan, A. A. Cohen, M. Park, A. F.-H. Hung, J. R. Keeffe, P. N. P. Gnanapragasam, Y. E. Lee, H. Gao, L. M. Kakutani, Z. Wu, H. Kleanthous, K. E. Malecek, J. C. Williams, P. J. Bjorkman, Neutralizing monoclonal antibodies elicited by mosaic RBD nanoparticles bind conserved sarbecovirus epitopes. *Immunity* **55**, 2419–2435.e10 (2022).
41. Y. Chen, X. Zhao, H. Zhou, H. Zhu, S. Jiang, P. Wang, Broadly neutralizing antibodies to SARS-CoV-2 and other human coronaviruses. *Nat. Rev. Immunol.*, 10.1038/s41577-022-00784-3 (2022).
42. P. Zhou, M. Yuan, G. Song, N. Beutler, N. Shaabani, D. Huang, W.-T. He, X. Zhu, S. Callaghan, P. Yong, F. Anzanello, L. Peng, J. Ricketts, M. Parren, E. Garcia, S. A. Rawlings, D. M. Smith, D. Nemazee, J. R. Teijaro, T. F. Rogers, I. A. Wilson, D. R. Burton, R. Andrabi, A human antibody reveals a conserved site on beta-coronavirus spike proteins and confers protection against SARS-CoV-2 infection. *Sci. Transl. Med.* **14**, eabi9215 (2022).
43. N. L. Kallewaard, D. Corti, P. J. Collins, U. Neu, J. M. McAuliffe, E. Benjamin, L. Wachter-Rosati, F. J. Palmer-Hill, A. Q. Yuan, P. A. Walker, M. K. Vorlaender, S. Bianchi, B. Guarino, A. D. Marco, F. Vanzetta, G. Agatic, M. Foglierini, D. Pinna, B. Fernandez-Rodriguez, A. Fruehwirth, C. Silacci, R. W. Ogrodowicz, S. R. Martin, F. Sallusto, J. A. Suzich, A. Lanzavecchia, Q. Zhu, S. J. Gamblin, J. J. Skehel, Structure and function analysis of an antibody recognizing all influenza A subtypes. *Cell* **166**, 596–608 (2016).
44. R. Kong, K. Xu, T. Zhou, P. Acharya, T. Lemmin, K. Liu, G. Ozorowski, C. Soto, J. D. Taft, R. T. Bailer, E. M. Cale, L. Chen, C. W. Choi, G.-Y. Chuang, N. A. Doria-Rose, A. Druz, I. S. Georgiev, J. Gorman, J. Huang, M. G. Joyce, M. K. Louder, X. Ma, K. McKee, S. O'Dell, M. Pancera, Y. Yang, S. C. Blanchard, W. Mothes, D. R. Burton, W. C. Koff, M. Connors, A. B. Ward, P. D. Kwong, J. R. Mascola, Fusion peptide of HIV-1 as a site of vulnerability to neutralizing antibody. *Science* **352**, 828–833 (2016).
45. K. Xu, P. Acharya, R. Kong, C. Cheng, G.-Y. Chuang, K. Liu, M. K. Louder, S. O'Dell, R. Rawi, M. Sastry, C.-H. Shen, B. Zhang, T. Zhou, M. Asokan, R. T. Bailer, M. Chambers, X. Chen, C. W. Choi, V. P. Dandey, N. A. Doria-Rose, A. Druz, E. T. Eng, S. K. Farney, K. E. Foulds, H. Geng, I. S. Georgiev, J. Gorman, K. R. Hill, A. J. Jafari, Y. D. Kwon, Y.-T. Lai, T. Lemmin, K. McKee, T. Y. Ohr, L. Ou, D. Peng, A. P. Rowshan, Z. Sheng, J.-P. Todd, Y. Tsybovsky, E. G. Viox, Y. Wang, H. Wei, Y. Yang, A. F. Zhou, R. Chen, L. Yang, D. G. Scorpio, A. B. McDermott, L. Shapiro, B. Carragher, C. S. Potter, J. R. Mascola, P. D. Kwong, Epitope-based vaccine design yields fusion peptide-directed antibodies that neutralize diverse strains of HIV-1. *Nat. Med.* **24**, 857–867 (2018).
46. Y. Yuan, D. Cao, Y. Zhang, J. Ma, J. Qi, Q. Wang, G. Lu, Y. Wu, J. Yan, Y. Shi, X. Zhang, G. F. Gao, Cryo-EM structures of MERS-CoV and SARS-CoV spike glycoproteins reveal the dynamic receptor binding domains. *Nat. Commun.* **8**, 15092 (2017).
47. A. C. Walls, X. Xiong, Y.-J. Park, M. A. Tortorici, J. Snijder, J. Quispe, E. Cameroni, R. Gopal, M. Dai, A. Lanzavecchia, M. Zambon, F. A. Rey, D. Corti, D. Veesler, Unexpected receptor functional mimicry elucidates activation of coronavirus fusion. *Cell* **176**, 1026–1039.e15 (2019).
48. Y. Shu, J. McCauley, GISAID: Global initiative on sharing all influenza data – from vision to reality. *Euro Surveill.* **22**, 30494 (2017).
49. B. T. Foley, B. T. M. Korber, T. K. Leitner, C. Apetrei, B. Hahn, I. Mizrachi, J. Mullins, A. Rambaut, S. Wolinsky, "HIV sequence compendium 2018" (Technical Report LA-UR-18-25673, Los Alamos National Laboratory (LANL), 2018).
50. L. Casalino, Z. Gaieb, J. A. Goldsmith, C. K. Hjorth, A. C. Dommer, A. M. Harbison, C. A. Fogarty, E. P. Barros, B. C. Taylor, J. S. McLellan, E. Fadda, R. E. Amaro, Beyond shielding: The roles of glycans in the SARS-CoV-2 spike protein. *ACS Cent. Sci.* **6**, 1722–1734 (2020).
51. International Committee on Taxonomy of Viruses Executive Committee, The new scope of virus taxonomy: Partitioning the virosphere into 15 hierarchical ranks. *Nat. Microbiol.* **5**, 668–674 (2020).
52. C. L. Schoch, S. Ciufo, M. Domrachev, C. L. Hotton, S. Kannan, R. Khovanskaya, D. Leipe, R. Mcveigh, K. O'Neill, B. Robbertse, S. Sharma, V. Soussov, J. P. Sullivan, L. Sun, S. Turner, I. Karsch-Mizrachi, NCBI Taxonomy: A comprehensive update on curation, resources and tools. *Database (Oxford)* **2020**, baaa062 (2020).
53. A. Dereeper, V. Guignon, G. Blanc, S. Audic, S. Buffet, F. Chevenet, J.-F. Dufayard, S. Guindon, V. Lefort, M. Lescot, J.-M. Claverie, O. Gascuel, Phylogeny.fr: Robust phylogenetic analysis for the non-specialist. *Nucleic Acids Res.* **36**, W465–W469 (2008).
54. R. De Gasparo, M. Pedotti, L. Simonelli, P. Nickl, F. Muecksch, I. Cassaniti, E. Percivalle, J. C. C. Lorenzi, F. Mazzola, D. Magrì, T. Michalcikova, J. Haviernik, V. Honig, B. Mrazkova, N. Polakova, A. Fortova, J. Tureckova, V. Iatsiuk, S. Di Girolamo, M. Palus, D. Zudova, P. Bednar, I. Bukova, F. Bianchini, D. Mehn, R. Nencka, O. Pavlis, J. Rozman, S. Gioria, J. C. Sammartino, F. Giardina, S. Gaiarsa, Q. Pan-Hammarström, C. O. Barnes, P. J. Bjorkman, L. Calzolai, A. Piralla, F. Baldanti, M. C. Nussenzweig, P. D. Bieniasz, T. Hatziioannou, J. Prochazka, R. Sedlacek, D. F. Robbiani, D. Ruzek, L. Varani, Bispecific IgG neutralizes SARS-CoV-2 variants and prevents escape in mice. *Nature* **593**, 424–428 (2021).
55. D. F. Robbiani, L. Bozzacco, J. R. Keeffe, R. Khouri, P. C. Olsen, A. Gazumyan, D. Schaefer-Babajew, S. Avila-Rios, L. Nogueira, R. Patel, S. A. Azzopardi, L. F. Uhl, M. Saeed, E. E. Sevilla-Reyes, M. Agudelo, K.-H. Yao, J. Golijanin, H. B. Gristick, A. Hurley, M. Caskey, J. Pai, T. Oliveira, E. A. Wunder, G. Sacramento, N. Nery Jr., C. Orge, F. Costa, M. G. Reis, N. M. Thomas, T. Eisenreich, D. M. Weinberger, A. R. P. de Almeida, A. P. West Jr., C. M. Rice, P. J. Bjorkman, G. Reyes-Teran, A. I. Ko, M. R. MacDonald, M. C. Nussenzweig, Recurrent potent human neutralizing antibodies to Zika virus in Brazil and Mexico. *Cell* **169**, 597–609.e11 (2017).
56. F. Schmidt, Y. Weisblum, F. Muecksch, H.-H. Hoffmann, E. Michailidis, J. C. C. Lorenzi, P. Mendoza, M. Rutkowska, E. Bednarski, C. Gaebler, M. Agudelo, A. Cho, Z. Wang, A. Gazumyan, M. Cipolla, M. Caskey, D. F. Robbiani, M. C. Nussenzweig, C. M. Rice, T. Hatziioannou, P. D. Bieniasz, Measuring SARS-CoV-2 neutralizing antibody activity using pseudotyped and chimeric viruses. *J. Exp. Med.* **217**, e20201181 (2020).
57. S. J. Zost, P. Gilchuk, J. B. Case, E. Binshtein, R. E. Chen, J. P. Nkolola, A. Schäfer, J. X. Reidy, A. Trivette, R. S. Nargi, R. E. Sutton, N. Suryadevara, D. R. Martinez, L. E. Williamson, E. C. Chen, T. Jones, S. Day, L. Myers, A. O. Hassan, N. M. Kafai, E. S. Winkler, J. M. Fox, S. Shrihari, B. K. Mueller, J. Meiler, A. Chandrashekar, N. B. Mercado, J. J. Steinhardt, K. Ren, Y.-M. Loo, N. L. Kallewaard, B. T. Mc Cune, S. P. Keeler, M. J. Holtzman, D. H. Barouch, L. E. Gralinski, R. S. Baric, L. B. Thackray, M. S. Diamond, R. H. Carnahan, J. E. Crowe Jr., Potently neutralizing and protective human antibodies against SARS-CoV-2. *Nature* **584**, 443–449 (2020).
58. A. O. Hassan, J. B. Case, E. S. Winkler, L. B. Thackray, N. M. Kafai, A. L. Bailey, B. T. McCune, J. M. Fox, R. E. Chen, W. B. Alsoussi, J. S. Turner, A. J. Schmitz, T. Lei, S. Shrihari, S. P. Keeler, D. H. Fremont, S. Greco, P. B. McCray Jr., S. Perlman, M. J. Holtzman, A. H. Ellebedy, M. S. Diamond, A SARS-CoV-2 infection model in mice demonstrates protection by neutralizing antibodies. *Cell* **182**, 744–753.e4 (2020).
59. W. Kabsch, Integration, scaling, space-group assignment and post-refinement. *Acta Crystallogr. D Biol. Crystallogr.* **66**, 133–144 (2010).
60. M. D. Winn, C. C. Ballard, K. D. Cowtan, E. J. Dodson, P. Emsley, P. R. Evans, R. M. Keegan, E. B. Krissinel, A. G. W. Leslie, A. McCoy, S. J. McNicholas, G. N. Murshudov, N. S. Pannu, E. A. Potterton, H. R. Powell, R. J. Read, A. Vagin, K. S. Wilson, Overview of the CCP4 suite and current developments. *Acta Crystallogr. D Biol. Crystallogr.* **67**, 235–242 (2011).
61. A. J. McCoy, R. W. Grosse-Kunstleve, P. D. Adams, M. D. Winn, L. C. Storoni, R. J. Read, Phaser crystallographic software. *J. Appl. Cryst.* **40**, 658–674 (2007).
62. P. D. Adams, P. V. Afonine, G. Bunkóczi, V. B. Chen, I. W. Davis, N. Echols, J. J. Headd, L.-W. Hung, G. J. Kapral, R. W. Grosse-Kunstleve, A. J. McCoy, N. W. Moriarty, R. Oeffner, R. J. Read, D. C. Richardson, J. S. Richardson, T. C. Terwilliger, P. H. Zwart, *PHENIX*: A comprehensive Python-based system for macromolecular structure solution. *Acta Crystallogr. D Biol. Crystallogr.* **66**, 213–221 (2010).
63. P. Emsley, B. Lohkamp, W. G. Scott, K. Cowtan, Features and development of *Coot*. *Acta Crystallogr. D Biol. Crystallogr.* **66**, 486–501 (2010).
64. D. N. Mastronarde, Automated electron microscope tomography using robust prediction of specimen movements. *J. Struct. Biol.* **152**, 36–51 (2005).
65. Z. Wang, F. Muecksch, A. Cho, C. Gaebler, H.-H. Hoffmann, V. Ramos, S. Zong, M. Cipolla, B. Johnson, F. Schmidt, J. DaSilva, E. Bednarski, T. Ben Tanfous, R. Raspe, K. Yao, Y. E. Lee, T. Chen, M. Turroja, K. G. Milard, J. Dizon, A. Kaczynska, A. Gazumyan, T. Y. Oliveira, C. M. Rice, M. Caskey, P. D. Bieniasz, T. Hatziioannou, C. O. Barnes, M. C. Nussenzweig, Analysis of memory B cells identifies conserved neutralizing epitopes on the N-terminal domain of variant SARS-Cov-2 spike proteins. *Immunity* **55**, 998–1012.e8 (2022).
66. A. Punjani, J. L. Rubinstein, D. J. Fleet, M. A. Brubaker, cryoSPARC: Algorithms for rapid unsupervised cryo-EM structure determination. *Nat. Methods* **14**, 290–296 (2017).
67. T. D. Goddard, C. C. Huang, T. E. Ferrin, Visualizing density maps with UCSF Chimera. *J. Struct. Biol.* **157**, 281–287 (2007).
68. V. B. Chen, W. B. Arendall III, J. J. Headd, D. A. Keedy, R. M. Immormino, G. J. Kapral, L. W. Murray, J. S. Richardson, D. C. Richardson, MolProbity: All-atom structure validation for macromolecular crystallography. *Acta Crystallogr. D Biol. Crystallogr.* **66**, 12–21 (2010).
69. X. Brochet, M.-P. Lefranc, V. Giudicelli, IMGT/V-QUEST: The highly customized and integrated system for IG and TR standardized V-J and V-D-J sequence analysis. *Nucleic Acids Res.* **36**, W503–W508 (2008).

Downloaded from https://www.science.org on May 03, 2024

70. T. D. Goddard, C. C. Huang, E. C. Meng, E. F. Pettersen, G. S. Couch, J. H. Morris, T. E. Ferrin, UCSF ChimeraX: Meeting modern challenges in visualization and analysis. *Protein Sci.* **27**, 14–25 (2018).
71. E. Krissinel, K. Henrick, Inference of macromolecular assemblies from crystalline state. *J. Mol. Biol.* **372**, 774–797 (2007).

Acknowledgments: We are grateful to all study participants and families, as well as to the medical personnel of the Clinica Luganese Moncucco. We further thank T. Hatziioannou and P. Bieniasz (Rockefeller University) for sharing plasmids and protocols for SARS-CoV-2 pseudovirus; D. Morone, I. Cassaniti, J. C. Sammartino, J. Kamis, and M. Spevakova for technical assistance; H. Jirincova (National Institute of Public Health, Prague) for providing virus isolates; P. Strakova for help with virus cultivation; N. Rezaei and Z. Chavoshzadeh (Tehran University of Medical Sciences) for contribution to the collection of vaccinated samples; and P. Bjorkman (California Institute of Technology) for sharing CoV expression plasmids. For the IMMUNO_COV study, we acknowledge the contribution of F. Montagnani, M. Fabbrini, I. Rancan, G. Pastore, J. Polvere, and S. Zirpoli (University of Siena and University Hospital of Siena) for participants' enrollment, clinical sample collection, and processing. Cryo-EM data for this work were collected at the Stanford-SLAC cryo-EM center with support from E. Montabana. X-ray crystallographic data were collected at the Stanford Synchrotron Radiation Lightsource, SLAC National Accelerator Laboratory, which is supported by the U.S. Department of Energy, Office of Science, Office of Basic Energy Sciences under contract no. DE-AC02-76SF00515. The SSRL Structural Molecular Biology Program is supported by the DOE Office of Biological and Environmental Research and by the National Institutes of Health, National Institute of General Medical Sciences (P30GM133894). **Funding:** This study was supported in part by the Swiss Vaccine Research Institute (SVRI); George Mason University Fast Grant; Fondation Philanthropique Famille Sandoz; NIH grants U01 AI151698 (United World Antiviral Research Network, UWARN), P01 AI138938, and U19 AI111825 (to D.F.R.); European Union's Horizon 2020 research and innovation programme under grant agreement no. 101003650: Antibody Therapy Against Coronavirus—ATAC (to Q.P.-H., H.M., F.Baldanti, L.C., L.V., and D.F.R.); BRIDGE 40B2-0_203488 (to A. Cavalli and D.F.R.); Department of Medical Biotechnologies, University of Siena (to D. Medaglini); EU Joint Research Centre Exploratory Research program (project "FUTURE," to G.G.); Swedish Research Council and Knut and Alice Wallenberg Foundation (to Q.P.-H.); Czech Ministry of Agriculture (RVO0518 to D.R.); National Institute of Virology and Bacteriology, Programme EXCELES, project no. LX22NPO5103 funded by the European Union-Next Generation EU (to D.R.); Strategy of the Czech Academy of Sciences, AV21-Virology and Antiviral Therapy (to D.R. and R.S.); Czech Science Foundation and Swiss National Science Foundation (21-05445L to D.R. and D.F.R.); 22-17139K by Czech Science Foundation (to R.S.); Czech Centre for Phenogenomics provided by Ministry of Education, Youth and Sports of the Czech Republic (LM2018126 to R.S.); and Czech Academy of Sciences (RVO68378050 to R.S.). A. Cavalli thanks F. Gruner for support. C.O.B. is supported by the Howard Hughes Medical Institute Hanna Gray Fellowship and is a Chan Zuckerberg Biohub investigator. **Author contributions:** F. Bianchini, V. Crivelli, A. Cavalli, C.O.B., and D.F.R. conceived the study. F. Bianchini, V. Crivelli, M.E.A., C. Guerra, M. Palus, M. Pedotti, L.C., R.S., D.R., L.V., A. Cavalli, C.O.B., and D.F.R. designed and analyzed the experiments. A.F.-P., M.U., D.F.R., and C. Garzoni designed human subject research protocols. F. Bianchini, V. Crivelli, M.E.A., C. Guerra, M. Palus, M. Pedotti, R.D.G., L.S., M.M., T.C.R., J.M., L.P., A.A.S., A. Celoria, M.S., V.H., V.P., T.M., J.P., G.G., A. Ciabattini, D.J., J.S., D.F., D. Mehn, P.S., and T.F. produced reagents and carried out experiments. H.M., A.P., H.A., D. Medaglini, Q.P.-H., and F. Baldanti contributed reagents and samples. M.B., V. Calvaruso, and A.F.-P. recruited participants and executed human subject research protocols. C.T. processed human samples. M.E.A. and C.O.B. performed structural analysis. V. Crivelli, L.S., M.M., L.V., and A. Cavalli performed bioinformatic analysis. F. Bianchini, V. Crivelli, M.E.A., C.O.B., and D.F.R. wrote the manuscript with input from all coauthors. **Competing interests:** The Institute for Research in Biomedicine has filed a provisional patent application in connection with this work on which F. Bianchini, V. Crivelli, L.V., A. Cavalli, and D.F.R. are inventors. **Data and materials availability:** The script for coldspot identification is available at GitHub (https://github.com/cavallilab/coldspot). The atomic models and corresponding maps for all structures are available online under the following accession codes. For fp.006-FP, the model and structure factor files are available in the Protein Data Bank (PDB) under accession code 8D47. For sd1.040-S, the model and cryo-EM maps are available both in the PDB and Electron Microscopy Data Bank (EMDB) under codes 8D48 and EMD-27177, respectively. Requests for materials should be addressed to D.F.R.; distribution may require a material transfer agreement. All data other needed to support the conclusions in the paper are present in the paper or the Supplementary Materials. This work is licensed under a Creative Commons Attribution 4.0 International (CC BY 4.0) license, which permits unrestricted use, distribution, and reproduction in any medium, provided the original work is properly cited. To view a copy of this license, visit http://creativecommons.org/licenses/by/4.0/. This license does not apply to figures/photos/artwork or other content included in the article that is credited to a third party; obtain authorization from the rights holder before using such material.

Submitted 24 July 2022
Accepted 23 January 2023
Published First Release 26 January 2023
Final published 10 March 2023
10.1126/sciimmunol.ade0958

Downloaded from https://www.science.org on May 03, 2024

Science Immunology
AAAS

Supplementary Materials for

Human neutralizing antibodies to cold linear epitopes and subdomain 1 of the SARS-CoV-2 spike glycoprotein

Filippo Bianchini *et al.*

Corresponding author: Daniel Ruzek, ruzekd@paru.ca.cz; Luca Varani, luca.varani@irb.usi.ch; Andrea Cavalli, andrea.cavalli@irb.usi.ch; Christopher O. Barnes, cobarnes@stanford.edu; Davide F. Robbiani, drobbiani@irb.usi.ch

Sci. Immunol., eade0958 (2023)
DOI: 10.1126/sciimmunol.ade0958

The PDF file includes:

Figs. S1 to S8
Tables S1 and S2

Other Supplementary Material for this manuscript includes the following:

Data files S1 to S3
MDAR Reproducibility Checklist

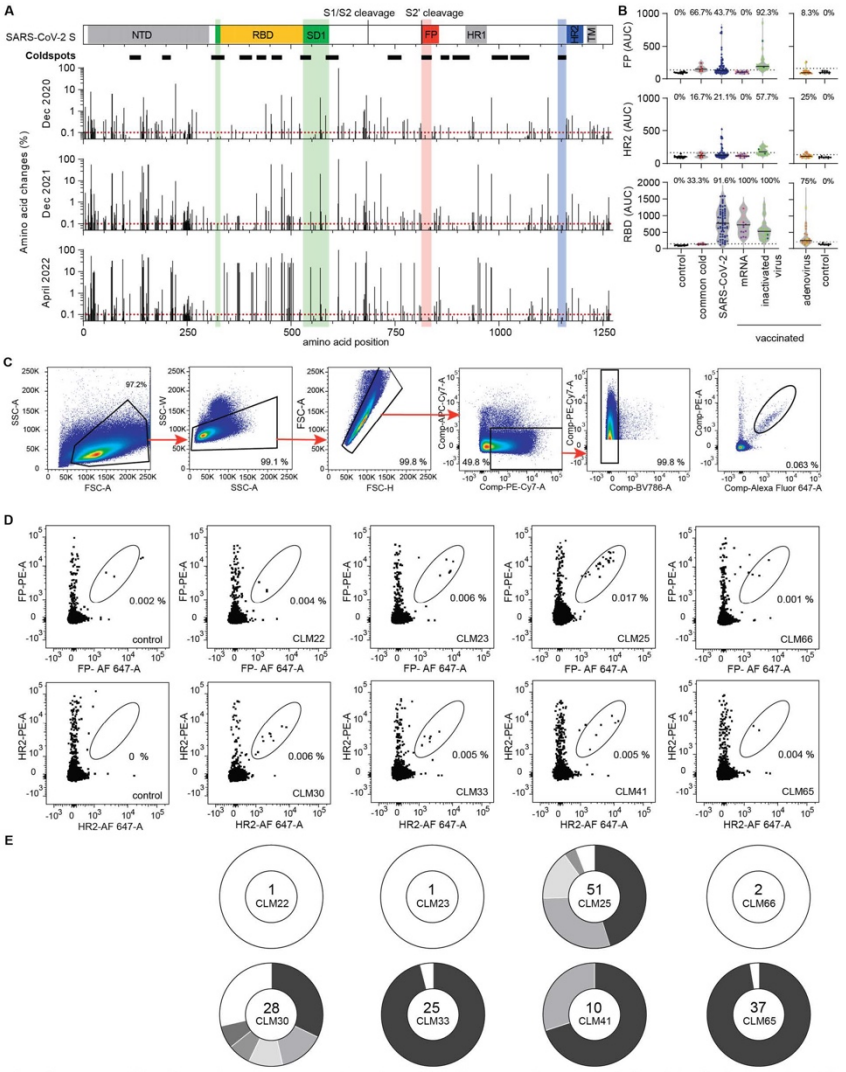

Fig. S1. Identification of coldspot antibodies. (A) Cartoon diagram of the SARS-CoV-2 S with highlighted coldspot regions at the fusion peptide (FP, red) and near heptad repeat 2 (HR2, blue), as well as subdomain 1 (SD1, green). The thick horizontal lines underneath indicate the location of all coldspots, and the histograms show the frequency of aa changes throughout S at different time points: 31.12.2020 (671,006), 31.12.2021 (7,526,116) and 29.04.2022 (10,480,461 sequences from GISAID). **(B)** ELISA reactivity of plasma IgG antibodies to FP (top) and HR2 (middle) peptides or to SARS-CoV-2 RBD (bottom). SARS-CoV-2 (n=67) and common cold CoV (n=6) convalescent samples are compared to COVID-19 vaccinees (mRNA: BNT162b2 n=11, purple; mRNA-1273 n=5, pink;

inactivated virus: Sinovac n=2, dark green; Sinopharm n=24, light green; adenovirus: ChAdOx1-S n=19, orange; Ad26.COV2.S n=4, yellow), and to non-infected controls (n=25). Area Under the Curve (AUC); average of two experiments. The percentage of samples with antibody levels 4 standard deviations above controls is shown on top. **(C)** Gating strategy for sorting peptide-specific or SD1-enriched B cells by flow cytometry. **(D)** Identification of FP-peptide specific (top) and HR2-peptide specific (bottom) B cells by flow cytometry. Numbers indicate percentage of gated double-positive cells. **(E)** Clonal analysis of antibody sequences derived from peptide-specific B cells identified in **(D)**. Pie charts show the total number of antibody sequences (center); the size of the slices is proportional to the number of clonally related sequences. White slices indicate antibody sequences that are not part of a clone.

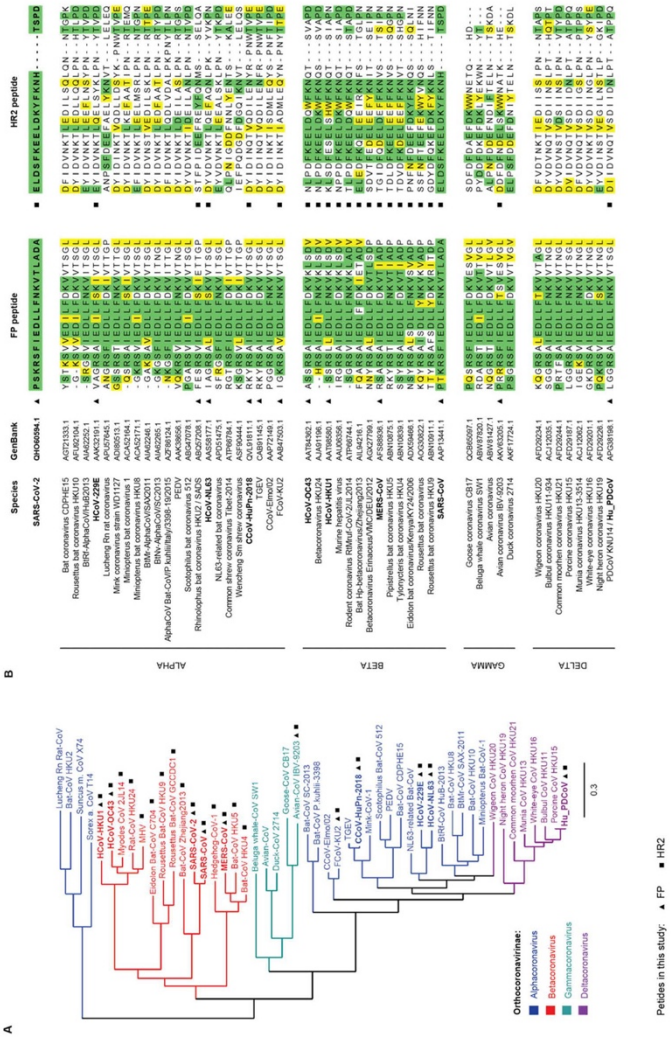

Fig. S2. Similarity of peptides at the FP and HR2 of Orthocoronavirinae. (A) Phylogenetic analysis of CoV species based on the aa sequence of S. **(B)** Alignment of SARS-CoV-2 FP and HR2 peptide sequences with those corresponding to related CoVs. In green identical residues; in yellow residues that are similar by side chain functionality.

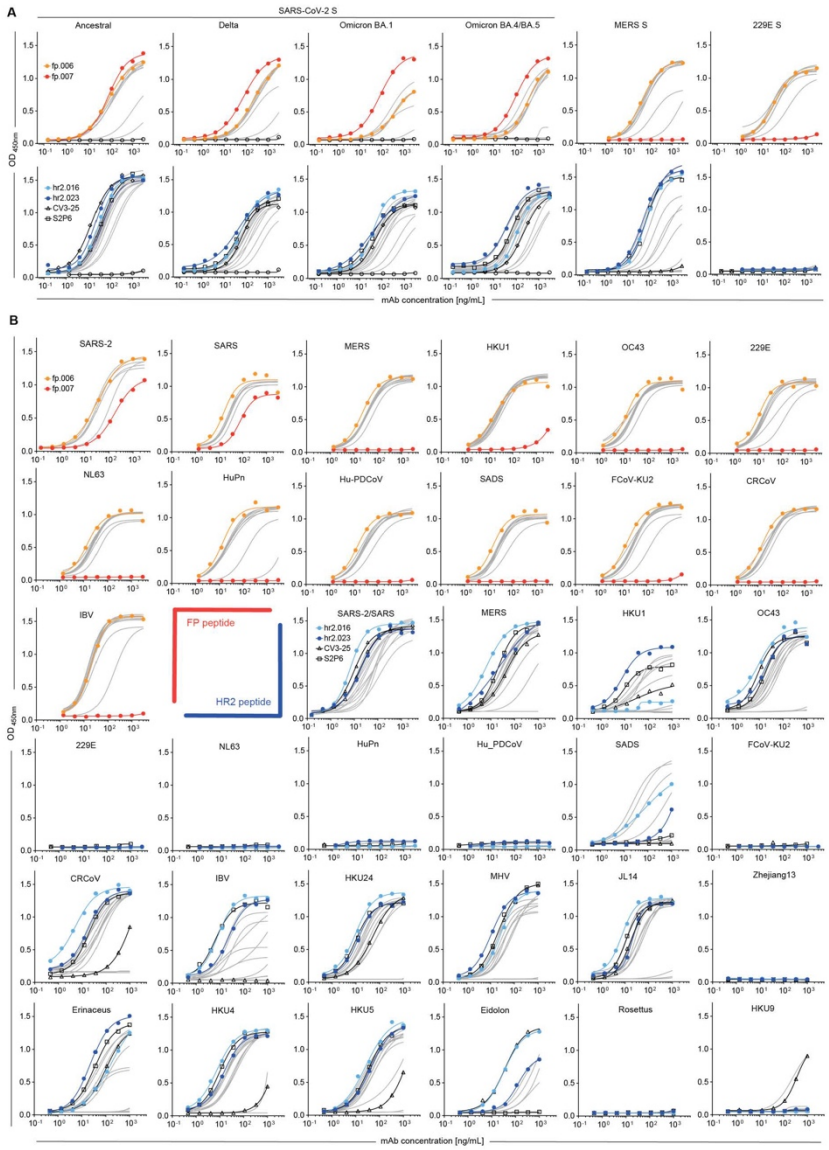

Fig. S3. Broadly crossreactive binding of FP and HR2 monoclonal antibodies. (A and **B)** Graphs show ELISAs measuring monoclonal antibodies reactivity to S **(A)** and to coldspot peptides **(B)** of coronaviruses. Mean of two independent experiments.

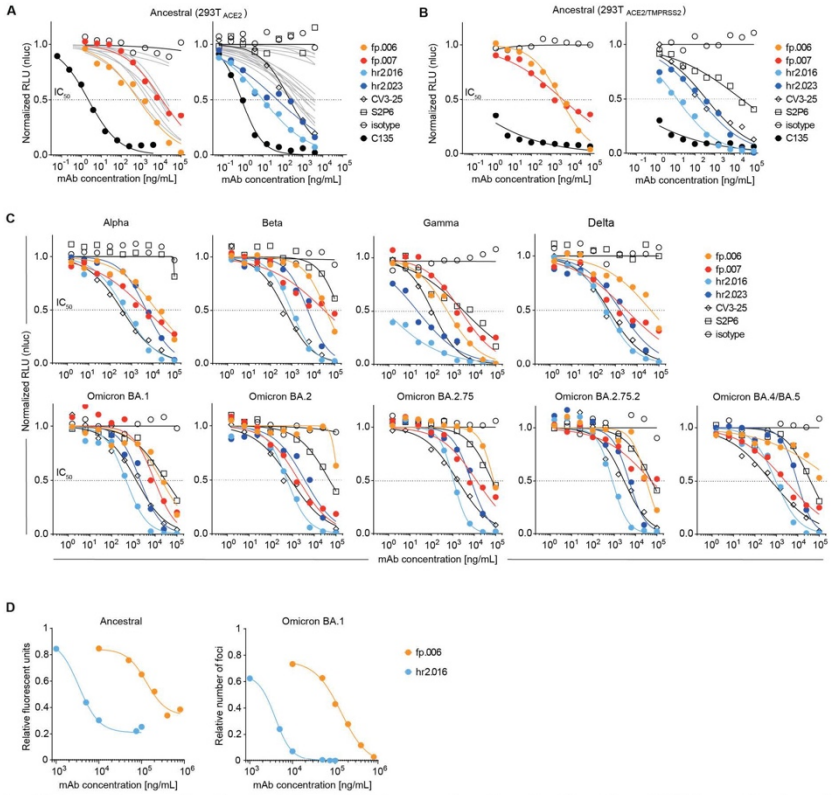

Fig. S4. Broad neutralization by FP and HR2 monoclonal antibodies. (A and **B)** Neutralization of ancestral SARS-CoV-2 pseudovirus. Graphs show normalized relative luminescence values in cell lysates of $293T_{ACE2}$ **(A)** or $293T_{ACE2/TMPRSS2}$ **(B)** cells 48 hours after infection with nanoluc-expressing SARS-CoV-2 pseudovirus in the presence of increasing concentrations of monoclonal antibodies to the FP (top) and HR2 (bottom). Isotype control and antibodies C135 (4), CV3-25 and S2P6 were assayed alongside for comparison; additional antibodies in grey (data file S2). Mean of at least two independent experiments. **(C)** Same as in **(A)**, but for SARS-CoV-2 pseudoviruses corresponding to VOC. **(D)** Neutralization of SARS-CoV-2 ancestral and Omicron BA.1 by Focus Reduction Neutralization Test (FRNT).

A

	heavy chain													light chain				
	CDRH1	CDRH2							CDRH3					FR1	CDRL3			
Residue Number	31	52	52A	53	55	56	57	58	97	98	99	100A	100F	1	93	94	95	95A
fp.006 Residue	N	S	Y	E	R	N	K	K	F	L	S	Y	Y	E	D	W	P	L
BSA (Å ²)	13	13	83	13	46	69	3	46	18	67	2	77	64	14	12	76	49	21

B

	fusion peptide																	
Residue Number	813	814	815	816	817	818	819	820	821	822	823	824	825	826	827	828	829	830
Conservation (%)	22	14	82	100	18	78	94	100	86	98	96	37	98	86	12	14	18	29
FP Residue	S	K	R	S	F	I	E	D	L	L	F	N	K	V	T	L	A	D
BSA (Å ²)	6	22	172	48	0	57	67*	48	0	89	175	3	71	0	0	22	0	0

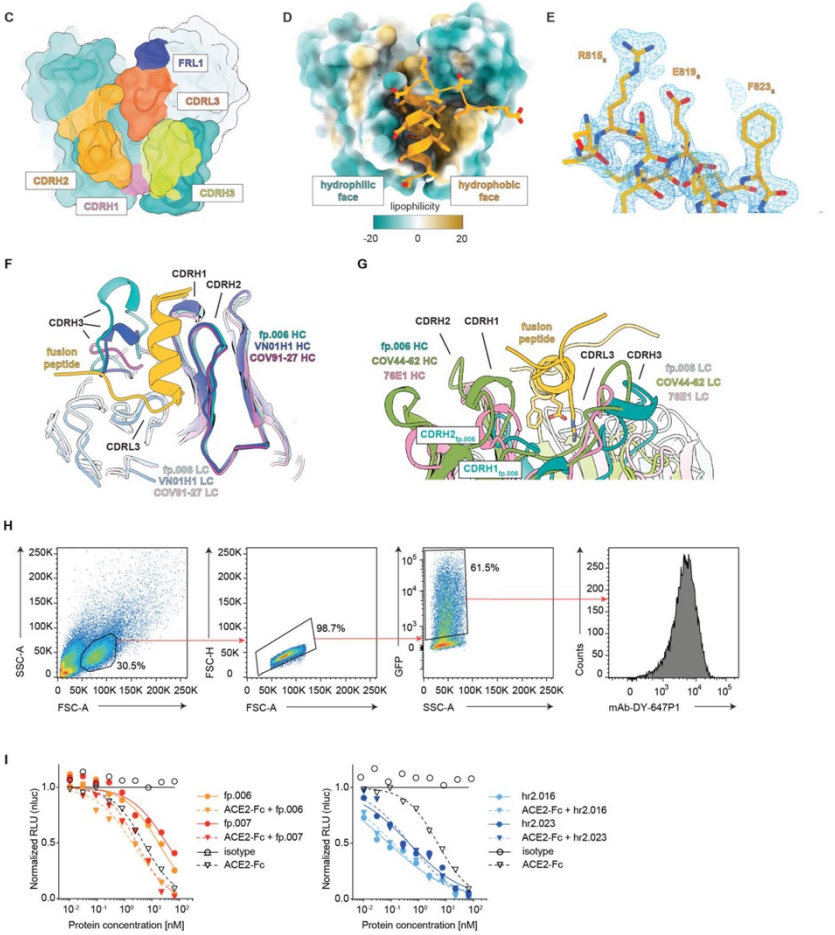

Fig. S5. Structure of fp.006 in complex with peptide antigen and effects of ACE2 engagement. (A) Contributions of fp.006 heavy and light chain paratope residues to the binding of the fusion peptide. Residue number, identity, and buried surface area (BSA) are shown, and colored as in panel **(C)**. **(B)**

Per residue contributions of the FP to the fp.006 epitope. Conservation calculated from the 49 CoV sequences listed in fig. S2B and BSA calculations per FP residue are listed. *Indicates that the BSA calculation does not include contacts mediated by water molecules. **(C)** Surface representation of the fp.006 paratope with interacting residues colored according to their CDR loop identity. Non-interacting heavy chain and light chain residues are colored teal and light teal, respectively. **(D)** Surface representation of the fp.006 paratope with per residue lipophilicity calculations shown. More hydrophobic patches are colored orange and more hydrophilic patches are colored teal, as calculated by ChimeraX. **(E)** Representative electron density for a portion of the FP contoured at 1.7σ. **(F)** Overlay of complex structures between the SARS-CoV-2 fusion peptide and fp.006 (this study; PDB 8D47), VN01H1 (PDB 7SKZ), and COV91-27 (PDB 8D6Z) illustrates a convergent binding mode independent of V gene usage. Structures are aligned on their fusion peptide chains and colored as shown. **(G)** Overlay of complex structures between the SARS-CoV-2 fusion peptide and fp.006 (this study; PDB 8D47), COV44-62 (PDB 8D36), and 76E1 (PDB 7X9E) Fabs, illustrating that anti-FP mAbs of different poses bind to the same face of the amphipathic fusion peptide α-helix, which includes highly-conserved residues, which are shown as sticks. **(H)** Gating strategy for measuring the binding of monoclonal antibodies to the SARS-CoV-2 S expressed by 293T cells by flow cytometry. **(I)** Normalized relative luminescence values in cell lysates of $293T_{ACE2}$ cells after infection with ancestral SARS-CoV-2 pseudovirus in the presence of increasing concentrations of FP or HR2 antibodies alone or as a cocktail with soluble ACE2. Isotype control in black. For the combination of fp.006+ACE2, P=0.0017 over fp.006 and P=0.0047 over ACE2; for the combination of fp.007+ACE2, P=0.0072 over fp.007 and P=0.2 over ACE2 (n=4; Welch's t-test, two-tailed).

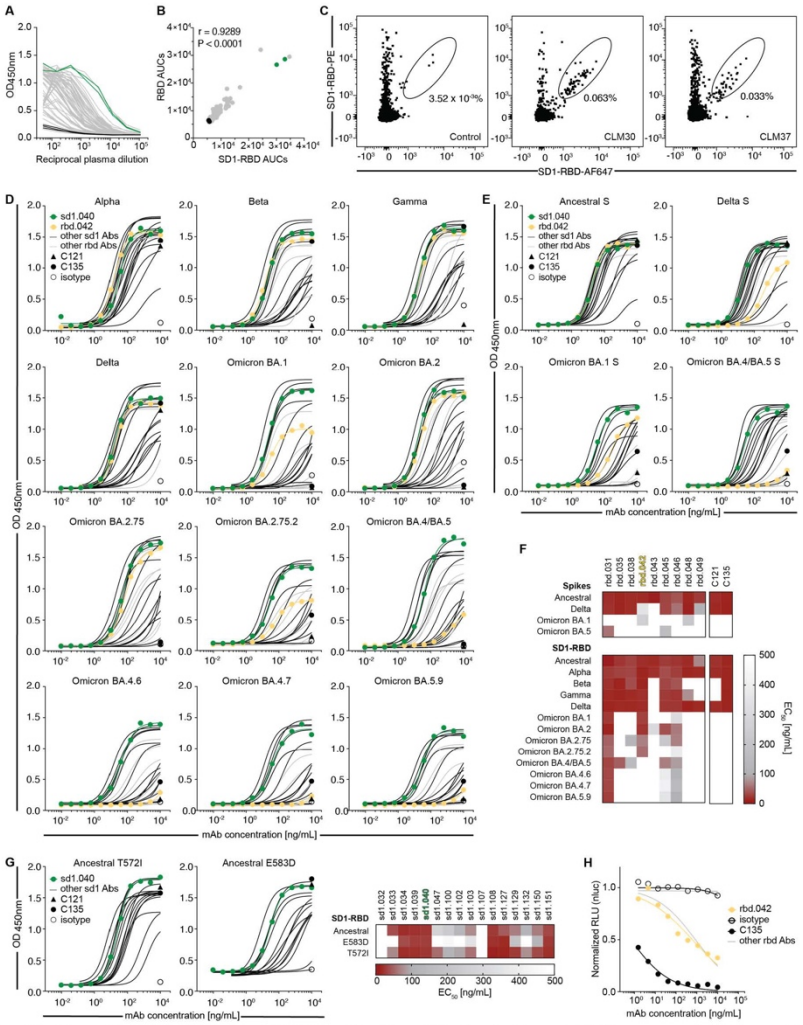

Fig. S6. Identification of SD1 and RBD antibodies. (A) Graph shows ELISAs measuring plasma IgG reactivity to RBD. Negative controls in black. Mean of two independent experiments. **(B)** Correlation of plasma IgG reactivities to SD1-RBD and RBD. Pearson correlation. **(C)** Identification of SD1-enriched B cells by flow cytometry. **(D** and **E)** Graphs show ELISAs measuring monoclonal antibodies reactivity to SD1-RBD **(D)** and S **(E)** corresponding to SARS-CoV-2 VOC. Mean of two independent experiments. **(F)** Heatmaps with the binding (EC_{50}) of RBD monoclonal antibodies to S (top) or SD1-RBD (bottom) proteins corresponding to SARS-CoV-2 VOC. Two experiments. **(G)** Graphs and summary heatmap for SD1 antibodies binding to SD1-RBD mutant proteins T572I and E583D. **(H)** Neutralization of ancestral SARS-CoV-2 pseudovirus by antibodies to the RBD that are broadly crossreactive to VOC.

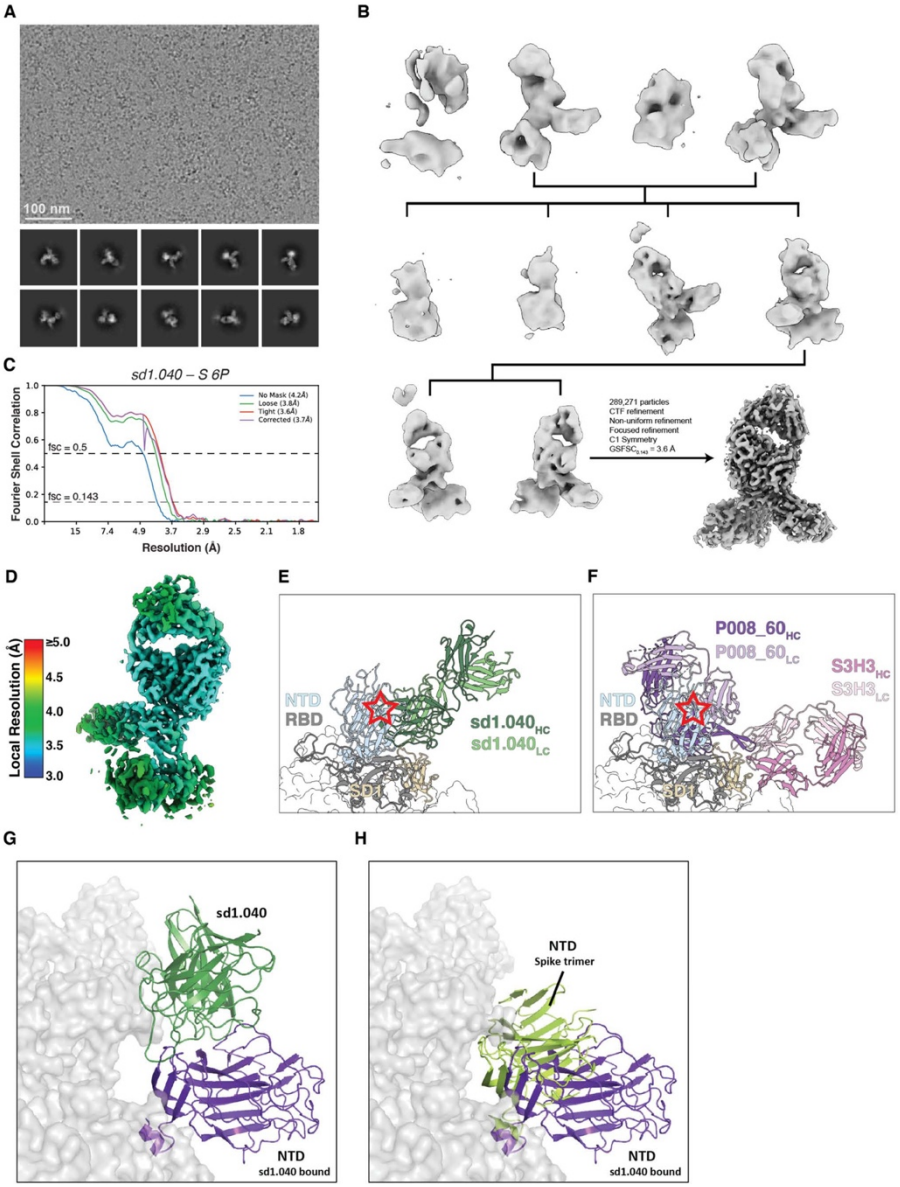

Fig. S7. Structure of sd1.040 in complex with S. (A) Representative micrograph and 2D class averages selected from the sd1.040-S dataset. **(B)** 3D classification workflow and final refinement strategy. **(C)** Gold-standard FSC plot for the final cryo-EM density map. **(D)** Local resolution estimates calculated

in cryoSPARC v3.1. **(E)** Close-up view of the sd1.040 Fab – S complex superimposed onto a prefusion S trimer (PDB 6VXX). Potential clashes with the NTD (cyan) on the neighboring S1 protomer are denoted by a red star. **(F)** Close-up views of the P008_60 Fab (PDB 7ZBU) and S3H3 Fab (PDB 7WD9) superposed onto a prefusion trimeric Spike. Antibody P008_60 shows prominent clashes with the adjacent NTD (red star), while the binding orientation of S3H3 does not clash with neighboring protomers. **(G and H)** According to docking simulations, sd1.040 binds also to the NTD of the adjacent protomer. In **(G)**, NTD moves from the position observed in the experimental structure of the free S to make room for antibody binding (sd1.040 in dark green bound to NTD in purple). In **(H)**, comparison between NTD bound to sd1.040 in simulations (purple) and NTD in the context of free spike trimer (lime).

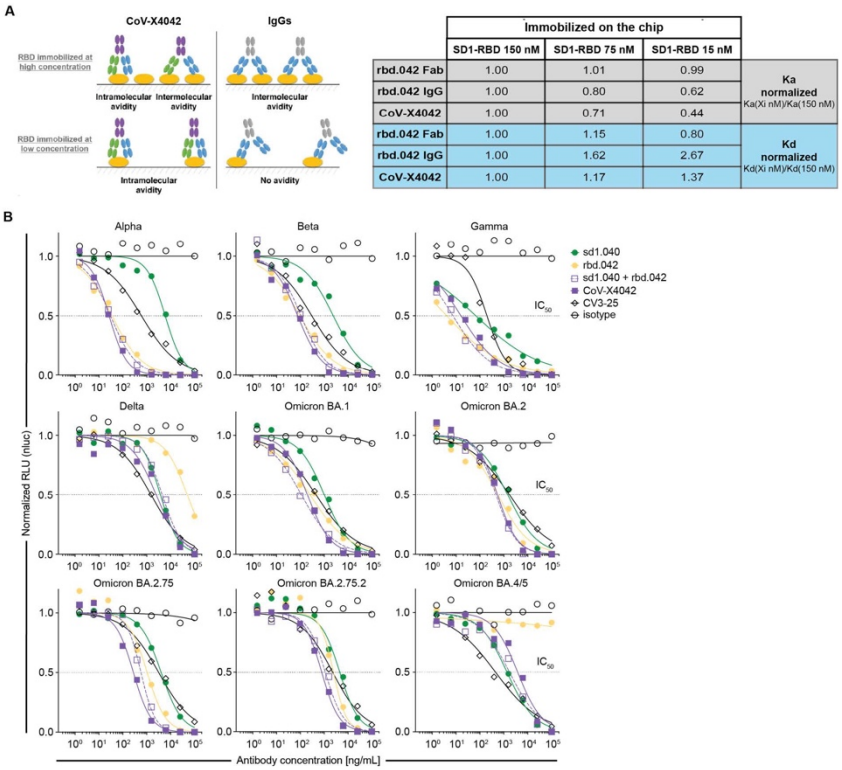

	Immobilized on the chip			
	SD1-RBD 150 nM	SD1-RBD 75 nM	SD1-RBD 15 nM	
rbd.042 Fab	1.00	1.01	0.99	Ka normalized Ka(Xi nM)/Ka(150 nM)
rbd.042 IgG	1.00	0.80	0.62	
CoV-X4042	1.00	0.71	0.44	
rbd.042 Fab	1.00	1.15	0.80	Kd normalized Kd(Xi nM)/Kd(150 nM)
rbd.042 IgG	1.00	1.62	2.67	
CoV-X4042	1.00	1.17	1.37	

Fig. S8. Binding and neutralizing properties of CoV-X4042. (A) Both arms of CoV-X4042 bind simultaneously to the same SD1-RBD molecule. Left, diagram showing that at high SD1-RBD concentrations, monoclonal antibodies have avidity effects owing to intermolecular binding (which results in a slower kd), but this is not the case at low SD1-RBD concentrations, because bivalent binding to a single SD1-RBD is impossible. By contrast, the bispecific antibody has avidity at both high and low concentrations, since bivalent binding to its two epitopes on a single SD1-RBD is possible. ka is not affected by avidity. Right, table summarizing the SPR results used to determine ka and kd of IgG, Fab and the bispecific antibody at different concentrations of immobilized SD1-RBD, which confirm experimentally that CoV-X4042 engages bivalently on a single SD1-RBD. **(B)** Neutralization of VOC by CoV-X4042 and parental monoclonal antibodies.

Table S1. Crystallographic data collection and refinement statistics

	fp.006-fusion peptide
PDB ID	8D47
Data collection[a,b]	
Space group	P 1 2_1 1
Cell dimensions	
a, b, c (Å)	90.0, 73.1, 90.1
α, β, γ (°)	90.0, 109.0, 90.0
Resolution (Å)	37.9 - 2.0 (2.04 - 2.00)
R_{merge}	0.117 (0.996)
I / σI	6.1 (1.5)
$CC_{1/2}$ (%)	0.988 (0.372)
Completeness (%)	97.9 (98.8)
Redundancy	3.0 (3.0)
Refinement	
Resolution (Å)	37.9 - 2.0
No. reflections	73148 (4545)
R_{work} / R_{free}	.1836/.2378
No. atoms	7723
Protein	6926
Ligand/ion	45
Water	752
B-factors (mean)	
Protein	30.7
Ligand/ion	41.7
Water	36.5
R.m.s. deviations	
Bond lengths (Å)	0.007
Bond angles (°)	0.840

[a]Data were derived from a single crystal
[b]Values in paratheses describe the highest resolution shell

Table S2. Cryo-EM data collection, refinement and validation statistics

	sd1.040 – S 2P (EMDB-27177) (PDB 8D48)
Data collection and processing	
Magnification	105,000x
Voltage (kV)	300
Electron exposure (e–/Å^2)	60
Defocus range (μm)	1.0 - 2.5
Pixel size (Å)	0.8521
Symmetry imposed	C1
Initial particle images (no.)	9,894
Final particle images (no.)	9,469
Map resolution (Å)	
FSC threshold (0.143)	3.7
Map resolution range (Å)	3.7 – 4.2
Refinement	
Initial model used (PDB code)	6VXX, 5AVE, 7D0D
Model resolution (Å)	
FSC threshold (0.143)	3.6
Model resolution range (Å)	3.5 – 3.8
Map sharpening B factor (Å^2)	114
Model composition	
Non-hydrogen atoms	5,545
Protein residues	714
Ligands	2
B factors (Å^2)	
Protein	44
Ligand	132
R.m.s. deviations	
Bond lengths (Å)	0.004
Bond angles (°)	0.8
Validation	
MolProbity score	2.0
Clashscore	11.7
Poor rotamers (%)	0
Ramachandran plot	
Favored (%)	92.8
Allowed (%)	7.2
Disallowed (%)	0

5. UNPUBLISHED DATA

Personal contribution:

- Experimental design and analysis,
- Design, generation, purification and characterization of reagents (i.e., SD1-RBD and benchmark monoclonal antibodies expression plasmids, mAb proteins),
- Execution of the experiments (i.e., ELISA on S and SD1-RBD VOCs).

5.1. RESULTS

sd1.040 recognizes the latest SARS-CoV-2 VOCs better than most benchmark antibodies

The continuous evolution of SARS-CoV-2 resulted in the spreading of new VOCs since publication of our findings in March 2023 (see above). Some of the latest VOCs are characterized by enhanced immune-escape and show resistance to the few clinically approved mAbs that were still effective on the previous Omicron variants[269]. To update the characterization of sd1.040, I produced SD1-RBD proteins corresponding to the latest Omicron variants (BQ.1.1, XBB.1, XBB.1.5, XBB.1.16, BA.2.86). I also produced a panel of benchmark RBD antibodies including some that were developed for the clinic: P2G3[287], Bebtelovimab[288], Tixagevimab, Cilgavimab[289], Sotrovimab[290], and Omi-42[291]. I also included the previously characterized antibodies C121 and C135 which were potent neutralizers of the ancestral SARS-CoV-2 lineage[292], and antibodies CR3022 and COVA1-16 which, together with Sotrovimab, are among the few known cross-reactive antibodies that recognize both SARS-CoV and SARS-CoV-2 RBDs[268,293,294]. I tested this panel of mAbs side-by-side with sd1.040 and CoV-X4042 in ELISA for binding to S and SD1-RBD variants (**Fig. UP1A, B**). I calculated the EC_{50} for each variant and built a heatmap showing the cross-reactivity pattern of the tested mAbs (**Fig. UP1C**). The potent neutralizing antibodies C121 and C135 completely lost their ability to bind the Omicron lineage, as did the SARS-CoV cross-reactive antibodies CR3022 and COVA1-16. Tixagevimab and Cilgavimab, which have been used in combination in the Evusheld cocktail, struggle to recognize Omicorn BA-2 derived variants, and are unable to bind the most recent VOCs. P2G3 and Bebtelovimab show a similar pattern, not binding the Omicron BQ.1.1 variant nor those that followed. Sotrovimab retains the ability to bind almost all the SD1-RBD variants, with the exception of the most recent Omicron BA.2.86. However, its binding is much reduced also on the other SD1-RBDs of the Omicron lineage. The best benchmark antibody was Omi-42, that was able to recognize all the VOCs with an EC_{50} between 9.2 and 47.1 ng/mL. The RBD antibody rbd.042 was unable to bind the Omicron BA.4/BA.5 derived

variants, even though it showed partial activity against the XBB sublineages (EC_{50} between 45.1 and 84.6 ng/mL).
The sd1.040 behaved similarly to Omi-42, recognizing all the variants with EC_{50} between 8.9 and 44.5 ng/mL. As predictable, the bispecific antibody CoV-X4042 was influenced by rbd.042's loss of binding, showing reduced EC_{50} on the latest Omicron variants (EC_{50} between 32.4 and 118.5). These data further support the hypothesis that SD1 antibodies have higher potential of resisting viral escape compared to RBD antibodies.

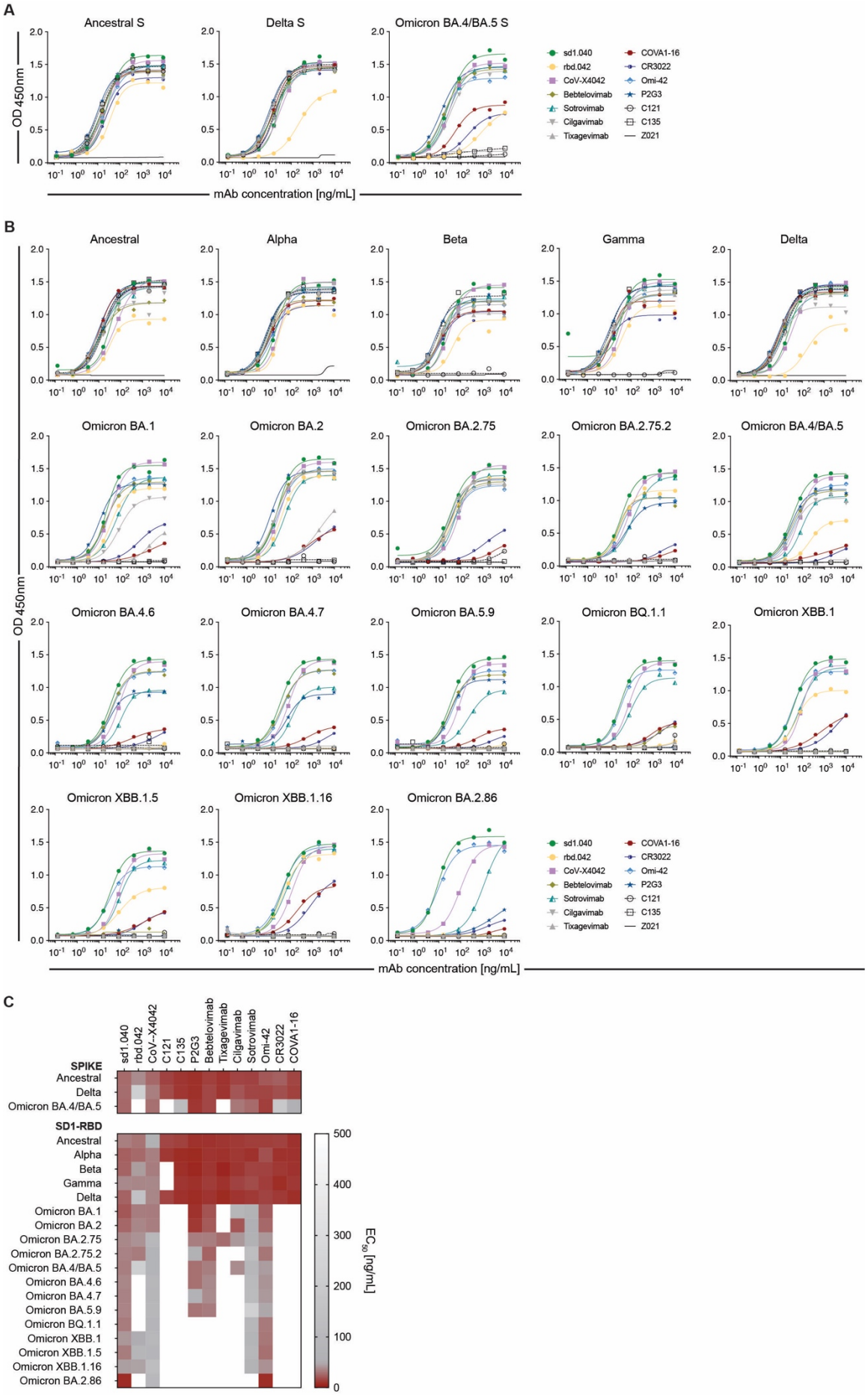
A
Ancestral S
Delta S
Omicron BA.4/BA.5 S
OD 450nm
mAb concentration [ng/mL]
sd1.040
rbd.042
CoV-X4042
Bebtelovimab
Sotrovimab
Cilgavimab
Tixagevimab
COVA1-16
CR3022
Omi-42
P2G3
C121
C135
Z021
B
Ancestral
Alpha
Beta
Gamma
Delta
Omicron BA.1
Omicron BA.2
Omicron BA.2.75
Omicron BA.2.75.2
Omicron BA.4/BA.5
Omicron BA.4.6
Omicron BA.4.7
Omicron BA.5.9
Omicron BQ.1.1
Omicron XBB.1
Omicron XBB.1.5
Omicron XBB.1.16
Omicron BA.2.86
C
SPIKE
SD1-RBD
Ancestral
Alpha
Beta
Gamma
Delta
Omicron BA.1
Omicron BA.2
Omicron BA.2.75
Omicron BA.2.75.2
Omicron BA.4/BA.5
Omicron BA.4.6
Omicron BA.4.7
Omicron BA.5.9
Omicron BQ.1.1
Omicron XBB.1
Omicron XBB.1.5
Omicron XBB.1.16
Omicron BA.2.86
EC50 [ng/mL]
500
400
300
200
100
0

Fig. UP1. sd1.040 cross-reactivity comparison with benchmark antibodies. ***(A** and **B)** Graphs showing ELISA reactivity of sd1.040, rbd.042, and CoV-X4042 in comparison with benchmark mAbs against S **(A)** or SD1-RBD **(B)** corresponding to SARS-CoV-2 VOCs. Average of two independent experiments.* ***(C)** Heatmap with the ELISA EC_{50} of sd1.040, rbd.042, CoV-X4042 and benchmark mAbs on SARS-CoV-2 VOCs on S (top) or RBD-SD1 (bottom). Average of two independent experiments.*

sd1.040, but not rbd.042, neutralizes Omicron BQ.1.1, EG.5.1, and BA.2.86 pseudoviruses

To evaluate the neutralizing potential of bispecific antibody CoV-X4042 and its parental antibodies sd1.040 and rbd.042 on the most recent Omicron variants, we performed in vitro neutralization assays with pseudoviruses corresponding to BQ.1.1, EG.5.1, and BA.2.86 (**Fig. UP2A**). rbd.042 was not able to neutralize Omicron BQ.1.1 and BA.2.86 but retained minimal neutralizing power against EG.5.1. sd1.040 was able to neutralize all the variants with IC_{50} values between 1'480 and 4'628 ng/mL. In general, CoV-X4042 showed intermediate neutralizing activity between sd1.040 and rbd.042. However, against Omicron EG.5.1 CoV-X4042 was more potent than sd1.040 (IC_{50} of 1'638 VS 4'628 ng/mL, respectively). This was probably due to the residual neutralizing activity of rbd.042 on Omicron EG.5.1.

By plotting the IC_{50} values of CoV-X4042 and its parental antibodies on different pseudovirus VOCs (**Fig. UP2B**), it is clear that sd1.040 is stably preserving its neutralizing power on the Omicron variants, while rbd.042 loses activity compared to earlier variants both as single monoclonal and as part of CoV-X4042 bispecific antibody.

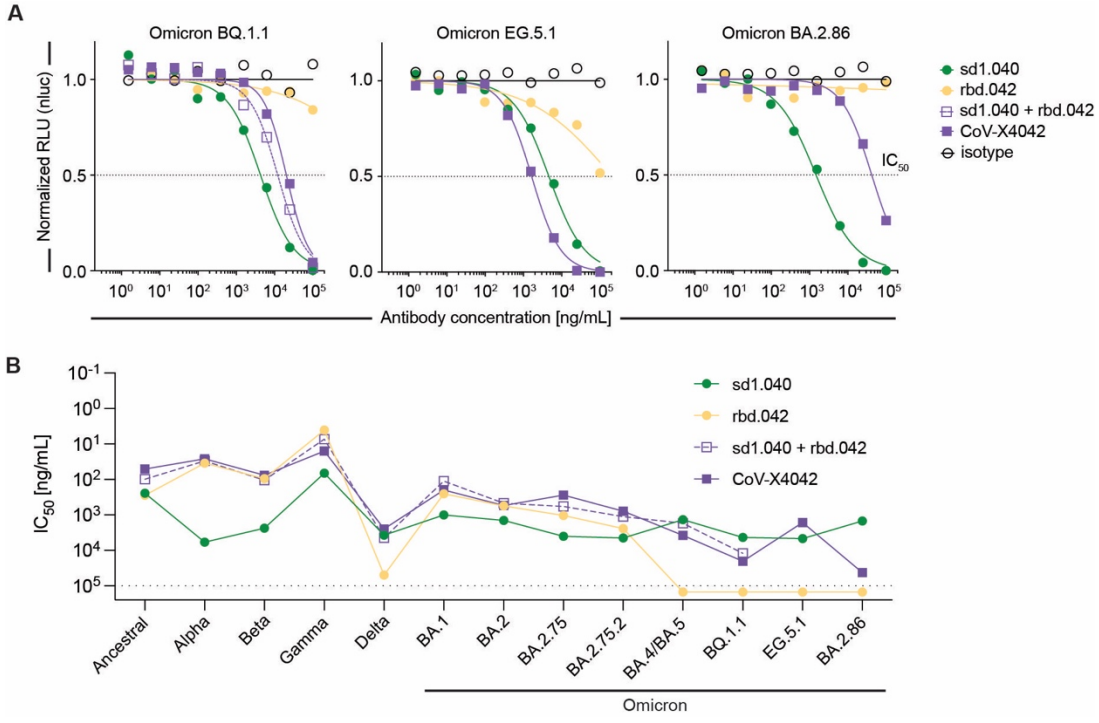

Fig. UP2. Neutralization of CoV-X4042 on latest SARS-CoV-2 pseudovirus VOCs. (A) *Normalized relative luminescence units (RLU) in 293T$_{ACE2}$ cell lysate upon infection with SARS-CoV-2 VOC pseudovirus in presence of variable concentration of CoV-X4042 or its parental mAbs. Negative control isotype is represented as empty circles. Average of two independent experiments.* ***(B)*** *Updated summary of CoV-X4042 and its parental mAbs IC$_{50}$ values on SARS-CoV-2 pseudovirus VOCs. Dotted line represents limit of detection. Average of two independent experiments. Neutralization experiments performed in collaboration with Virginia Crivelli and Concetta Guerra.*

Identification of broadly cross-reactive RBD mAbs

In published work (see above) we demonstrated that SD1 and RBD antibodies can be successfully combined to achieve potent neutralization and they can even act synergistically[272]. Unfortunately, the loss of neutralizing activity by the RBD antibody rbd.042 against the more recent variants deeply impaired the efficacy of the bispecific CoV-X4042 (**Fig. UP2B**). To address this problem, we characterized 37 additional RBD antibodies from SARS-CoV-2 convalescent individuals[272]. The antibodies were tested in ELISA on the S and SD1-RBD proteins corresponding to the main SARS-CoV-2 VOCs (**Fig. UP3A-B**). As predictable, most of the RBD antibodies completely or partially lost binding to SD1-RBD corresponding to the Omicron variants (**Fig. UP3C**). We selected 10 among the best cross-reactive antibodies (rbd.104, rbd.106, rbd.110, rbd.112, rbd.113, rbd.117, rbd.123, rbd.141, rbd.142, and rbd.143) and tested them in neutralization on SARS-CoV-2 ancestral pseudovirus. Three antibodies, rbd.106 (IC_{50} = 67.44 ng/mL), rbd.112 (IC_{50} = 86.73 ng/mL), and rbd.141 (IC_{50} = 163.6 ng/mL), were more potent than rbd.042 (IC_{50} = 176.8 ng/mL; **Fig. UP3D**). Thus, we identified three promising candidates to combine in bispecific format with sd1.040 in future studies.

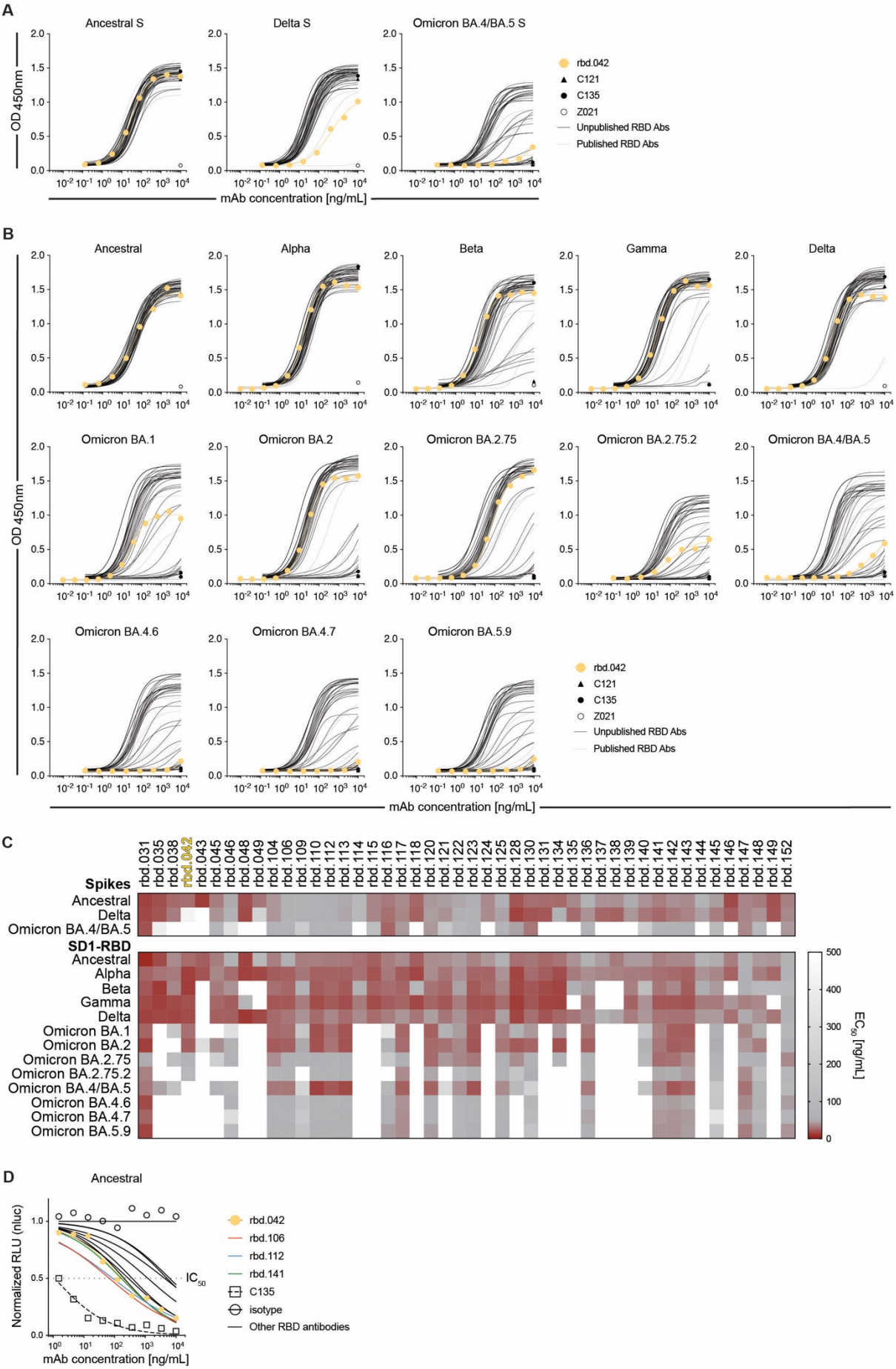
A
Ancestral S
Delta S
Omicron BA.4/BA.5 S
OD 450nm
mAb concentration [ng/mL]
rbd.042
C121
C135
Z021
Unpublished RBD Abs
Published RBD Abs
B
Ancestral
Alpha
Beta
Gamma
Delta
Omicron BA.1
Omicron BA.2
Omicron BA.2.75
Omicron BA.2.75.2
Omicron BA.4/BA.5
Omicron BA.4.6
Omicron BA.4.7
Omicron BA.5.9
C
Spikes
Ancestral
Delta
Omicron BA.4/BA.5
SD1-RBD
Alpha
Beta
Gamma
Omicron BA.1
Omicron BA.2
Omicron BA.2.75
Omicron BA.2.75.2
Omicron BA.4.6
Omicron BA.4.7
Omicron BA.5.9
EC50 [ng/mL]
D
Ancestral
Normalized RLU (nluc)
IC50
mAb concentration [ng/mL]
rbd.042
rbd.106
rbd.112
rbd.141
C135
isotype
Other RBD antibodies

Fig. UP3. Characterization of additional RBD-specific mAbs. ***(A*** *and* ***B)*** *Graphs showing ELISA reactivity of 37 additional RBD-specific mAbs (black lines) tested side-by-side with the 9 previously reported mAbs (gray lines) on S* ***(A)*** *or SD1-RBD* ***(B)*** *corresponding to SARS-CoV-2 VOCs. rbd.042 is in yellow. Average of two independent experiments.* ***(C)*** *Heatmap with the ELISA* EC_{50} *values of all RBD-specific mAbs on SARS-CoV-2 VOCs S (top) or RBD-SD1 (bottom). Average of two independent experiments.* ***(D)*** *Neutralization of ancestral SARS-CoV-2 pseudovirus by broadly cross-reactive RBD mAbs. Antibodies that are more potent than rbd.042 (in yellow) have distinctive colors. Antibodies less potent than rbd.042 are in black. Positive control (C135) is represented as empty squares, negative control isotype as empty circles. Average of two independent experiments. Neutralization experiment performed in collaboration with Virginia Crivelli and Concetta Guerra.*

5.2. MATERIALS AND METHODS

All the protocols used in the "Unpublished data" section have been previously described in the "Published manuscript" section.
RBD-SD1 proteins and SARS-CoV-2 pseudoviruses corresponding to the most recent variants were based on the following publicly available sequences: Omicron BQ.1.1, GenBank UWM38596.1; Omicron XBB.1, PDB 8IOV; Omicron XBB.1.5, GenBank UZG29433.1; Omicron XBB.1.16, GenBank UZG29433.1 + K474R; Omicron EG.5.1, GenBank WGM84363.1; and Omicron BA.2.86, GenBank WRK62249.1 + N17M + N17_L18insPLFN + I670V.

6. DISCUSSION

The rapid evolution of SARS-CoV-2 leads to the periodic emergence of new variants[225]. Latest variants are characterized by an increased number of mutations in their S glycoprotein and therefore increase the chances of immune escape and reinfection[239]. Luckily, the latest variants also seem to be less pathogenic than earlier ones, probably due to both intrinsic properties of the virus and pre-existing immunity at the population level[260]. However, we cannot exclude that a new variant with more pathogenic properties will appear in the future[233]. Furthermore, current circulating variants can still be a threat for fragile individuals (e.g., immunocompromised, elderly people)[295,296] or they can cause long-term sequelae known as "long COVID"[297]. mAbs are a potent weapon in the fight against infectious diseases, but most of the clinically approved antibodies for SARS-CoV-2 infection treatment target regions of the S which mutate rapidly (i.e., RBD and NTD)[265].

Herein, we identified the SD1 of the S glycoprotein of SARS-CoV-2 as target of broadly protective antibodies due to its highly conserved amino acid sequence. We designed a sorting strategy that allowed the enrichment of SD1-specific B cells among the sorted pool, and produced 16 SD1-specific antibodies. We demonstrated that some SD1 antibodies can recognize all the main SARS-CoV-2 variants and focused on the characterization of the best neutralizer: sd1.040.

The sd1.040 mAb was able to neutralize all the SARS-CoV-2 pseudovirus VOCs that were tested with IC_{50} values between 245 and 5'844 ng/mL, including Omicron BA.2.86 (IC_{50} = 1'480 ng/mL). As far as we know, sd1.040 is the only SD1 mAb reported that still retains neutralizing activity on Omicron BA.2.86. Even if the IC_{50} value of sd1.040 in our in vitro neutralization assay increases on the Omicron variants, its epitope binding ability measured by ELISA on SD1-RBD variants remains quite stable. It is well documented that antibodies can protect *in vivo* through the activation of FcRs, and this mechanism is independent from the intrinsic neutralizing activity of the antibody. Non-neutralizing antibodies have been shown to protect mice in SARS-CoV-2 infection models through the activation of antibody-dependent cellular phagocytosis and cytotoxicity[298,299]. Therefore, the fact that sd1.040 neutralization decreases on the Omicron variants *in vitro* does not necessarily mean that it would be less effective in protecting *in vivo*.

To investigate the mechanism of neutralization of sd1.040, we resolved its epitope by Cryo-EM. sd1.040 appears to bind a cryptic epitope on SD1 that is hidden by the NTD of the adjacent protomer in the S prefusion conformation. Based on molecular dynamic simulations, we hypothesized that sd1.040 could interact with residues of the NTD (P295-K300), crosslinking two protomers and stabilizing the spike trimer in the prefusion conformation. This

model was supported by flow cytometry data that showed reduced exposure of the fusion loop upon ACE2 binding to the S in presence of sd1.040. However, this model could not explain why we observed sd1.040 only in complex with single protomers in Cryo-EM, and never with the full S trimer. After our publication reporting the discovery of sd1.040, we contributed to a second paper[300] in which we investigated the conformational changes of the S trimer following sd1.040 binding using analytical ultracentrifugation. Based on these additional data, we proposed a new model where sd1.040 locks the S trimer in a conformation where the protomers are more loosely associated, in particular in the apical part of the S. This conformation would still be able to bind ACE2 but would not allow the rearrangements needed for membrane fusion.

Although this model requires further investigation to be confirmed, the comparison of sd1.040 with other reported SD1 antibodies could help in understanding the general features of this antibody class. Only few SD1 antibodies have been characterized in detail, and most of them have been published after sd1.040[273,274,277–280]. Because of the small size of SD1, all these antibodies recognize partially overlapping epitopes. However, by mapping the interacting residues on the SD1 structure it is possible to distinguish two main groups of SD1 antibodies binding preferentially near the loops connecting the SD1 to the RBD or to the main SD1 core (**Fig. D1A**). In the first group we find mAbs S3H3[274], SD1-1, SD1-2[279], and MO11[280]. All of them have been shown to bind the S trimer in Cryo-EM. S3H3 and MO11 seem to neutralize by locking the S in the prefusion conformation or in an intermediate conformation preventing S1 shedding. SD1-1 and SD1-2, instead, could block ACE2 binding and even impair S trimer oligomerization. The other group of SD1 antibodies bind the SD1 farther from the connection with the RBD and interact mostly with the loops 3 and 5 of SD1. This group includes sd1.040, P008_60[273], and C68.59[277]. sd1.040 and P008_60 have been found to form complexes only with S protomers in Cryo-EM, while C68.59 can bind the S trimer. The complexes formed by P008_60 and C68.59 with the full S have also been characterized using hydrogen-deuterium exchange coupled to mass spectrometry (HDX-MS). This technique showed that both these antibodies induce destabilization of the S2 portion without release of the S1. HDX-MS data are compatible with the neutralization mechanism hypothesized for sd1.040, which also involves loosening of protomer-protomer interactions. The fact that the sd1.040 epitope largely overlaps with those of P008_60 and C68.59 supports the idea that all these antibodies could have similar effects on the structure of the S trimer (**Fig. D1A-B**).

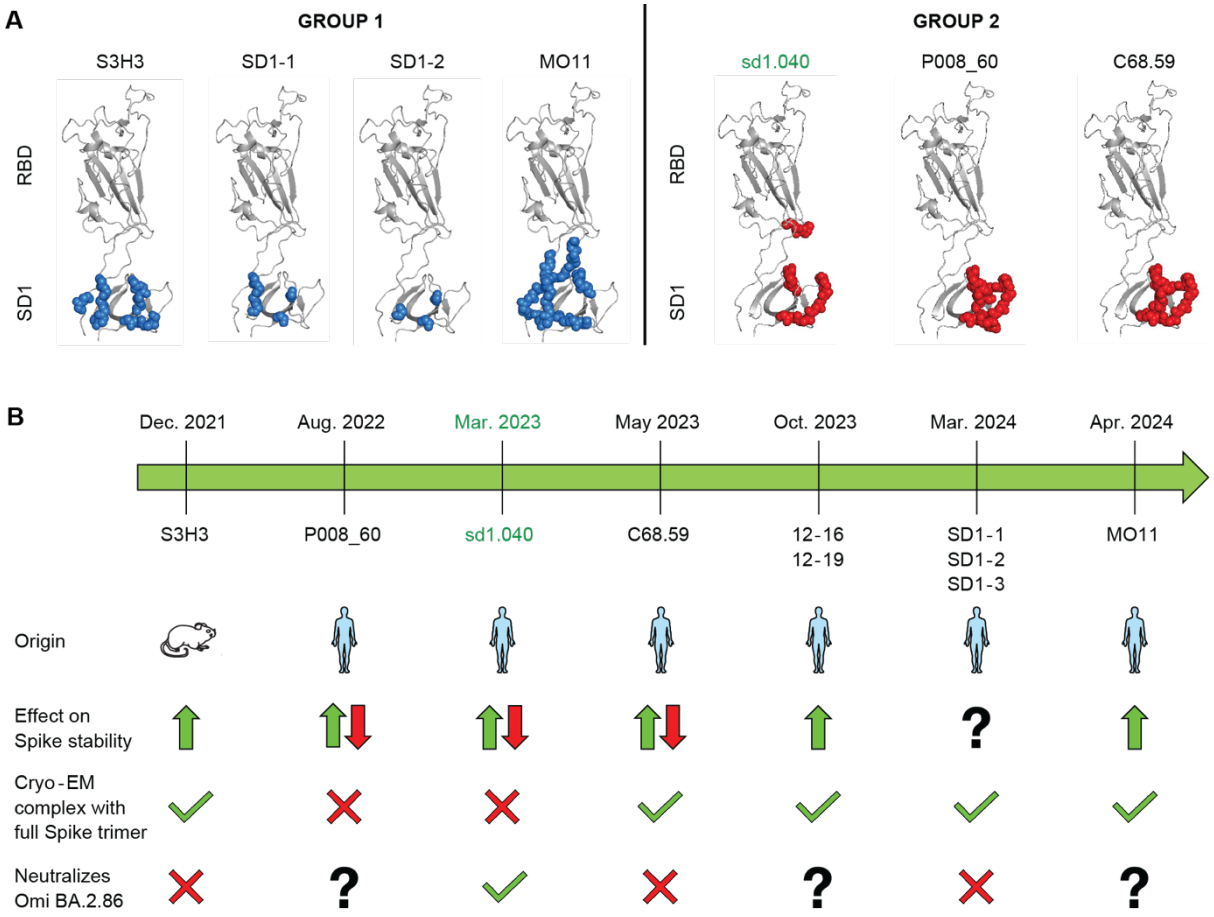

Fig. D1. Features of published SD1 monoclonal antibodies. ***(A)*** *Contacting residues of the indicated SD1 antibodies are shown on the SD1-RBD structure as spheres (blue for group 1, on the left; red for group 2, on the right).* ***(B)*** *Summary of the main features of published SD1 antibodies. Antibodies are ordered based on their date of publication. Question marks indicate features that have not being investigated or reported to date.*

Due to the small exposed surface of SD1, another common feature of SD1 antibodies is to bind residues outside this region, cross-linking different domains of the same protomer or even adjacent protomers. As previously mentioned, this seems to be the case for sd1.040, which could cross-link the SD1 with NTD and RBD domains. C68.59 binds both SD1 and the SD2 of the adjacent protomer[277], while MO11 interacts with SD1 and both RBD and SD2[280]. Whether these interactions outside the SD1 are necessary for neutralization or they just reinforce antibody binding is not clear. Instead, antibodies 12-16 and 12-19 both bind a quaternary epitope made by SD1 and NTD. In this case, both the domains contribute to a similar extent to antibody binding and neutralize by locking the RBD in the ”down” conformation[278].
SD1 antibodies are generally less potent in neutralization than RBD or NTD antibodies, but they show higher resistance to viral escape by recent SARS-CoV-2 variants[280]. In order to investigate the contribution of SD1 antibodies to the plasma neutralizing activity in humans, Zhou et al.[279] used a

recombinant form of SD1 to deplete sera of vaccinated and infected individuals of SD1 antibodies. Interestingly, depletion of SD1 antibodies had negligible effect when the sera were used to neutralize an early pandemic strain, but a significant reduction in neutralizing potency was observed on the recent variant Omicron XBB.1.5. This difference could be due to loss of neutralization from the RBD and NTD antibody pools, with consequent unmasking of the contribution of SD1 antibodies. Another explanation is that reinfection and vaccination could boost pre-existing cross-reactive SD1-specific B cells. The experiment demonstrated an increasing contribution of SD1 antibodies in mediating protection to the latest variants of SARS-CoV-2 but, on the other side, suggested that the sudden appearance of two mutations in the SD1 domain of the variant Omicron BA.2.86 could be due to increased immunological pressure. If this is true, we should expect accumulation of new mutations in this region in future variants. At present, the neutralizing ability of most SD1 antibodies on the Omicron BA.2.86 variant has been completely abolished by mutation E554K. Our sd1.040 is the only SD1 antibody, which has been demonstrated to retain neutralizing activity against Omicron BA.2.86.

A strategy to prevent viral escape from antibody treatment is to combine two or more antibodies in a cocktail or bispecific molecule targeting different epitopes at the same time[165]. We developed a bispecific antibody (CoV-X4042) combining sd1.040 with the RBD antibody rbd.042, which showed potent neutralizing activity on the early Omicron variants. sd1.040 and rbd.042 neutralize synergistically the ancestral pseudovirus when coupled in the CoV-X4042 antibody, and even protected mice infected with ancestral or Omicron BA.1 virus from weight loss and reduced viral replication in lungs.

Unfortunately, rbd.042 completely lost the ability to bind and neutralize the latest SARS-CoV-2 variants, and this impaired CoV-X4042 potency considerably. We observed similar behavior with clinically approved RBD antibodies (i.e., Bebtelovimab[288], Sotrovimab[290], Tixagevimab, Cilgavimab[289]) and even with antibodies that were able to recognize both SARS-CoV and ancestral SARS-CoV-2 RBDs (i.e., CR3022, COVA1-16)[268,293,294]. To find a substitute of rbd.042, we characterized 37 additional RBD antibodies from memory B cells. As expected, most of them did not bind SD1-RBD proteins corresponding to the latest Omicron variants. However, we were able to identify some that are broadly cross-reactive and also neutralizing. Such antibodies could be combined with sd1.040 in a bispecific formulation in future experiments.

In conclusion, this work demonstrates the potential of SD1 antibodies in the ongoing fight against SARS-CoV-2 and its variants. The sorting strategy that we devised could help future discovery of additional SD1 antibodies from individuals with hybrid immunity because of exposure to both virus and vaccination, as well as from those who suffered repeated exposure to distinct

VOCs. The study of this class of antibodies may be relevant especially in light of recent evidence showing that they are an increasingly relevant component of the human polyclonal response against the latest VOCs. We furthermore discovered and characterized the only SD1 antibody that remains effective against Omicron BA.2.86 and showed that its combination with RBD antibodies can improve neutralization in a synergistic way. Despite the WHO declaring the end of the COVID-19 emergency on May 5th, 2023[177], we expect SARS-CoV-2 to remain endemic with likely seasonal fluctuations in the number of clinically relevant infections, in addition to the periodical emergence of new variants[233]. In this regard, finding neutralizing antibodies that are resilient to the emergence of new variants may be more important than finding potent neutralizers specific for few variants. SD1 antibodies seem to fulfill this requirement and thus have the potential to become a novel class of drugs for passive immunotherapy.

7. ADDENDUM

During my PhD, I collaborated to the publication of 4 other papers from our and other research groups. These papers, which are not part of my thesis project, are listed below.

BISPECIFIC IgG NEUTRALIZES SARS-COV-2 VARIANTS AND PREVENTS ESCAPE IN MICE

Raoul De Gasparo[1,16], Mattia Pedotti[1,16], Luca Simonelli[1], Petr Nickl[2], Frauke Muecksch[3], Irene Cassaniti[4], Elena Percivalle[4], Julio C. C. Lorenzi[5], Federica Mazzola[1], Davide Magrì[6], Tereza Michalcikova[2], Jan Haviernik[7], Vaclav Honig[7,8], Blanka Mrazkova[2], Natalie Polakova[2], Andrea Fortova[7], Jolana Tureckova[2], Veronika Iatsiuk[2], Salvatore Di Girolamo[1], Martin Palus[7,8], Dagmar Zudova[2], Petr Bednar[7,9], Ivana Bukova[2], **Filippo Bianchini**[1], Dora Mehn[6], Radim Nencka[10], Petra Strakova[7], Oto Pavlis[11], Jan Rozman[2], Sabrina Gioria[6], Josè Camilla Sammartino[4], Federica Giardina[4], Stefano Gaiarsa[4], Qiang Pan-Hammarström[12], Christopher O. Barnes[13], Pamela J. Bjorkman[13], Luigi Calzolai[6], Antonio Piralla[4], Fausto Baldanti[4,14], Michel C. Nussenzweig[5,15], Paul D. Bieniasz[3,15], Theodora Hatziioannou[3], Jan Prochazka[2], Radislav Sedlacek[2], Davide F. Robbiani[1] ✉, Daniel Ruzek[7,8] ✉ & Luca Varani[1] ✉

[1]Institute for Research in Biomedicine, Università della Svizzera italiana (USI), Bellinzona, Switzerland. [2]Czech Centre of Phenogenomics and Laboratory of Transgenic Models of Diseases, Institute of Molecular Genetics of the Czech Academy of Sciences, Vestec, Czech Republic. [3]Laboratory of Retrovirology, The Rockefeller University, New York, NY, USA. [4]Molecular Virology Unit, Microbiology and Virology Department, Fondazione IRCCS Policlinico San Matteo, Pavia, Italy. [5]Laboratory of Molecular Immunology, The Rockefeller University, New York, NY, USA. [6]European Commission, Joint Research Centre, Ispra, Italy. [7]Veterinary Research Institute, Brno, Czech Republic. [8]Institute of Parasitology, Biology Centre of the Czech Academy of Sciences, Ceske Budejovice, Czech Republic. [9]Faculty of Science, University of South Bohemia, Ceske Budejovice, Czech Republic. [10]Institute of Organic Chemistry and Biochemistry of the Czech Academy of Sciences, Prague, Czech Republic. [11]Center of Biological Defense, Military Health Institute, Military Medical Agency, Techonin, Czech Republic. [12]Department of Biosciences and Nutrition, Karolinska Institutet, Huddinge, Sweden. [13]Division of Biology and Biological Engineering, California Institute of Technology, Pasadena, CA, USA. [14]Department of Clinical Surgical Diagnostic and Pediatric Sciences, Università degli Studi di Pavia, Pavia, Italy. [15]Howard Hughes Medical Institute, The Rockefeller University, New York, NY, USA.
[16]These authors contributed equally: Raoul De Gasparo, Mattia Pedotti.
✉e-mail: drobbiani@irb.usi.ch; ruzekd@paru.cas.cz; luca.varani@irb.usi.ch

Personal contribution:

- Preparation and sequencing of cDNA samples from viral RNA extracted from mouse lungs.

Status: published in Nature (10.1038/s41586-021-03461-y), March 2021.

BROAD AND POTENT NEUTRALIZING HUMAN ANTIBODIES TO TICK-BORNE FLAVIVIRUSES PROTECT MICE FROM DISEASE

Marianna Agudelo[1], MartinPalus[2,3*], Jennifer R. Keeffe[4*], **Filippo Bianchini**[1,5], Pavel Svoboda[3,6], Jirı Salat[2,3], AveryPeace[7], Anna Gazumyan[1], Melissa Cipolla[1], Tania Kapoor[1], Francesca Guidetti[1], Kai-Hui Yao[1], Jana Elsterova[2,3], Dana Teislerova[8], Ales Chrdle[8,9,10], Vaclav Honig[2,3], Thiago Oliveira[1], Anthony P. West Jr.[4], Yu E. Lee[4], Charles M. Rice[7], Margaret R. MacDonald[7], Pamela J. Bjorkman[4], Daniel Ruzek[2,3], Davide F. Robbiani[1,5], and Michel C. Nussenzweig[1,11]

[1]Laboratory of Molecular Immunology, The Rockefeller University, New York, NY; [2]Institute of Parasitology, Biology Centre of the Czech Academy of Sciences, Ceske Budejovice, Czech Republic; [3]Veterinary Research Institute, Brno, Czech Republic; [4]Division of Biology and Biological Engineering, California Institute of Technology, Pasadena, CA; [5]Institute for Research in Biomedicine, Università della Svizzera italiana, Bellinzona, Switzerland; [6]Department of Pharmacology and Pharmacy, Faculty of Veterinary Medicine, University of Veterinary and Pharmaceutical Sciences Brno, Brno, Czech Republic; [7]Laboratory of Virology and Infectious Disease, The Rockefeller University, New York, NY; [8]Hospital Ceske Budejovice, Ceske Budejovice, Czech Republic; [9]Faculty of Social and Health Sciences, University of South Bohemia, Ceske Budejovice, Czech Republic; [10]Royal Liverpool University Hospital, Liverpool, UK; [11]Howard Hughes Medical Institute, The Rockefeller University, New York, NY.
*M. Palus and J.R. Keeffe contributed equally to this paper;
Correspondence to Michel C. Nussenzweig: nussen@rockefeller.edu; Davide F. Robbiani: drobbiani@ irb.usi.ch; Daniel Ruzek: ruzekd@paru.cas.cz; Pamela J. Bjorkman: bjorkman@caltech.edu.

Personal contribution:

- Experimental analysis,
- Monoclonal antibodies cloning, purification and characterization,
- Execution of the experiments (i.e., antibody PCRs, cloning, expression and purification; ELISA on mAbs; neutralization of flavivirus RVPs),

Status: published in Journal of Experimental Medicine (10.1084/jem.20210236), April 2021.

AUTOANTIBODIES AGAINST CHEMOKINES POST-SARS-COV-2 INFECTION CORRELATE WITH DISEASE COURSE

Jonathan Muri[1,23], Valentina Cecchinato[1,23], Andrea Cavalli[1,2], Akanksha A. Shanbhag[1], Milos Matkovic[1], Maira Biggiogero[3], Pier Andrea Maida[3], Jacques Moritz[1], Chiara Toscano[1], Elaheh Ghovehoud[1], Raffaello Furlan[4,5], Franca Barbic[4,5], Antonio Voza[4,6], Guendalina De Nadai[7], Carlo Cervia[8], Yves Zurbuchen[8], Patrick Taeschler[8] , Lilly A. Murray[9], Gabriela Danelon-Sargenti[1], Simone Moro[1], Tao Gong[1], Pietro Piffaretti[1], **Filippo Bianchini**[1], Virginia Crivelli[1], Lucie Podešvová[1], Mattia Pedotti[1], David Jarrossay[1], Jacopo Sgrignani[1], Sylvia Thelen[1], Mario Uhr[10], Enos Bernasconi[11,12], Andri Rauch[13], Antonio Manzo[14], Adrian Ciurea[15], Marco B. L. Rocchi[16], Luca Varani[1] , Bernhard Moser[17], Barbara Bottazzi[18], Marcus Thelen[1], Brian A. Fallon[9,19], Onur Boyman[8,20], Alberto Mantovani[4,18,21], Christian Garzoni[22], Alessandra Franzetti-Pellanda[3], Mariagrazia Uguccioni[1,4,24] & Davide F. Robbiani[1,24]

[1]Institute for Research in Biomedicine, Università della Svizzera italiana, Bellinzona, Switzerland. [2]Swiss Institute of Bioinformatics, Lausanne, Switzerland. [3]Clinical Research Unit, Clinica Luganese Moncucco, Lugano, Switzerland. [4]Department of Biomedical Sciences, Humanitas University, Milan, Italy. [5]Department of Internal Medicine, IRCCS Humanitas Research Hospital, Milan, Italy. [6]Department of Emergency, IRCCS Humanitas Research Hospital, Milan, Italy. [7]Emergency Medicine Residency School, Department of Biomedical Sciences, Humanitas University, Milan, Italy. [8]Department of Immunology, University Hospital Zurich, University of Zurich, Zurich, Switzerland. [9]Lyme and Tick-Borne Diseases Research Center at Columbia University Irving Medical Center, New York, NY, USA. [10]Synlab Suisse, Bioggio, Switzerland. [11]Regional Hospital Lugano, Ente Ospedaliero Cantonale, Lugano, Switzerland. [12]Università della Svizzera italiana, Lugano, Switzerland. [13]Department of Infectious Diseases, Inselspital, Bern University Hospital, University of Bern, Bern, Switzerland. [14]Rheumatology and Translational Immunology Research Laboratories (LaRIT), Division of Rheumatology, IRCCS Policlinico San Matteo Foundation, University of Pavia, Pavia, Italy. [15]Department of Rheumatology, University Hospital Zurich, University of Zurich, Zurich, Switzerland. [16]Department of Biomolecular Sciences, Biostatistics Unit, University of Urbino, Urbino, Italy. [17]Division of Infection & Immunity, Cardiff University School of Medicine, Cardiff, UK. [18]IRCCS Humanitas Research Hospital, Milan, Italy. [19]Lyme Research Program at the New York State Psychiatric Institute, New York, NY, USA. [20]Faculty of Medicine and Faculty of Science, University of Zurich, Zurich, Switzerland. [21]The William Harvey Research Institute, Queen Mary University of London, London, UK. [22]Internal Medicine and Infectious Diseases, Clinica Luganese Moncucco, Lugano, Switzerland.
[23]These authors contributed equally: Jonathan Muri, Valentina Cecchinato.
[24]These authors jointly supervised this work: Davide F. Robbiani and Mariagrazia Uguccioni.
e-mail: andrea.cavalli@irb.usi.ch; mariagrazia.uguccioni@irb.usi.ch; drobbiani@irb.usi.ch

Personal contribution:

- Experimental analysis,
- Design, generation, purification and characterization of RBD expression plasmid and protein,
- Execution of the experiments (i.e., buffy coat processing; antibody expression and purification; ELISA on plasma),

Status: published in Nature Immunology (10.1038/s41590-023-01445-w), March 2023.

ANALYTICAL ULTRACENTRIFUGATION DETECTS QUATERNARY REARRANGEMENTS AND ANTIBODY-INDUCED CONFORMATIONAL SELECTION OF THE SARS-COV-2 SPIKE TRIMER

Giuditta Guerrini[1], Dora Mehn[1], Francesco Fumagalli[1], Sabrina Gioria[1], Mattia Pedotti[2], Luca Simonelli[2], **Filippo Bianchini**[2], Davide F. Robbiani[2], Luca Varani[2,*] and Luigi Calzolai[1,*]

[1]European Commission, Joint Research Centre (JRC), 21027 Ispra, Italy; giuditta.guerrini@ec.europa.eu (G.G.); dora.mehn@ec.europa.eu (D.M.); francesco-sirio.fumagalli@ec.europa.eu (F.F.); sabrina.gioria@ec.europa.eu (S.G.)
[2]Institute for Research in Biomedicine, Università della Svizzera Italiana, 6500 Bellinzona, Switzerland; mattia.pedotti@irb.usi.ch (M.P.); luca.simonelli@irb.usi.ch (L.S.); filippo.bianchini@irb.usi.ch (F.B.); drobbiani@irb.usi.ch (D.F.R.)
*Correspondence: luca.varani@irb.usi.ch (L.V.); luigi.calzolai@ec.europa.eu (L.C.)

Personal contribution:

- Design, generation, purification and characterization of monoclonal antibodies.

Status: published in International Journal of Molecular Sciences (10.3390/ijms241914875), October 2023.

8. BIBLIOGRAPHY

1. Abbas, A. K., Lichtman, A. H., Pillai, S., Baker, D. L. & Baker, A. *Cellular and Molecular Immunology*. (Elsevier, Philadelphia, PA, 2018).
2. Hayday, A. C. & Vantourout, P. The Innate Biologies of Adaptive Antigen Receptors. *Annu. Rev. Immunol.* **38**, 487–510 (2020).
3. Takeuchi, O. & Akira, S. Pattern Recognition Receptors and Inflammation. *Cell* **140**, 805–820 (2010).
4. Murphy, K. & Weaver, C. *Janeway's Immunobiology*. (Garland Science, 2016).
5. Charles A Janeway, J., Travers, P., Walport, M. & Shlomchik, M. J. Principles of innate and adaptive immunity. in *Immunobiology: The Immune System in Health and Disease. 5th edition* (Garland Science, 2001).
6. Netea, M. G. *et al.* Trained immunity: A program of innate immune memory in health and disease. *Science* **352**, aaf1098 (2016).
7. Netea, M. G. *et al.* Defining trained immunity and its role in health and disease. *Nat. Rev. Immunol.* **20**, 375–388 (2020).
8. Althwaiqeb, S. A. & Bordoni, B. Histology, B Cell Lymphocyte. in *StatPearls* (StatPearls Publishing, Treasure Island (FL), 2024).
9. Nagasawa, T. Microenvironmental niches in the bone marrow required for B-cell development. *Nat. Rev. Immunol.* **6**, 107–116 (2006).
10. Nutt, S. L., Eberhard, D., Horcher, M., Rolink, A. G. & Busslinger, M. Pax5 Determines the Identity of B Cells from the Beginning to the End of B-lymphopoiesis. *Int. Rev. Immunol.* **20**, 65–82 (2001).
11. Zandi, S. *et al.* EBF1 Is Essential for B-Lineage Priming and Establishment of a Transcription Factor Network in Common Lymphoid Progenitors1. *J. Immunol.* **181**, 3364–3372 (2008).
12. Herzog, S., Reth, M. & Jumaa, H. Regulation of B-cell proliferation and differentiation by pre-B-cell receptor signalling. *Nat. Rev. Immunol.* **9**, 195–205 (2009).
13. Hardy, R. R. B-1 B Cell Development1. *J. Immunol.* **177**, 2749–2754 (2006).
14. Pieper, K., Grimbacher, B. & Eibel, H. B-cell biology and development. *J. Allergy Clin. Immunol.* **131**, 959–971 (2013).
15. Wang, Y., Liu, J., Burrows, P. D. & Wang, J.-Y. B Cell Development and Maturation. in *B Cells in Immunity and Tolerance* (ed. Wang, J.-Y.) 1–22 (Springer, Singapore, 2020). doi:10.1007/978-981-15-3532-1_1.
16. Wang, H., Morse, H. C. & Bolland, S. Transcriptional Control of Mature B Cell Fates. *Trends Immunol.* **41**, 601–613 (2020).
17. Zouali, M. & Richard, Y. Marginal Zone B-Cells, a Gatekeeper of Innate Immunity. *Front. Immunol.* **2**, (2011).

18. Deenen, G. J. & Kroese, F. G. M. Kinetics of peritoneal B-1a cells (CD5 B cells) in young adult mice. *Eur. J. Immunol.* **23**, 12–16 (1993).
19. Kageyama, Y. & Katayama, N. Ontogeny of human B1 cells. *Int. J. Hematol.* **111**, 628–633 (2020).
20. Griffin, D. & Rothstein, T. L. Human B1 Cell Frequency: Isolation and Analysis of Human B1 Cells. *Front. Immunol.* **3**, (2012).
21. Matsuuchi, L. & Gold, M. R. New views of BCR structure and organization. *Curr. Opin. Immunol.* **13**, 270–277 (2001).
22. Kurosaki, T. Regulation of BCR signaling. *Mol. Immunol.* **48**, 1287–1291 (2011).
23. Rickert, R. C. Regulation of B lymphocyte activation by complement C3 and the B cell coreceptor complex. *Curr. Opin. Immunol.* **17**, 237–243 (2005).
24. Nemazee, D. Mechanisms of central tolerance for B cells. *Nat. Rev. Immunol.* **17**, 281–294 (2017).
25. Gururajan, M., Sindhava, V. J. & Bondada, S. B Cell Tolerance in Health and Disease. *Antibodies* **3**, 116–129 (2014).
26. Gonzalez, S. F. *et al.* Trafficking of B Cell Antigen in Lymph Nodes. *Annu. Rev. Immunol.* **29**, 215–233 (2011).
27. Ohl, L. *et al.* Cooperating Mechanisms of CXCR5 and CCR7 in Development and Organization of Secondary Lymphoid Organs. *J. Exp. Med.* **197**, 1199–1204 (2003).
28. Hardtke, S., Ohl, L. & Förster, R. Balanced expression of CXCR5 and CCR7 on follicular T helper cells determines their transient positioning to lymph node follicles and is essential for efficient B-cell help. *Blood* **106**, 1924–1931 (2005).
29. MacLennan, I. C. M. Germinal Centers. *Annu. Rev. Immunol.* **12**, 117–139 (1994).
30. Victora, G. D. *et al.* Germinal Center Dynamics Revealed by Multiphoton Microscopy with a Photoactivatable Fluorescent Reporter. *Cell* **143**, 592–605 (2010).
31. Shlomchik, M. J., Luo, W. & Weisel, F. Linking signaling and selection in the germinal center. *Immunol. Rev.* **288**, 49–63 (2019).
32. Shimoda, M., Li, T., Pihkala, J. P. S. & Koni, P. A. Role of MHC Class II on Memory B Cells in Post-Germinal Center B Cell Homeostasis and Memory Response1. *J. Immunol.* **176**, 2122–2133 (2006).
33. Khalil, A. M., Cambier, J. C. & Shlomchik, M. J. B Cell Receptor Signal Transduction in the GC Is Short-Circuited by High Phosphatase Activity. *Science* **336**, 1178–1181 (2012).
34. Anderson, S. M. *et al.* Taking Advantage: High-Affinity B Cells in the Germinal Center Have Lower Death Rates, but Similar Rates of Division, Compared to Low-Affinity Cells1. *J. Immunol.* **183**, 7314–7325 (2009).

35. Weisel, F. J., Zuccarino-Catania, G. V., Chikina, M. & Shlomchik, M. J. A Temporal Switch in the Germinal Center Determines Differential Output of Memory B and Plasma Cells. *Immunity* **44**, 116–130 (2016).
36. Shinnakasu, R. *et al.* Regulated selection of germinal-center cells into the memory B cell compartment. *Nat. Immunol.* **17**, 861–869 (2016).
37. Zhang, Y. *et al.* Plasma cell output from germinal centers is regulated by signals from Tfh and stromal cells. *J. Exp. Med.* **215**, 1227–1243 (2018).
38. Ionescu, L. & Urschel, S. Memory B Cells and Long-lived Plasma Cells. *Transplantation* **103**, 890 (2019).
39. Nutt, S. L., Hodgkin, P. D., Tarlinton, D. M. & Corcoran, L. M. The generation of antibody-secreting plasma cells. *Nat. Rev. Immunol.* **15**, 160–171 (2015).
40. Kabashima, K. *et al.* Plasma cell S1P1 expression determines secondary lymphoid organ retention versus bone marrow tropism. *J. Exp. Med.* **203**, 2683–2690 (2006).
41. Chu, V. T. & Berek, C. The establishment of the plasma cell survival niche in the bone marrow. *Immunol. Rev.* **251**, 177–188 (2013).
42. Peperzak, V. *et al.* Mcl-1 is essential for the survival of plasma cells. *Nat. Immunol.* **14**, 290–297 (2013).
43. Saini, A. S., Shenoy, G. N., Rath, S., Bal, V. & George, A. Inducible nitric oxide synthase is a major intermediate in signaling pathways for the survival of plasma cells. *Nat. Immunol.* **15**, 275–282 (2014).
44. Xiang, Z. *et al.* FcγRIIb controls bone marrow plasma cell persistence and apoptosis. *Nat. Immunol.* **8**, 419–429 (2007).
45. Trepel, F. Number and distribution of lymphocytes in man. A critical analysis. *Klin. Wochenschr.* **52**, 511–515 (1974).
46. Terstappen, L., Johnsen, S., Segers-Nolten, I. & Loken, M. Identification and characterization of plasma cells in normal human bone marrow by high-resolution flow cytometry. *Blood* **76**, 1739–1747 (1990).
47. Radbruch, A. *et al.* Competence and competition: the challenge of becoming a long-lived plasma cell. *Nat. Rev. Immunol.* **6**, 741–750 (2006).
48. Odendahl, M. *et al.* Generation of migratory antigen-specific plasma blasts and mobilization of resident plasma cells in a secondary immune response. *Blood* **105**, 1614–1621 (2005).
49. Schauer, U. *et al.* Levels of Antibodies Specific to Tetanus Toxoid, Haemophilus influenzae Type b, and Pneumococcal Capsular Polysaccharide in Healthy Children and Adults. *Clin. Vaccine Immunol.* **10**, 202–207 (2003).
50. Human Immunoglobulin (Ig)M+IgD+ Peripheral Blood B Cells Expressing the CD27 Cell Surface Antigen Carry Somatically Mutated Variable Region Genes: CD27 as a General Marker for Somatically Mutated (Memory) B Cells | Journal of Experimental Medicine |

Rockefeller University Press. https://rupress.org/jem/article/188/9/1679/7789/Human-Immunoglobulin-Ig-M-IgD-Peripheral-Blood-B.
51. Schittek, B. & Rajewsky, K. Natural occurrence and origin of somatically mutated memory B cells in mice. *J. Exp. Med.* **176**, 427–438 (1992).
52. Amanna, I. J., Carlson, N. E. & Slifka, M. K. Duration of Humoral Immunity to Common Viral and Vaccine Antigens. *N. Engl. J. Med.* **357**, 1903–1915 (2007).
53. Inoue, T. & Kurosaki, T. Memory B cells. *Nat. Rev. Immunol.* 1–13 (2023) doi:10.1038/s41577-023-00897-3.
54. Taylor, J. J., Pape, K. A. & Jenkins, M. K. A germinal center–independent pathway generates unswitched memory B cells early in the primary response. *J. Exp. Med.* **209**, 597–606 (2012).
55. Paus, D. *et al.* Antigen recognition strength regulates the choice between extrafollicular plasma cell and germinal center B cell differentiation. *J. Exp. Med.* **203**, 1081–1091 (2006).
56. Viant, C. *et al.* Antibody Affinity Shapes the Choice between Memory and Germinal Center B Cell Fates. *Cell* **183**, 1298-1311.e11 (2020).
57. Glaros, V. *et al.* Limited access to antigen drives generation of early B cell memory while restraining the plasmablast response. *Immunity* **54**, 2005-2023.e10 (2021).
58. Exit from germinal center to become quiescent memory B cells depends on metabolic reprograming and provision of a survival signal | Journal of Experimental Medicine | Rockefeller University Press. https://rupress.org/jem/article/218/1/e20200866/211457/Exit-from-germinal-center-to-become-quiescent.
59. Chen, S. T., Oliveira, T. Y., Gazumyan, A., Cipolla, M. & Nussenzweig, M. C. B cell receptor signaling in germinal centers prolongs survival and primes B cells for selection. *Immunity* **56**, 547-561.e7 (2023).
60. Finkin, S., Hartweger, H., Oliveira, T. Y., Kara, E. E. & Nussenzweig, M. C. Protein Amounts of the MYC Transcription Factor Determine Germinal Center B Cell Division Capacity. *Immunity* **51**, 324-336.e5 (2019).
61. Ersching, J. *et al.* Germinal Center Selection and Affinity Maturation Require Dynamic Regulation of mTORC1 Kinase. *Immunity* **46**, 1045-1058.e6 (2017).
62. Viant, C. *et al.* Germinal center–dependent and –independent memory B cells produced throughout the immune response. *J. Exp. Med.* **218**, e20202489 (2021).
63. Ehrhardt, G. R. A. *et al.* Expression of the immunoregulatory molecule FcRH4 defines a distinctive tissue-based population of memory B cells. *J. Exp. Med.* **202**, 783–791 (2005).

64. Zhang, Y. *et al.* Recycling of memory B cells between germinal center and lymph node subcapsular sinus supports affinity maturation to antigenic drift. *Nat. Commun.* **13**, 2460 (2022).
65. Fazilleau, N. *et al.* Lymphoid reservoirs of antigen-specific memory T helper cells. *Nat. Immunol.* **8**, 753–761 (2007).
66. Moran, I. *et al.* Memory B cells are reactivated in subcapsular proliferative foci of lymph nodes. *Nat. Commun.* **9**, 3372 (2018).
67. Mesin, L. *et al.* Restricted Clonality and Limited Germinal Center Reentry Characterize Memory B Cell Reactivation by Boosting. *Cell* **180**, 92-106.e11 (2020).
68. Pape, K. A., Taylor, J. J., Maul, R. W., Gearhart, P. J. & Jenkins, M. K. Different B Cell Populations Mediate Early and Late Memory During an Endogenous Immune Response. *Science* **331**, 1203–1207 (2011).
69. Leach, S. *et al.* Requirement for memory B-cell activation in protection from heterologous influenza virus reinfection. *Int. Immunol.* **31**, 771–779 (2019).
70. Wong, R. *et al.* Affinity-Restricted Memory B Cells Dominate Recall Responses to Heterologous Flaviviruses. *Immunity* **53**, 1078-1094.e7 (2020).
71. Purtha, W. E., Tedder, T. F., Johnson, S., Bhattacharya, D. & Diamond, M. S. Memory B cells, but not long-lived plasma cells, possess antigen specificities for viral escape mutants. *J. Exp. Med.* **208**, 2599–2606 (2011).
72. V(D)J recombination, somatic hypermutation and class switch recombination of immunoglobulins: mechanism and regulation - Chi - 2020 - Immunology - Wiley Online Library. https://onlinelibrary.wiley.com/doi/10.1111/imm.13176.
73. Woof, J. M. & Russell, M. W. Structure and function relationships in IgA. *Mucosal Immunol.* **4**, 590–597 (2011).
74. Dechant, M. *et al.* Effector Mechanisms of Recombinant IgA Antibodies against Epidermal Growth Factor Receptor. *J. Immunol.* **179**, 2936–2943 (2007).
75. Lohse, S. *et al.* Effector mechanisms of IgA antibodies against CD20 include recruitment of myeloid cells for antibody-dependent cell-mediated cytotoxicity and complement-dependent cytotoxicity. *Br. J. Haematol.* **181**, 413–417 (2018).
76. Johansen, F.-E., Braathen, R. & Brandtzaeg, P. The J Chain Is Essential for Polymeric Ig Receptor-Mediated Epithelial Transport of IgA1. *J. Immunol.* **167**, 5185–5192 (2001).
77. Furtado, P. B. *et al.* Solution Structure Determination of Monomeric Human IgA2 by X-ray and Neutron Scattering, Analytical Ultracentrifugation and Constrained Modelling: A Comparison with Monomeric Human IgA1. *J. Mol. Biol.* **338**, 921–941 (2004).

78. Steffen, U. *et al.* IgA subclasses have different effector functions associated with distinct glycosylation profiles. *Nat. Commun.* **11**, 120 (2020).
79. Josephs, D. H., Spicer, J. F., Karagiannis, P., Gould, H. J. & Karagiannis, S. N. IgE immunotherapy. *mAbs* **6**, 54–72 (2014).
80. Kretschmer, A., Schwanbeck, R., Valerius, T. & Rösner, T. Antibody Isotypes for Tumor Immunotherapy. *Transfus. Med. Hemotherapy* **44**, 320–326 (2017).
81. Hlavacek, W. S. *et al.* Quantifying aggregation of IgE-FcepsilonRI by multivalent antigen. *Biophys. J.* **76**, 2421–2431 (1999).
82. Brüggemann, M. *et al.* Comparison of the effector functions of human immunoglobulins using a matched set of chimeric antibodies. *J. Exp. Med.* **166**, 1351–1361 (1987).
83. Garred, P., Michaelsen, T. E. & Aase, A. The IgG Subclass Pattern of Complement Activation Depends on Epitope Density and Antibody and Complement Concentration. *Scand. J. Immunol.* **30**, 379–382 (1989).
84. Rösner, T. *et al.* An IgG3 switch variant of rituximab mediates enhanced complement-dependent cytotoxicity against tumour cells with low CD20 expression levels. *Br. J. Haematol.* **161**, 282–286 (2013).
85. Bruhns, P. Properties of mouse and human IgG receptors and their contribution to disease models. *Blood* **119**, 5640–5649 (2012).
86. van der Neut Kolfschoten, M. *et al.* Anti-Inflammatory Activity of Human IgG4 Antibodies by Dynamic Fab Arm Exchange. *Science* **317**, 1554–1557 (2007).
87. Johansen, Braathen, & Brandtzaeg. Role of J Chain in Secretory Immunoglobulin Formation. *Scand. J. Immunol.* **52**, 240–248 (2000).
88. Michaelsen, T. E. *et al.* Human Secretory IgM Antibodies Activate Human Complement and Offer Protection at Mucosal Surface. *Scand. J. Immunol.* **85**, 43–50 (2017).
89. Wang, H., Coligan, J. E. & Morse, H. C. Emerging Functions of Natural IgM and Its Fc Receptor FCMR in Immune Homeostasis. *Front. Immunol.* **7**, 99 (2016).
90. Kubagawa, H. *et al.* The Long Elusive IgM Fc Receptor, FcμR. *J. Clin. Immunol.* **34**, S35 (2014).
91. Enders, A. *et al.* Zinc-finger protein ZFP318 is essential for expression of IgD, the alternatively spliced Igh product made by mature B lymphocytes. *Proc. Natl. Acad. Sci.* **111**, 4513–4518 (2014).
92. Quách, T. D. *et al.* Anergic Responses Characterize a Large Fraction of Human Autoreactive Naive B Cells Expressing Low Levels of Surface IgM. *J. Immunol.* **186**, 4640–4648 (2011).
93. Arpin, C. *et al.* The Normal Counterpart of IgD Myeloma Cells in Germinal Center Displays Extensively Mutated IgVH Gene, C□–C? Switch, and □ Light Chain Expression.

94. Gutzeit, C., Chen, K. & Cerutti, A. The enigmatic function of IgD: some answers at last. *Eur. J. Immunol.* **48**, 1101–1113 (2018).
95. Drenth, J. P. H., Göertz, J., Daha, M. R. & Van Der Meer, J. W. M. Immunoglobulin D enhances the release of tumour necrosis factor-α, and interleukin-1β as well as interleukin-1 receptor antagonist from human mononuclear cells. *Immunology* **88**, 355–362 (1996).
96. Chen, K. *et al.* Immunoglobulin D enhances immune surveillance by activating antimicrobial, proinflammatory and B cell–stimulating programs in basophils. *Nat. Immunol.* **10**, 889–898 (2009).
97. Sechet, B., Meseri-Delwail, A., Arock, M., Wijdenes, J. & Sarrouilhe, D. Immunoglobulin D Enhances Interleukin-6 Release from the KU812 Human Prebasophil Cell Line.
98. Carmona, L. M. & Schatz, D. G. New insights into the evolutionary origins of the recombination-activating gene proteins and V(D)J recombination. *FEBS J.* **284**, 1590–1605 (2017).
99. Hwang, J. K., Alt, F. W. & Yeap, L.-S. Related Mechanisms of Antibody Somatic Hypermutation and Class Switch Recombination. *Microbiol. Spectr.* **3**, 10.1128/microbiolspec.mdna3-0037–2014 (2015).
100. Kim, M.-S., Lapkouski, M., Yang, W. & Gellert, M. Crystal structure of the V(D)J recombinase RAG1–RAG2. *Nature* **518**, 507–511 (2015).
101. Panchakshari, R. A. *et al.* DNA double-strand break response factors influence end-joining features of IgH class switch and general translocation junctions. *Proc. Natl. Acad. Sci.* **115**, 762–767 (2018).
102. Ru, H. *et al.* Molecular Mechanism of V(D)J Recombination from Synaptic RAG1-RAG2 Complex Structures. *Cell* **163**, 1138–1152 (2015).
103. Motea, E. A. & Berdis, A. J. Terminal deoxynucleotidyl transferase: The story of a misguided DNA polymerase. *Biochim. Biophys. Acta BBA - Proteins Proteomics* **1804**, 1151–1166 (2010).
104. Roldán, E. *et al.* Locus 'decontraction' and centromeric recruitment contribute to allelic exclusion of the immunoglobulin heavy-chain gene. *Nat. Immunol.* **6**, 31–41 (2005).
105. Ebert, A., Hill, L. & Busslinger, M. Chapter Three - Spatial Regulation of V–(D)J Recombination at Antigen Receptor Loci. in *Advances in Immunology* (ed. Murre, C.) vol. 128 93–121 (Academic Press, 2015).
106. Zan, H. & Casali, P. Regulation of Aicda expression and AID activity. *Autoimmunity* **46**, 83–101 (2013).
107. Jiricny, J. Postreplicative Mismatch Repair. *Cold Spring Harb. Perspect. Biol.* **5**, a012633 (2013).
108. Krokan, H. E. & Bjørås, M. Base Excision Repair. *Cold Spring Harb. Perspect. Biol.* **5**, a012583 (2013).
109. Di Noia, J. M. & Neuberger, M. S. Molecular Mechanisms of Antibody Somatic Hypermutation. *Annu. Rev. Biochem.* **76**, 1–22 (2007).

110. Matthews, A. J., Zheng, S., DiMenna, L. J. & Chaudhuri, J. Chapter One - Regulation of Immunoglobulin Class-Switch Recombination: Choreography of Noncoding Transcription, Targeted DNA Deamination, and Long-Range DNA Repair. in *Advances in Immunology* (ed. Alt, F. W.) vol. 122 1–57 (Academic Press, 2014).
111. Feldman, S. *et al.* 53BP1 Contributes to Igh Locus Chromatin Topology during Class Switch Recombination. *J. Immunol.* **198**, 2434–2444 (2017).
112. Eccleston, J., Yan, C., Yuan, K., Alt, F. W. & Selsing, E. Mismatch repair proteins MSH2, MLH1, and EXO1 are important for class-switch recombination events occurring in B cells that lack nonhomologous end joining. *J. Immunol. Baltim. Md 1950* **186**, 2336–2343 (2011).
113. Boboila, C., Alt, F. W. & Schwer, B. Chapter One - Classical and Alternative End-Joining Pathways for Repair of Lymphocyte-Specific and General DNA Double-Strand Breaks. in *Advances in Immunology* (ed. Alt, F. W.) vol. 116 1–49 (Academic Press, 2012).
114. Stavnezer, J. & Schrader, C. E. IgH Chain Class Switch Recombination: Mechanism and Regulation. *J. Immunol.* **193**, 5370–5378 (2014).
115. Koenderman, L. Inside-Out Control of Fc-Receptors. *Front. Immunol.* **10**, (2019).
116. Daëron, M. Fc Receptors as Adaptive Immunoreceptors. in *Fc Receptors* (eds. Daeron, M. & Nimmerjahn, F.) 131–164 (Springer International Publishing, Cham, 2014). doi:10.1007/978-3-319-07911-0_7.
117. Mancardi, D. A. *et al.* FcγRIV is a mouse IgE receptor that resembles macrophage FcεRI in humans and promotes IgE-induced lung inflammation. *J. Clin. Invest.* **118**, 3738–3750 (2008).
118. Bruhns, P. *et al.* Specificity and affinity of human Fcγ receptors and their polymorphic variants for human IgG subclasses. *Blood* **113**, 3716–3725 (2009).
119. Bezman, N. & Koretzky, G. A. Compartmentalization of ITAM and integrin signaling by adapter molecules. *Immunol. Rev.* **218**, 9–28 (2007).
120. Nakamura, K., Malykhin, A. & Coggeshall, K. M. The Src homology 2 domain–containing inositol 5-phosphatase negatively regulates Fcγ receptor–mediated phagocytosis through immunoreceptor tyrosine-based activation motif–bearing phagocytic receptors. *Blood* **100**, 3374–3382 (2002).
121. Gimborn, K., Lessmann, E., Kuppig, S., Krystal, G. & Huber, M. SHIP Down-Regulates FcεR1-Induced Degranulation at Supraoptimal IgE or Antigen Levels. *J. Immunol.* **174**, 507–516 (2005).
122. Lesourne, R., Fridman, W. H. & Daëron, M. Dynamic Interactions of Fcγ Receptor IIB with Filamin-Bound SHIP1 Amplify Filamentous Actin-

Dependent Negative Regulation of Fcε Receptor I Signaling1. *J. Immunol.* **174**, 1365–1373 (2005).
123. Daëron, M., Malbec, O., Latour, S., Arock, M. & Fridman, W. H. Regulation of high-affinity IgE receptor-mediated mast cell activation by murine low-affinity IgG receptors. *J. Clin. Invest.* **95**, 577–585 (1995).
124. Forthal, D. N. Functions of Antibodies. *Microbiol. Spectr.* **2**, 10.1128/microbiolspec.aid-0019–2014 (2014).
125. Phalipon, A. *et al.* Secretory Component: A New Role in Secretory IgA-Mediated Immune Exclusion In Vivo. *Immunity* **17**, 107–115 (2002).
126. Brandtzaeg, P. Induction of secretory immunity and memory at mucosal surfaces. *Vaccine* **25**, 5467–5484 (2007).
127. Brioen, P., Dekegel, D. & Boeyé, A. Neutralization of poliovirus by antibody-mediated polymerization. *Virology* **127**, 463–468 (1983).
128. Campodónico, V. L. *et al.* Evaluation of Flagella and Flagellin of Pseudomonas aeruginosa as Vaccines. *Infect. Immun.* **78**, 746–755 (2010).
129. McCullough, K. C. *et al.* Conformational alteration in foot-and-mouth disease virus virion capsid structure after complexing with monospecific antibody. *Immunology* **60**, 75–82 (1987).
130. Hernandez, R., Paredes, A. & Brown, D. T. Sindbis Virus Conformational Changes Induced by a Neutralizing Anti-E1 Monoclonal Antibody. *J. Virol.* **82**, 5750–5760 (2008).
131. Pachl, J. *et al.* A Randomized, Blinded, Multicenter Trial of Lipid-Associated Amphotericin B Alone versus in Combination with an Antibody-Based Inhibitor of Heat Shock Protein 90 in Patients with Invasive Candidiasis. *Clin. Infect. Dis.* **42**, 1404–1413 (2006).
132. Preclinical Assessment of the Efficacy of Mycograb, a Human Recombinant Antibody against Fungal HSP90 | Antimicrobial Agents and Chemotherapy. https://journals.asm.org/doi/full/10.1128/aac.47.7.2208-2216.2003.
133. McClelland, E. E., Nicola, A. M., Prados-Rosales, R. & Casadevall, A. Ab binding alters gene expression in *Cryptococcus neoformans* and directly modulates fungal metabolism. *J. Clin. Invest.* **120**, 1355–1361 (2010).
134. Booy, F. P., Roden, R. B. S., Greenstone, H. L., Schiller, J. T. & Trus, B. L. Two antibodies that neutralize papillomavirus by different mechanisms show distinct binding patterns at 13 Å resolution1. *J. Mol. Biol.* **281**, 95–106 (1998).
135. Smith, T. J. *et al.* Structure of human rhinovirus complexed with Fab fragments from a neutralizing antibody. *J. Virol.* **67**, 1148–1158 (1993).
136. Klasse, P. J., Sanders, R. W., Cerutti, A. & Moore, J. P. How Can HIV-Type-1-Env Immunogenicity Be Improved to Facilitate Antibody-Based Vaccine Development? *AIDS Res. Hum. Retroviruses* **28**, 1–15 (2012).

137. He, R.-T. *et al.* Antibodies that block virus attachment to vero cells are a major component of the human neutralizing antibody response against dengue virus type 2. *J. Med. Virol.* **45**, 451–461 (1995).
138. Iorio, R. M., Glickman, R. L., Riel, A. M., Sheehan, J. P. & Bratt, M. A. Functional and neutralization profile of seven overlapping antigenic sites on the HN glycoprotein of Newcastle disease virus: monoclonal antibodies to some sites prevent viral attachment. *Virus Res.* **13**, 245–261 (1989).
139. Platt, E. J., Gomes, M. M. & Kabat, D. Kinetic mechanism for HIV-1 neutralization by antibody 2G12 entails reversible glycan binding that slows cell entry. *Proc. Natl. Acad. Sci.* **109**, 7829–7834 (2012).
140. Della-Porta, A. J. & Westaway, E. G. A Multi-Hit Model for the Neutralization of Animal Viruses. *J. Gen. Virol.* **38**, 1–19 (1978).
141. Klemm, P., Vejborg, R. M. & Hancock, V. Prevention of bacterial adhesion. *Appl. Microbiol. Biotechnol.* **88**, 451–459 (2010).
142. Khan, M. N. & Pichichero, M. E. Vaccine candidates PhtD and PhtE of *Streptococcus pneumoniae* are adhesins that elicit functional antibodies in humans. *Vaccine* **30**, 2900–2907 (2012).
143. Sui, X., Yan, L. & Jiang, Y. The vaccines and antibodies associated with Als3p for treatment of *Candida albicans* infections. *Vaccine* **35**, 5786–5793 (2017).
144. Kaufmann, B. *et al.* West Nile virus in complex with the Fab fragment of a neutralizing monoclonal antibody. *Proc. Natl. Acad. Sci.* **103**, 12400–12404 (2006).
145. de Rosny, E., Vassell, R., Jiang, S., Kunert, R. & Weiss, C. D. Binding of the 2F5 Monoclonal Antibody to Native and Fusion-Intermediate Forms of Human Immunodeficiency Virus Type 1 gp41: Implications for Fusion-Inducing Conformational Changes. *J. Virol.* **78**, 2627–2631 (2004).
146. Edwards, M. J. & Dimmock, N. J. Hemagglutinin 1-Specific Immunoglobulin G and Fab Molecules Mediate Postattachment Neutralization of Influenza A Virus by Inhibition of an Early Fusion Event. *J. Virol.* **75**, 10208–10218 (2001).
147. Ishii, Y. *et al.* Inhibition of nuclear entry of HPV16 pseudovirus-packaged DNA by an anti-HPV16 L2 neutralizing antibody. *Virology* **406**, 181–188 (2010).
148. Mallery, D. L. *et al.* Antibodies mediate intracellular immunity through tripartite motif-containing 21 (TRIM21). *Proc. Natl. Acad. Sci.* **107**, 19985–19990 (2010).
149. Preparation and Properties of Antibody Directed Specifically Against the Neuraminidase of Influenza Virus | The Journal of Immunology | American Association of Immunologists. https://journals.aai.org/jimmunol/article-abstract/99/1/49/68973/Preparation-and-Properties-of-Antibody-Directed.

150. DiScipio, R. G. & Schraufstatter, I. U. The role of the complement anaphylatoxins in the recruitment of eosinophils. *Int. Immunopharmacol.* **7**, 1909–1923 (2007).
151. Charles A Janeway, J., Travers, P., Walport, M. & Shlomchik, M. J. The complement system and innate immunity. in *Immunobiology: The Immune System in Health and Disease. 5th edition* (Garland Science, 2001).
152. Poorly Neutralizing Cross-Reactive Antibodies against the Fusion Loop of West Nile Virus Envelope Protein Protect In Vivo via Fcγ Receptor and Complement-Dependent Effector Mechanisms | Journal of Virology. https://journals.asm.org/doi/full/10.1128/jvi.05859-11.
153. Forthal, D. N. & Moog, C. Fc receptor-mediated antiviral antibodies. *Curr. Opin. HIV AIDS* **4**, 388–393 (2009).
154. Brunner, K. T., Hurez, D., McCluskey, R. T. & Benacerraf, B. Blood Clearance of P32-Labeled Vesicular Stomatitis and Newcastle Disease Viruses by the Reticuloendothelial System in Mice1. *J. Immunol.* **85**, 99–105 (1960).
155. Igarashi, T. *et al.* Human immunodeficiency virus type 1 neutralizing antibodies accelerate clearance of cell–free virions from blood plasma. *Nat. Med.* **5**, 211–216 (1999).
156. Fan, G., Wang, Z., Hao, M. & Li, J. Bispecific antibodies and their applications. *J. Hematol. Oncol.J Hematol Oncol* **8**, 130 (2015).
157. Kontermann, R. E. & Brinkmann, U. Bispecific antibodies. *Drug Discov. Today* **20**, 838–847 (2015).
158. Brinkmann, U. & Kontermann, R. E. The making of bispecific antibodies. *mAbs* **9**, 182–212 (2017).
159. Ma, J. *et al.* Bispecific Antibodies: From Research to Clinical Application. *Front. Immunol.* **12**, (2021).
160. Schaefer, W. *et al.* Immunoglobulin domain crossover as a generic approach for the production of bispecific IgG antibodies. *Proc. Natl. Acad. Sci.* **108**, 11187–11192 (2011).
161. Labrijn, A. F., Janmaat, M. L., Reichert, J. M. & Parren, P. W. H. I. Bispecific antibodies: a mechanistic review of the pipeline. *Nat. Rev. Drug Discov.* **18**, 585–608 (2019).
162. Fenis, A., Demaria, O., Gauthier, L., Vivier, E. & Narni-Mancinelli, E. New immune cell engagers for cancer immunotherapy. *Nat. Rev. Immunol.* 1–16 (2024) doi:10.1038/s41577-023-00982-7.
163. Deak, L. L. C. *et al.* Abstract 2270: RG7769 (PD1-TIM3), a novel heterodimeric avidity-driven T cell specific PD-1/TIM-3 bispecific antibody lacking Fc-mediated effector functions for dual checkpoint inhibition to reactivate dysfunctional T cells. *Cancer Res.* **80**, 2270 (2020).

164. Gadkar, K. *et al.* Mathematical PKPD and safety model of bispecific TfR/BACE1 antibodies for the optimization of antibody uptake in brain. *Eur. J. Pharm. Biopharm.* **101**, 53–61 (2016).
165. Schäfer, A. *et al.* Antibody potency, effector function, and combinations in protection and therapy for SARS-CoV-2 infection in vivo. *J. Exp. Med.* **218**, e20201993 (2020).
166. De Gasparo, R. *et al.* Bispecific IgG neutralizes SARS-CoV-2 variants and prevents escape in mice. *Nature* **593**, 424–428 (2021).
167. Helmy, Y. A. *et al.* The COVID-19 Pandemic: A Comprehensive Review of Taxonomy, Genetics, Epidemiology, Diagnosis, Treatment, and Control. *J. Clin. Med.* **9**, 1225 (2020).
168. Lefkowitz, E. J. *et al.* Virus taxonomy: the database of the International Committee on Taxonomy of Viruses (ICTV). *Nucleic Acids Res.* **46**, D708–D717 (2018).
169. Tyrrell, D. A. J. & Bynoe, M. L. Cultivation of a Novel Type of Common-cold Virus in Organ Cultures. *Br. Med. J.* **1**, 1467–1470 (1965).
170. Summary of probable SARS cases with onset of illness from 1 November 2002 to 31 July 2003. https://www.who.int/publications/m/item/summary-of-probable-sars-cases-with-onset-of-illness-from-1-november-2002-to-31-july-2003.
171. Severe acute respiratory syndrome (SARS). https://www.who.int/publications-detail-redirect/severe-acute-respiratory-syndrome-(sars)-executive-board-113.
172. CSR. MERS outbreaks. *World Health Organization - Regional Office for the Eastern Mediterranean* http://www.emro.who.int/health-topics/mers-cov/mers-outbreaks.html.
173. Zaki, A. M., van Boheemen, S., Bestebroer, T. M., Osterhaus, A. D. M. E. & Fouchier, R. A. M. Isolation of a Novel Coronavirus from a Man with Pneumonia in Saudi Arabia. *N. Engl. J. Med.* **367**, 1814–1820 (2012).
174. Zhou, P. *et al.* A pneumonia outbreak associated with a new coronavirus of probable bat origin. *Nature* **579**, 270–273 (2020).
175. Huang, C. *et al.* Clinical features of patients infected with 2019 novel coronavirus in Wuhan, China. *The Lancet* **395**, 497–506 (2020).
176. Transmission of 2019-nCoV Infection from an Asymptomatic Contact in Germany | NEJM. https://www.nejm.org/doi/full/10.1056/nejmc2001468.
177. Coronavirus disease (COVID-19) pandemic. https://www.who.int/europe/emergencies/situations/covid-19.
178. Cowling, B. J. & Leung, G. M. Epidemiological research priorities for public health control of the ongoing global novel coronavirus (2019-nCoV) outbreak. *Eurosurveillance* **25**, 2000110 (2020).
179. Coronavirus disease (COVID-19) – World Health Organization. https://www.who.int/emergencies/diseases/novel-coronavirus-2019.

180. Cui, J., Li, F. & Shi, Z.-L. Origin and evolution of pathogenic coronaviruses. *Nat. Rev. Microbiol.* **17**, 181–192 (2019).
181. Zhang, S. *et al.* Bat and pangolin coronavirus spike glycoprotein structures provide insights into SARS-CoV-2 evolution. *Nat. Commun.* **12**, 1607 (2021).
182. Bai, C., Zhong, Q. & Gao, G. F. Overview of SARS-CoV-2 genome-encoded proteins. *Sci. China Life Sci.* **65**, 280–294 (2022).
183. Surjit, M. & Lal, S. K. The SARS-CoV nucleocapsid protein: A protein with multifarious activities. *Infect. Genet. Evol.* **8**, 397–405 (2008).
184. Verdiá-Báguena, C. *et al.* Coronavirus E protein forms ion channels with functionally and structurally-involved membrane lipids. *Virology* **432**, 485–494 (2012).
185. Venkatagopalan, P., Daskalova, S. M., Lopez, L. A., Dolezal, K. A. & Hogue, B. G. Coronavirus envelope (E) protein remains at the site of assembly. *Virology* **478**, 75–85 (2015).
186. Lim, K. P. & Liu, D. X. The Missing Link in Coronavirus Assembly: RETENTION OF THE AVIAN CORONAVIRUS INFECTIOUS BRONCHITIS VIRUS ENVELOPE PROTEIN IN THE PRE-GOLGI COMPARTMENTS AND PHYSICAL INTERACTION BETWEEN THE ENVELOPE AND MEMBRANE PROTEINS *. *J. Biol. Chem.* **276**, 17515–17523 (2001).
187. Jimenez-Guardeño, J. M. *et al.* The PDZ-Binding Motif of Severe Acute Respiratory Syndrome Coronavirus Envelope Protein Is a Determinant of Viral Pathogenesis. *PLOS Pathog.* **10**, e1004320 (2014).
188. Teoh, K.-T. *et al.* The SARS Coronavirus E Protein Interacts with PALS1 and Alters Tight Junction Formation and Epithelial Morphogenesis. *Mol. Biol. Cell* **21**, 3838–3852 (2010).
189. Bcl-xL inhibits T-cell apoptosis induced by expression of SARS coronavirus E protein in the absence of growth factors | Biochemical Journal | Portland Press. https://portlandpress.com/biochemj/article/392/1/135/44065/Bcl-xL-inhibits-T-cell-apoptosis-induced-by.
190. Neuman, B. W. *et al.* A structural analysis of M protein in coronavirus assembly and morphology. *J. Struct. Biol.* **174**, 11–22 (2011).
191. Tortorici, M. A. & Veesler, D. Chapter Four - Structural insights into coronavirus entry. in *Advances in Virus Research* (ed. Rey, F. A.) vol. 105 93–116 (Academic Press, 2019).
192. Thoms, M. *et al.* Structural basis for translational shutdown and immune evasion by the Nsp1 protein of SARS-CoV-2. *Science* **369**, 1249–1255 (2020).
193. Deng, X. *et al.* Coronavirus nonstructural protein 15 mediates evasion of dsRNA sensors and limits apoptosis in macrophages. *Proc. Natl. Acad. Sci.* **114**, E4251–E4260 (2017).

194. Bartlam, M., Xu, Y. & Rao, Z. Structural proteomics of the SARS coronavirus: a model response to emerging infectious diseases. *J. Struct. Funct. Genomics* **8**, 85–97 (2007).
195. Arya, R. *et al.* Structural insights into SARS-CoV-2 proteins. *J. Mol. Biol.* **433**, 166725 (2021).
196. Adedeji, A. O. *et al.* Mechanism of Nucleic Acid Unwinding by SARS-CoV Helicase. *PLOS ONE* **7**, e36521 (2012).
197. Bouvet, M. *et al.* Coronavirus Nsp10, a Critical Co-factor for Activation of Multiple Replicative Enzymes *. *J. Biol. Chem.* **289**, 25783–25796 (2014).
198. Viswanathan, T. *et al.* Structural basis of RNA cap modification by SARS-CoV-2. *Nat. Commun.* **11**, 3718 (2020).
199. Ferron, F. *et al.* Structural and molecular basis of mismatch correction and ribavirin excision from coronavirus RNA. *Proc. Natl. Acad. Sci.* **115**, E162–E171 (2018).
200. Eckerle, L. D. *et al.* Infidelity of SARS-CoV Nsp14-Exonuclease Mutant Virus Replication Is Revealed by Complete Genome Sequencing. *PLOS Pathog.* **6**, e1000896 (2010).
201. Gorkhali, R. *et al.* Structure and Function of Major SARS-CoV-2 and SARS-CoV Proteins. *Bioinforma. Biol. Insights* **15**, 11779322211025876 (2021).
202. Gordon, D. E. *et al.* A SARS-CoV-2 protein interaction map reveals targets for drug repurposing. *Nature* **583**, 459–468 (2020).
203. Kopecky-Bromberg, S. A., Martinez-Sobrido, L. & Palese, P. 7a Protein of Severe Acute Respiratory Syndrome Coronavirus Inhibits Cellular Protein Synthesis and Activates p38 Mitogen-Activated Protein Kinase. *J. Virol.* **80**, 785–793 (2006).
204. Flower, T. G. *et al.* Structure of SARS-CoV-2 ORF8, a rapidly evolving immune evasion protein. *Proc. Natl. Acad. Sci.* **118**, e2021785118 (2021).
205. Gordon, D. E. *et al.* Comparative host-coronavirus protein interaction networks reveal pan-viral disease mechanisms. *Science* **370**, eabe9403 (2020).
206. Zhang, J. *et al.* Understanding the Role of SARS-CoV-2 ORF3a in Viral Pathogenesis and COVID-19. *Front. Microbiol.* **13**, (2022).
207. Chorba, T. The Concept of the Crown and Its Potential Role in the Downfall of Coronavirus. *Emerg. Infect. Dis.* **26**, 2302–2305 (2020).
208. Takeda, M. Proteolytic activation of SARS-CoV-2 spike protein. *Microbiol. Immunol.* **66**, 15–23 (2022).
209. Walls, A. C. *et al.* Structure, Function, and Antigenicity of the SARS-CoV-2 Spike Glycoprotein. *Cell* **181**, 281-292.e6 (2020).
210. Papa, G. *et al.* Furin cleavage of SARS-CoV-2 Spike promotes but is not essential for infection and cell-cell fusion. *PLOS Pathog.* **17**, e1009246 (2021).

211. Jackson, C. B., Farzan, M., Chen, B. & Choe, H. Mechanisms of SARS-CoV-2 entry into cells. *Nat. Rev. Mol. Cell Biol.* **23**, 3–20 (2022).
212. Henderson, R. *et al.* Controlling the SARS-CoV-2 spike glycoprotein conformation. *Nat. Struct. Mol. Biol.* **27**, 925–933 (2020).
213. Yuan, Y. *et al.* Cryo-EM structures of MERS-CoV and SARS-CoV spike glycoproteins reveal the dynamic receptor binding domains. *Nat. Commun.* **8**, 15092 (2017).
214. Clausen, T. M. *et al.* SARS-CoV-2 Infection Depends on Cellular Heparan Sulfate and ACE2. *Cell* **183**, 1043-1057.e15 (2020).
215. Benton, D. J. *et al.* Receptor binding and priming of the spike protein of SARS-CoV-2 for membrane fusion. *Nature* **588**, 327–330 (2020).
216. Yurkovetskiy, L. *et al.* Structural and Functional Analysis of the D614G SARS-CoV-2 Spike Protein Variant. *Cell* **183**, 739-751.e8 (2020).
217. Gobeil, S. M.-C. *et al.* D614G Mutation Alters SARS-CoV-2 Spike Conformation and Enhances Protease Cleavage at the S1/S2 Junction. *Cell Rep.* **34**, (2021).
218. Shi, W. *et al.* Cryo-EM structure of SARS-CoV-2 postfusion spike in membrane. *Nature* **619**, 403–409 (2023).
219. Malone, B., Urakova, N., Snijder, E. J. & Campbell, E. A. Structures and functions of coronavirus replication–transcription complexes and their relevance for SARS-CoV-2 drug design. *Nat. Rev. Mol. Cell Biol.* **23**, 21–39 (2022).
220. Bhatt, P. R. *et al.* Structural basis of ribosomal frameshifting during translation of the SARS-CoV-2 RNA genome. *Science* **372**, 1306–1313 (2021).
221. Brant, A. C., Tian, W., Majerciak, V., Yang, W. & Zheng, Z.-M. SARS-CoV-2: from its discovery to genome structure, transcription, and replication. *Cell Biosci.* **11**, 136 (2021).
222. Pasternak, A. O., Spaan, W. J. M. & Snijder, E. J. Nidovirus transcription: how to make sense…? *J. Gen. Virol.* **87**, 1403–1421 (2006).
223. Sola, I., Almazán, F., Zúñiga, S. & Enjuanes, L. Continuous and Discontinuous RNA Synthesis in Coronaviruses. *Annu. Rev. Virol.* **2**, 265–288 (2015).
224. Sawicki, S. G., Sawicki, D. L. & Siddell, S. G. A Contemporary View of Coronavirus Transcription. *J. Virol.* **81**, 20–29 (2007).
225. CDC. Coronavirus Disease 2019 (COVID-19). *Centers for Disease Control and Prevention* https://www.cdc.gov/coronavirus/2019-ncov/variants/variant-classifications.html (2020).
226. Rawson, J. M. O., Landman, S. R., Reilly, C. S. & Mansky, L. M. HIV-1 and HIV-2 exhibit similar mutation frequencies and spectra in the absence of G-to-A hypermutation. *Retrovirology* **12**, 60 (2015).

227. Ribeiro, R. M. *et al.* Quantifying the Diversification of Hepatitis C Virus (HCV) during Primary Infection: Estimates of the In Vivo Mutation Rate. *PLOS Pathog.* **8**, e1002881 (2012).
228. Amicone, M. *et al.* Mutation rate of SARS-CoV-2 and emergence of mutators during experimental evolution. *Evol. Med. Public Health* **10**, 142–155 (2022).
229. Kim, K. *et al.* The roles of APOBEC-mediated RNA editing in SARS-CoV-2 mutations, replication and fitness. *Sci. Rep.* **12**, 14972 (2022).
230. Impact of ADAR-induced editing of minor viral RNA populations on replication and transmission of SARS-CoV-2 | PNAS. https://www.pnas.org/doi/abs/10.1073/pnas.2112663119.
231. Carabelli, A. M. *et al.* SARS-CoV-2 variant biology: immune escape, transmission and fitness. *Nat. Rev. Microbiol.* **21**, 162–177 (2023).
232. Hilleman, M. R. Strategies and mechanisms for host and pathogen survival in acute and persistent viral infections. *Proc. Natl. Acad. Sci.* **101**, 14560–14566 (2004).
233. Markov, P. V. *et al.* The evolution of SARS-CoV-2. *Nat. Rev. Microbiol.* **21**, 361–379 (2023).
234. SARS-CoV-2 D614G spike mutation increases entry efficiency with enhanced ACE2-binding affinity | Nature Communications. https://www.nature.com/articles/s41467-021-21118-2.
235. Liu, H. *et al.* The basis of a more contagious 501Y.V1 variant of SARS-CoV-2. *Cell Res.* **31**, 720–722 (2021).
236. Wrobel, A. G. *et al.* Evolution of the SARS-CoV-2 spike protein in the human host. *Nat. Commun.* **13**, 1178 (2022).
237. Lamers, M. M. *et al.* SARS-CoV-2 Omicron efficiently infects human airway, but not alveolar epithelium. 2022.01.19.476898 Preprint at https://doi.org/10.1101/2022.01.19.476898 (2022).
238. Harvey, W. T. *et al.* SARS-CoV-2 variants, spike mutations and immune escape. *Nat. Rev. Microbiol.* **19**, 409–424 (2021).
239. Viana, R. *et al.* Rapid epidemic expansion of the SARS-CoV-2 Omicron variant in southern Africa. *Nature* **603**, 679–686 (2022).
240. Increased risk of SARS-CoV-2 reinfection associated with emergence of Omicron in South Africa | Science. https://www.science.org/doi/full/10.1126/science.abn4947.
241. Konings, F. *et al.* SARS-CoV-2 Variants of Interest and Concern naming scheme conducive for global discourse. *Nat. Microbiol.* **6**, 821–823 (2021).
242. Davies, N. G. *et al.* Estimated transmissibility and impact of SARS-CoV-2 lineage B.1.1.7 in England. *Science* **372**, eabg3055 (2021).
243. Tegally, H. *et al.* Detection of a SARS-CoV-2 variant of concern in South Africa. *Nature* **592**, 438–443 (2021).

244. Faria, N. R. *et al.* Genomics and epidemiology of the P.1 SARS-CoV-2 lineage in Manaus, Brazil. *Science* **372**, 815–821 (2021).
245. Dhar, M. S. *et al.* Genomic characterization and epidemiology of an emerging SARS-CoV-2 variant in Delhi, India. *Science* **374**, 995–999 (2021).
246. Campbell, F. *et al.* Increased transmissibility and global spread of SARS-CoV-2 variants of concern as at June 2021. *Eurosurveillance* **26**, 2100509 (2021).
247. Attwood, S. W., Hill, S. C., Aanensen, D. M., Connor, T. R. & Pybus, O. G. Phylogenetic and phylodynamic approaches to understanding and combating the early SARS-CoV-2 pandemic. *Nat. Rev. Genet.* **23**, 547–562 (2022).
248. Tegally, H. *et al.* Emergence of SARS-CoV-2 Omicron lineages BA.4 and BA.5 in South Africa. *Nat. Med.* **28**, 1785–1790 (2022).
249. Ito, J. *et al.* Convergent evolution of SARS-CoV-2 Omicron subvariants leading to the emergence of BQ.1.1 variant. *Nat. Commun.* **14**, 2671 (2023).
250. Khare, S. *et al.* GISAID's Role in Pandemic Response. *China CDC Wkly.* **3**, 1049–1051 (2021).
251. Adepoju, P. Challenges of SARS-CoV-2 genomic surveillance in Africa. *Lancet Microbe* **2**, e139 (2021).
252. Wilkinson, E. *et al.* A year of genomic surveillance reveals how the SARS-CoV-2 pandemic unfolded in Africa. *Science* **374**, 423–431 (2021).
253. Hale, V. L. *et al.* SARS-CoV-2 infection in free-ranging white-tailed deer. *Nature* **602**, 481–486 (2022).
254. Oude Munnink, B. B. *et al.* Transmission of SARS-CoV-2 on mink farms between humans and mink and back to humans. *Science* **371**, 172–177 (2021).
255. Schlottau, K. *et al.* SARS-CoV-2 in fruit bats, ferrets, pigs, and chickens: an experimental transmission study. *Lancet Microbe* **1**, e218–e225 (2020).
256. Choi, B. *et al.* Persistence and Evolution of SARS-CoV-2 in an Immunocompromised Host. *N. Engl. J. Med.* **383**, 2291–2293 (2020).
257. Wilkinson, S. A. J. *et al.* Recurrent SARS-CoV-2 mutations in immunodeficient patients. *Virus Evol.* **8**, veac050 (2022).
258. Clark, S. A. *et al.* SARS-CoV-2 evolution in an immunocompromised host reveals shared neutralization escape mechanisms. *Cell* **184**, 2605-2617.e18 (2021).
259. Funk, T. *et al.* Characteristics of SARS-CoV-2 variants of concern B.1.1.7, B.1.351 or P.1: data from seven EU/EEA countries, weeks 38/2020 to 10/2021. *Eurosurveillance* **26**, 2100348 (2021).
260. Assessment of the further spread and potential impact of the SARS-CoV-2 Omicron variant of concern in the EU/EEA, 19th update.

https://www.ecdc.europa.eu/en/publications-data/covid-19-omicron-risk-assessment-further-emergence-and-potential-impact (2022).
261. Cevik, M. *et al.* SARS-CoV-2, SARS-CoV, and MERS-CoV viral load dynamics, duration of viral shedding, and infectiousness: a systematic review and meta-analysis. *Lancet Microbe* **2**, e13–e22 (2021).
262. Taylor, P. C. *et al.* Neutralizing monoclonal antibodies for treatment of COVID-19. *Nat. Rev. Immunol.* **21**, 382–393 (2021).
263. Li, D., Sempowski, G. D., Saunders, K. O., Acharya, P. & Haynes, B. F. SARS-CoV-2 Neutralizing Antibodies for COVID-19 Prevention and Treatment. *Annu. Rev. Med.* **73**, 1–16 (2022).
264. Piccoli, L. *et al.* Mapping Neutralizing and Immunodominant Sites on the SARS-CoV-2 Spike Receptor-Binding Domain by Structure-Guided High-Resolution Serology. *Cell* **183**, 1024-1042.e21 (2020).
265. Chen, Y. *et al.* Broadly neutralizing antibodies to SARS-CoV-2 and other human coronaviruses. *Nat. Rev. Immunol.* 1–11 (2022) doi:10.1038/s41577-022-00784-3.
266. Barnes, C. O. *et al.* SARS-CoV-2 neutralizing antibody structures inform therapeutic strategies. *Nature* **588**, 682–687 (2020).
267. Planas, D. *et al.* Considerable escape of SARS-CoV-2 Omicron to antibody neutralization. *Nature* **602**, 671–675 (2022).
268. Pinto, D. *et al.* Cross-neutralization of SARS-CoV-2 by a human monoclonal SARS-CoV antibody. *Nature* **583**, 290–295 (2020).
269. Touret, F. *et al.* Enhanced neutralization escape to therapeutic monoclonal antibodies by SARS-CoV-2 omicron sub-lineages. *iScience* **26**, (2023).
270. Jennewein, M. F. *et al.* Isolation and characterization of cross-neutralizing coronavirus antibodies from COVID-19+ subjects. *Cell Rep.* **36**, 109353 (2021).
271. McCallum, M. *et al.* N-terminal domain antigenic mapping reveals a site of vulnerability for SARS-CoV-2. *Cell* **184**, 2332-2347.e16 (2021).
272. Bianchini, F. *et al.* Human neutralizing antibodies to cold linear epitopes and subdomain 1 of the SARS-CoV-2 spike glycoprotein. *Sci. Immunol.* **8**, eade0958 (2023).
273. Seow, J. *et al.* A neutralizing epitope on the SD1 domain of SARS-CoV-2 spike targeted following infection and vaccination. *Cell Rep.* **40**, (2022).
274. Xu, S. *et al.* Mapping cross-variant neutralizing sites on the SARS-CoV-2 spike protein. *Emerg. Microbes Infect.* **11**, 351–367 (2022).
275. Wang, Q. *et al.* Antigenicity and receptor affinity of SARS-CoV-2 BA.2.86 spike. *Nature* **624**, 639–644 (2023).
276. Tanaka, S. *et al.* Rapid identification of neutralizing antibodies against SARS-CoV-2 variants by mRNA display. *Cell Rep.* **38**, (2022).

277. Guenthoer, J. *et al.* Identification of broad, potent antibodies to functionally constrained regions of SARS-CoV-2 spike following a breakthrough infection. *Proc. Natl. Acad. Sci.* **120**, e2220948120 (2023).
278. Liu, L. *et al.* Antibodies targeting a quaternary site on SARS-CoV-2 spike glycoprotein prevent viral receptor engagement by conformational locking. *Immunity* **56**, 2442-2455.e8 (2023).
279. Zhou, D. *et al.* The SARS-CoV-2 neutralizing antibody response to SD1 and its evasion by BA.2.86. *Nat. Commun.* **15**, 2734 (2024).
280. Epitopes of an antibody that neutralizes a wide range of SARS-CoV-2 variants in a conserved subdomain 1 of the spike protein | Journal of Virology. https://journals.asm.org/doi/10.1128/jvi.00416-24.
281. Shrestha, L. B., Tedla, N. & Bull, R. A. Broadly-Neutralizing Antibodies Against Emerging SARS-CoV-2 Variants. *Front. Immunol.* **12**, (2021).
282. Pinto, D. *et al.* Broad betacoronavirus neutralization by a stem helix–specific human antibody. *Science* **373**, 1109–1116 (2021).
283. Shi, W. *et al.* Vaccine-elicited murine antibody WS6 neutralizes diverse beta-coronaviruses by recognizing a helical stem supersite of vulnerability. *Structure* **30**, 1233-1244.e7 (2022).
284. Dacon, C. *et al.* Broadly neutralizing antibodies target the coronavirus fusion peptide. *Science* **377**, 728–735 (2022).
285. Sun, X. *et al.* Neutralization mechanism of a human antibody with pan-coronavirus reactivity including SARS-CoV-2. *Nat. Microbiol.* **7**, 1063–1074 (2022).
286. Low, J. S. *et al.* ACE2-binding exposes the SARS-CoV-2 fusion peptide to broadly neutralizing coronavirus antibodies. *Science* **377**, 735–742 (2022).
287. Fenwick, C. *et al.* Patient-derived monoclonal antibody neutralizes SARS-CoV-2 Omicron variants and confers full protection in monkeys. *Nat. Microbiol.* **7**, 1376–1389 (2022).
288. Westendorf, K. *et al.* LY-CoV1404 (bebtelovimab) potently neutralizes SARS-CoV-2 variants. *Cell Rep.* **39**, 110812 (2022).
289. Focosi, D. & Casadevall, A. A Critical Analysis of the Use of Cilgavimab plus Tixagevimab Monoclonal Antibody Cocktail (Evusheld™) for COVID-19 Prophylaxis and Treatment. *Viruses* **14**, 1999 (2022).
290. Drysdale, M. *et al.* Real-world effectiveness of sotrovimab for the treatment of SARS-CoV-2 infection during Omicron BA.2 and BA.5 subvariant predominance: a systematic literature review. *Infection* (2024) doi:10.1007/s15010-024-02245-6.
291. Zhou, D., Ren, J., Fry, E. E. & Stuart, D. I. Broadly neutralizing antibodies against COVID-19. *Curr. Opin. Virol.* **61**, 101332 (2023).
292. Robbiani, D. F. *et al.* Convergent antibody responses to SARS-CoV-2 in convalescent individuals. *Nature* **584**, 437–442 (2020).

293. Atyeo, C. *et al.* Dissecting strategies to tune the therapeutic potential of SARS-CoV-2–specific monoclonal antibody CR3022. *JCI Insight* **6**, e143129.
294. Liu, H. *et al.* Cross-Neutralization of a SARS-CoV-2 Antibody to a Functionally Conserved Site Is Mediated by Avidity. *Immunity* **53**, 1272-1280.e5 (2020).
295. Malahe, S. R. K. *et al.* Clinical Characteristics and Outcomes of Immunocompromised Patients With Coronavirus Disease 2019 Caused by the Omicron Variant: A Prospective, Observational Study. *Clin. Infect. Dis.* **76**, e172–e178 (2023).
296. Fericean, R. M. *et al.* Outcomes of Elderly Patients Hospitalized with the SARS-CoV-2 Omicron B.1.1.529 Variant: A Systematic Review. *Int. J. Environ. Res. Public. Health* **20**, 2150 (2023).
297. Boufidou, F. *et al.* SARS-CoV-2 Reinfections and Long COVID in the Post-Omicron Phase of the Pandemic. *Int. J. Mol. Sci.* **24**, 12962 (2023).
298. Paciello, I., Maccari, G., Pantano, E., Andreano, E. & Rappuoli, R. High-resolution map of the Fc functions mediated by COVID-19-neutralizing antibodies. *Proc. Natl. Acad. Sci.* **121**, e2314730121 (2024).
299. Pierre, C. N. *et al.* Non-neutralizing SARS-CoV-2 N-terminal domain antibodies protect mice against severe disease using Fc-mediated effector functions. 2023.07.25.550460 Preprint at https://doi.org/10.1101/2023.07.25.550460 (2023).
300. Guerrini, G. *et al.* Analytical Ultracentrifugation Detects Quaternary Rearrangements and Antibody-Induced Conformational Selection of the SARS-CoV-2 Spike Trimer. *Int. J. Mol. Sci.* **24**, 14875 (2023).

ACKNOWLEDGEMENTS

The very first acknowledgement of this thesis goes, of course, to my PhD supervisor, **Davide**. Not only you gave me a life-changing opportunity when I was still a young master student scared to leave Italy, but you took care of me both scientifically and personally since the beginning of the COVID-19 pandemic. I am short of words to express my gratitude, but I can say that I couldn't wish for a better mentor for my PhD.

I thank **Lucie** for being my best workmate and gossiping buddy. Even if we couldn't find almost any common interest (ok, maybe one…), we still got to stay together until the very end. But you know, we shouldn't be surprised. After all, Sagittarius and Gemini are opposites but compatible. With you, I learned about Czech black humour, curses, fat food and, of course, science.

Jacques, I know that you don't want to read this, so I'm asking Lucie to force you. You joined the lab later than others, and I think that's a pity because the environment is much funnier since you are around. I really enjoyed your (very French) personality and your… particular jokes. I thank you for always trying to make Bellinzona a more bearable place for people that hate nature, like me. Please, don't change.

Thanks to **Jasmine** for your kindness and huuuge help with the experiments. You learned a lot very fast and became a sort of "lab mom", always available for everyone and ready to solve conflicts in a pacific way.

Acknowledgements are also due to all the other people that are currently part of the lab (i.e., **Benedetta**, **Tao**, **Amara**, **Joanna**, **Vaiva**, **Virginia** and **Tomàs**), but also to those people that left. Just to mention some of the most important for me and my thesis, I want to thank **Victoria** for being our moral compass and a caring friend. Even if we disagree on fundamental ideals, like the role of Harry Potter in modern society, it was inspiring to see how you were standing up for your principles.

Thanks to **Andrea** for all the help that you gave me even when the ELISA background was overwhelming us. Unfortunately, it won, but you fought as a hero.

Akanksha, you also helped me with many experiments but, honestly, I thank you mainly for all the nice moments we spent together as a fake-couple. Similarly to what I've written for Jacques, I would have liked you to stay with us longer.

Thanks to **Chiara** for being the very first person joining the lab after me, saving me from solitude, and for the help you gave me when we had to set up the lab from scratch.

Thank you, **Jonathan**. You have been a fundamental and reliable part of the lab for so long that we were all astonished when you decided to leave. I will

remember you as a model of the perfect Postdoc, despite your weird obsession for Egyptians.
And of course, **Pietro** (aka PIETROOOH). I've never met a genuinely happy and funny person like you. Thank you for being always ready to joke about everything, while trading bitcoins and doing ELISA. You made me re-discover baking as an important stress-relief.
There are also people from other labs that I would like to thank. First of all, **Gabriela**, for being my first tutor when I joined IRB and for all the help in setting up the new lab. Thank you also for the intensive course of "IRB history and backstage".
Thanks to all the guys from **Uguccioni**, **Cavalli** and **Varani labs** for the precious collaborations and for the nice time spent together.
Last but not the least, I want to thank **my parents and my family** for having supported me also in this last journey toward the end of the "student" life. I know you will always be here for me, and that the achievement of a PhD will not change this, but I think that the bare minimum from my side is to let you know that I notice how much you do and I appreciate every single act. We are not used, as family, to express our love out loud, and we do it mainly through little gestures. But I mean, is it so bad?

Take life lightly, for lightness is not superficiality, but gliding above things, not having weights on your heart.

-Italo Calvino, American Lessons

RINGRAZIAMENTI

Il primo ringraziamento di questa tesi va, ovviamente, al mio supervisore, **Davide**. Non solo mi hai offerto un'opportunità unica quando ancora ero un giovane studente di magistrale spaventato dall'idea di lasciare l'Italia, ma ti sei anche preso cura di me sia scientificamente che umanamente sin dall'inizio della pandemia di COVID-19. Non ho parole per esprimerti la mia gratitudine, ma posso affermare che non avrei potuto desiderare un mentore migliore per il mio PhD.

Ringrazio **Lucie** per essere stata la mia miglior compagna di lavoro e di pettegolezzi. Anche se non siamo riusciti a trovare alcun interesse comune (ok, forse uno…), siamo comunque riusciti a stare uniti fino alla fine. Ma sai, non dovremmo essere sorpresi. In fondo, sagittario e gemelli sono segni opposti ma compatibili. Grazie a te ho ampliato la mia conoscenza del black humour, gli insulti e il cibo grasso della Repubblica Ceca, oltre, ovviamente, alla scienza.

Jacques, so che non vuoi leggere tutto questo, quindi chiedo a Lucie di obbligarti. Ti sei unito a questo laboratorio più tardi di altri, e ritengo che sia un peccato perché l'ambiente è molto più divertente da quando ci sei. Ho apprezzato moltissimo la tua personalità (molto francese) e le tue battute… particolari. Ti ringrazio per aver provato a rendere Bellinzona un posto più sopportabile per quelle persone che odiano la natura, come me. Per favore, non cambiare.

Grazie a **Jasmine** per la tua gentilezza e il graaande aiuto con gli esperimenti. Hai imparato così tanto così in fretta e sei diventata una sorta di "mamma di laboratorio", sempre pronta ad aiutare chiunque e a risolvere conflitti in maniera pacifica.

Dei ringraziamenti sono anche dovuti a tutte le altre persone che fanno attualmente parte del laboratorio (ovvero **Benedetta**, **Tao**, **Amara**, **Joanna**, **Vaiva**, **Virginia** e **Tomàs**), e a quelle che l'hanno già lasciato. Giusto per menzionare alcune delle più significative per me e per la mia tesi, vorrei ringraziare **Victoria** per essere stata la nostra bussola morale e amica premurosa. Anche se siamo stati in disaccordo su ideali fondamentali, come il ruolo di Harry Potter nella società moderna, è stato d'ispirazione vedere come tu ti sia sempre battuta per i tuoi principi.

Grazie ad **Andrea** per tutto l'aiuto che mi hai dato anche quando il background dell'ELISA stava per avere la meglio su di noi. Alla fine ha vinto lui, ma hai combattuto da eroe.

Akanksha, anche tu mi hai aiutato con diversi esperimenti, ma vorrei ringraziarti principalmente per tutti i bei momenti passati insieme come finta-coppietta. Come ho già detto per Jacques, avrei voluto che fossi rimasta con noi più a lungo.

Grazie a **Chiara** per essere stata la primissima persona ad unirsi al laboratorio dopo di me, salvandomi dalla solitudine, e per l'aiuto che mi hai dato nell'organizzarlo.
Graze anche a te, **Jonathan**. Tu sei stato una parte fondamentale e affidabile del laboratorio così a lungo da averci sorpresi tutti quando hai deciso di andartene. Ti ricorderò come un modello del Postdoc perfetto, nonostante la tua strana ossessione per gli egiziani.
E ovviamente, **Pietro** (o PIETROOOH). Non ho mai incontrato una persona genuinamente felice e divertente come te. Grazie per essere sempre stato pronto a scherzare su tutto, tra un investimento di bitcoin e un ELISA. Mi hai fatto riscoprire la panificazione come importante attività anti-stress.
Ci sono anche persone di altri laboratory che vorrei ringraziare. Prima tra tutti, **Gabriela**, per essere stata la mia prima vera tutor quando sono arrivato in IRB e per tutto l'aiuto nell'organizzazione del nuovo lab. Grazie anche per il corso intensivo di "storia e retroscena dell'IRB".
Grazie a tutti I ragazzi dei **laboratori Uguccioni**, **Cavalli** e **Varani** per le preziose collaborazioni e per i bei momenti passati insieme.
In ultimo, ma non meno importante, voglio ringraziare **i miei genitori e la mia famiglia** per avermi supportato anche in quest'ultimo viaggio verso la fine della vita da studente. So che sarete sempre qui per me, e che l'ottenimento del PhD non cambierà nulla, ma penso che sia il minimo da parte mia farvi sapere che noto tutto quello che fate per me e apprezzo ogni singolo gesto. In famiglia non siamo soliti esprimere il nostro affetto esplicitamente, e di solito lo facciamo attraverso piccoli gesti. Ma in fondo, anche così non è male, no?

Prendete la vita con leggerezza, che leggerezza non è superficialità,
ma planare sulle cose dall'alto, non avere macigni sul cuore.

-Italo Calvino, Lezioni Americane